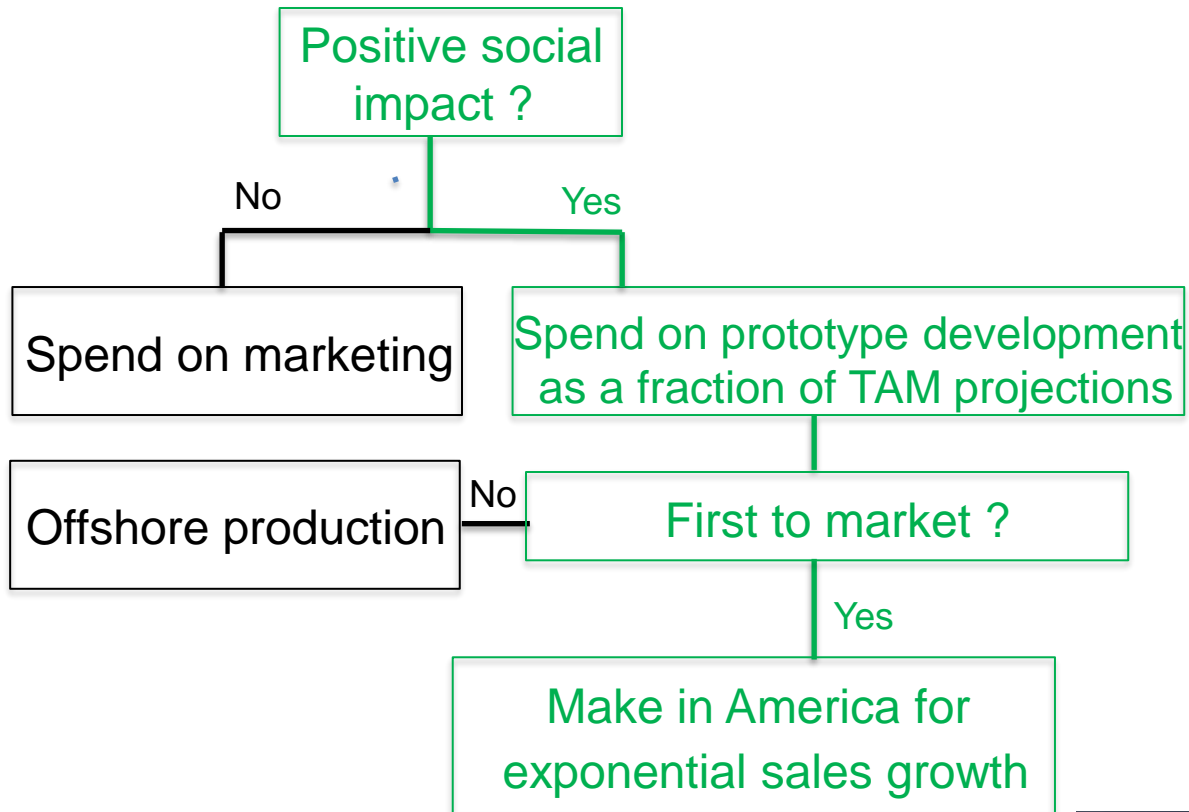
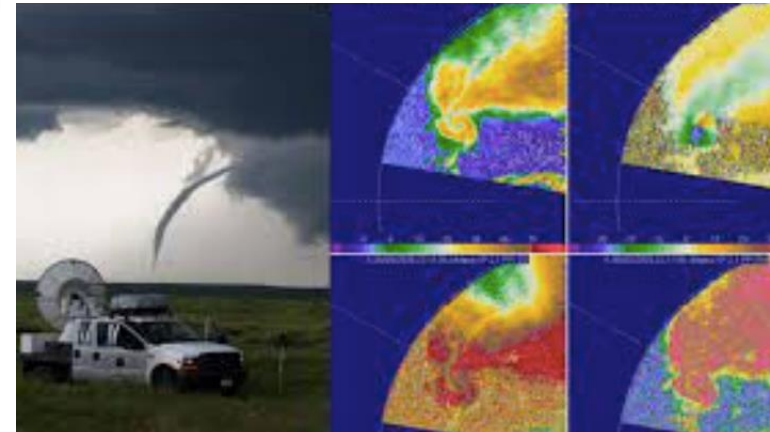

Stereo sensor electronics and algorithms for autonomous systems

Vijay Venkatesh

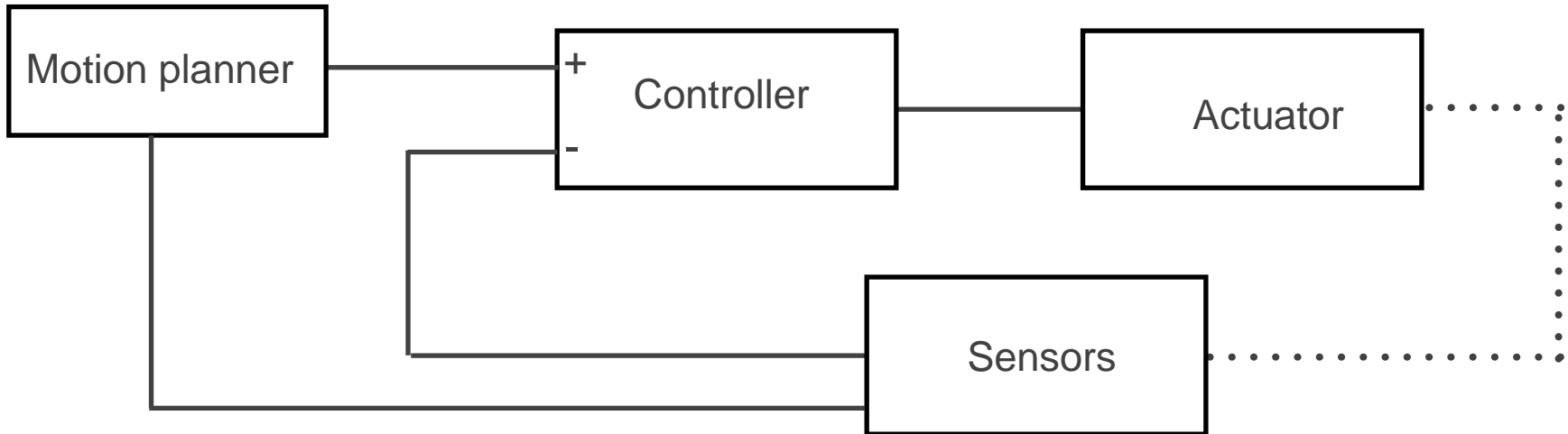
Introduction



- Autonomous systems and stereo vision.
- First ever stereo radar 2-D velocity demonstration on an automotive platform.
- First ever stereo radar 2-D velocity demonstration at automotive radar frequency.



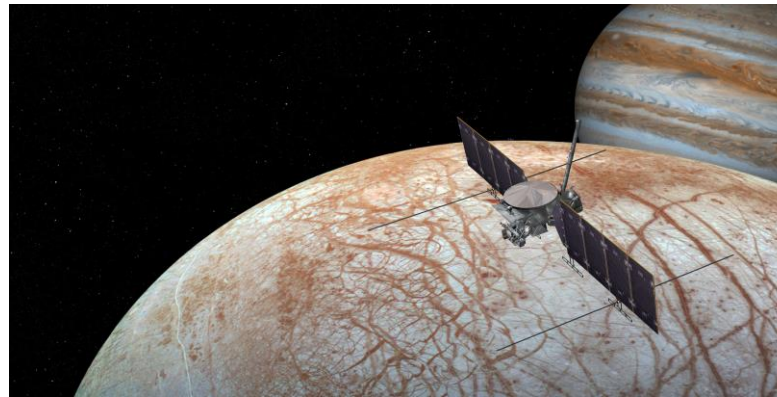
Anatomy of autonomous systems



- Motion plan involves computing path/steering/velocity to go from source to destination, while avoiding obstacles and respecting safety.
- Using motion plan as a reference, controller actuates vehicle.
- Sensors provide feedback, e.g. internal and environmental awareness.



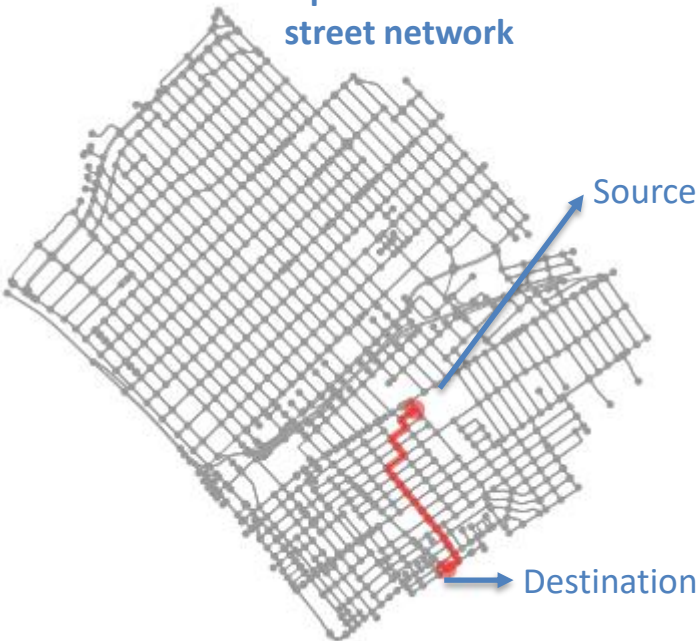
Adventure Actuators – Pickup truck, UAV, Europa spacecraft and snake robot



- Focus of talk is on rovers and vehicle experience.
- Experience gained on other autonomous systems can fuel innovation.

Motion Planning - Mission

Open source
street network



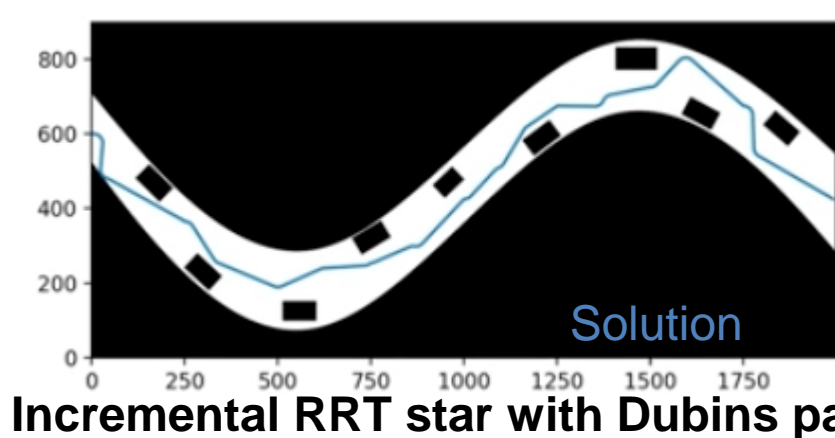
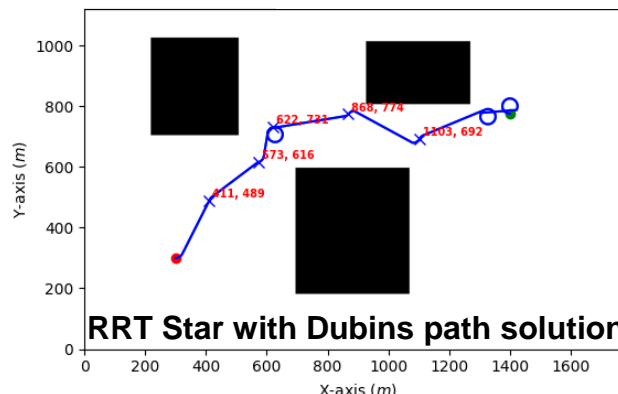
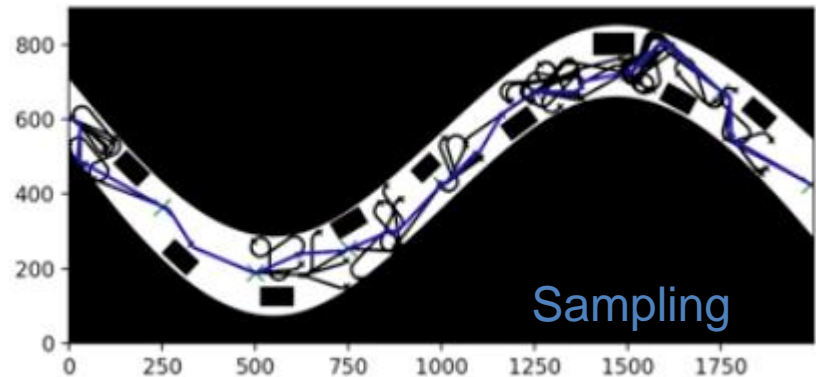
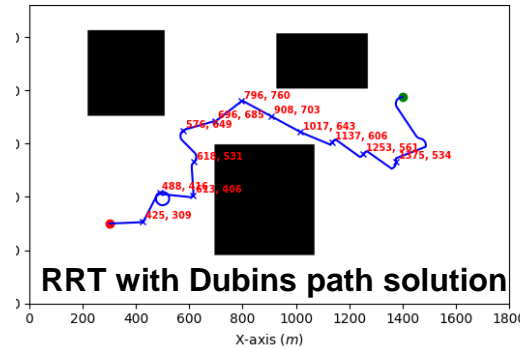
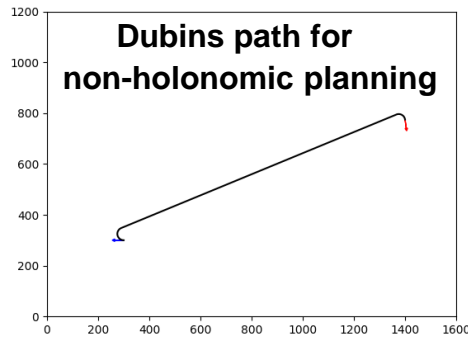
- Intersections represented as nodes, roads as edges of a graph.
- A* algorithm computes least cost path from source to destination.
- Selection of stepping stone node_{interim} intermediate nodes based on cost.
- Cost[node_{interim}] = Distance from source to node_{interim} + Distance from node_{interim} to destination

Algorithm 1 A*(G, s, t)

```
1: open ← MinHeap()
2: closed ← Set()
3: predecessors ← Dict()
4: costs ← Dict()
5: open.push(s, 0)
6: costs[s] ← 0
7: while !open.isEmpty() do
8:   u ← open.pop()
9:   uCost ← costs[u]
10:  if isGoal(u) then
11:    return extractPath(u, predecessors)
12:  for all v ∈ u.successors do
13:    if v ∈ closed then
14:      continue
15:    uvCost ← edgeCost(G, u, v)
16:    if v ∈ open then
17:      if uCost + uvCost + h(v) < open[v] then
18:        open[v] ← uCost + uvCost + h(v)
19:        costs[v] ← uCost + uvCost
20:        predecessors[v] ← u
21:    else
22:      open.push(v, uCost + uvCost + h(v))
23:      costs[v] ← uCost + uvCost
24:      predecessors[v] ← u
25:  closed.add(u)
```

Motion Planning - Behavior

- ❖ Behavior planning avoids obstacles within each road.
 - Dubins algorithm guarantees nearly optimal path assuming reverse gear is irrelevant.
 - Rapidly exploring Random Trees (RRT) “samples” space until collision free path is found.
 - RRT star algorithm searches for shorter path even after initial path is found.



Control systems

$$\sum F = ma \quad \sum M = I\ddot{\psi}$$

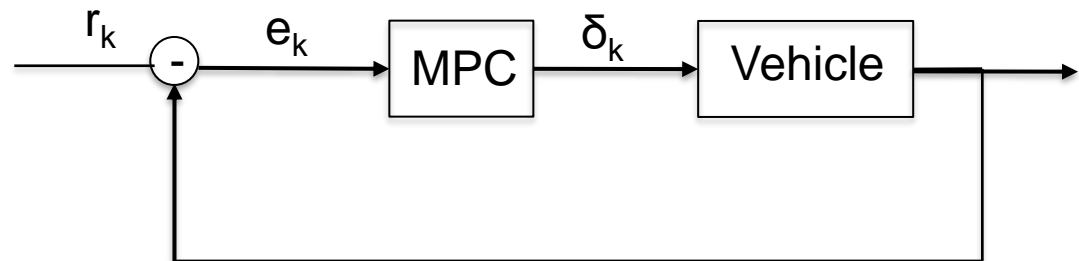
$$\dot{\psi} = \frac{v}{L} \tan \delta$$

$$x_{k+1} = Ax_k + Bu_k$$

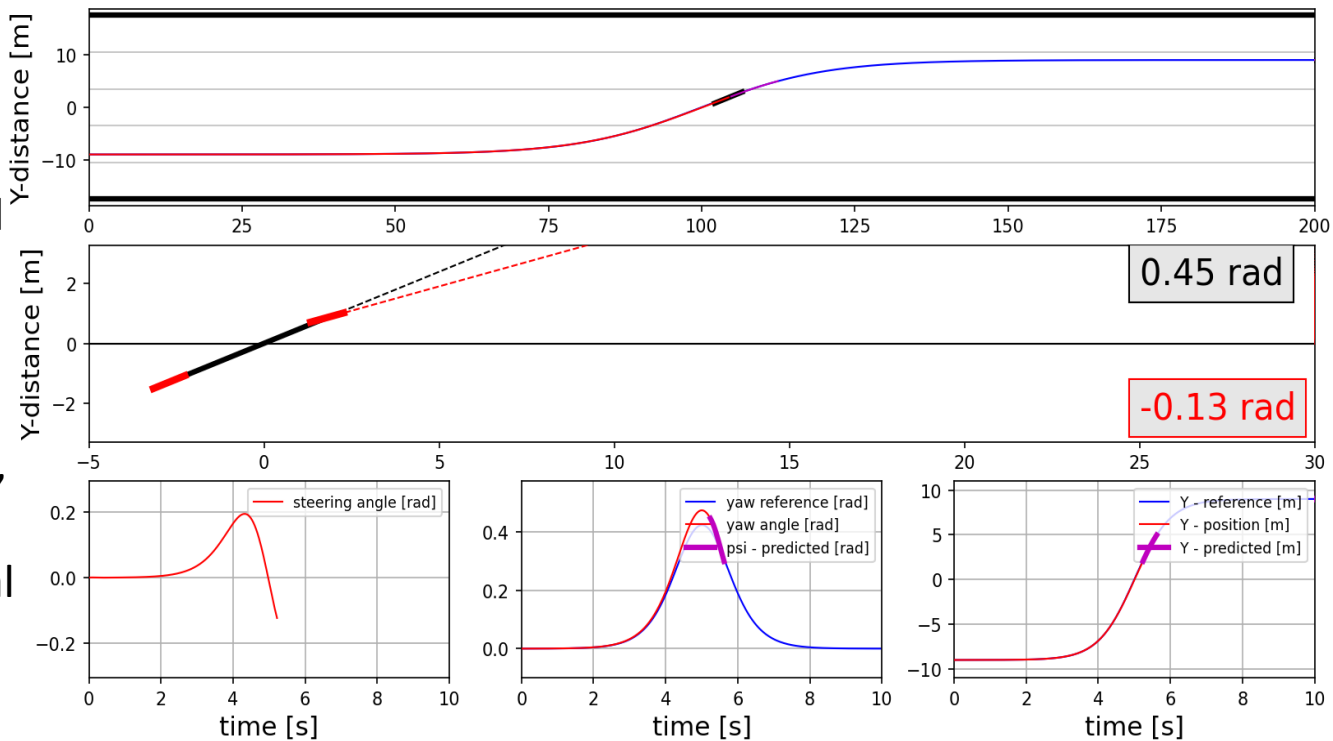
$$y_{k+1} = Cx_k + Du_k$$

$$e_k = r_k - y_k$$

$$J = f(S, e_{k,k+1\dots,k+N}, u_{k,k+1\dots,k+N}, Q)$$



- ❖ Tracking controllers allow vehicle to maintain desired lane discipline.



(e.g. jerk free driving vs aggressive pursuit of speed).

Control systems

$$\vec{u}_k = [\delta_k, a_k]$$

❖ Cost function optimized over predictive horizon N.

$$\vec{x}_k = [\dot{x}_k, \dot{y}_k, \psi_k, \dot{\psi}_k, X, Y]$$

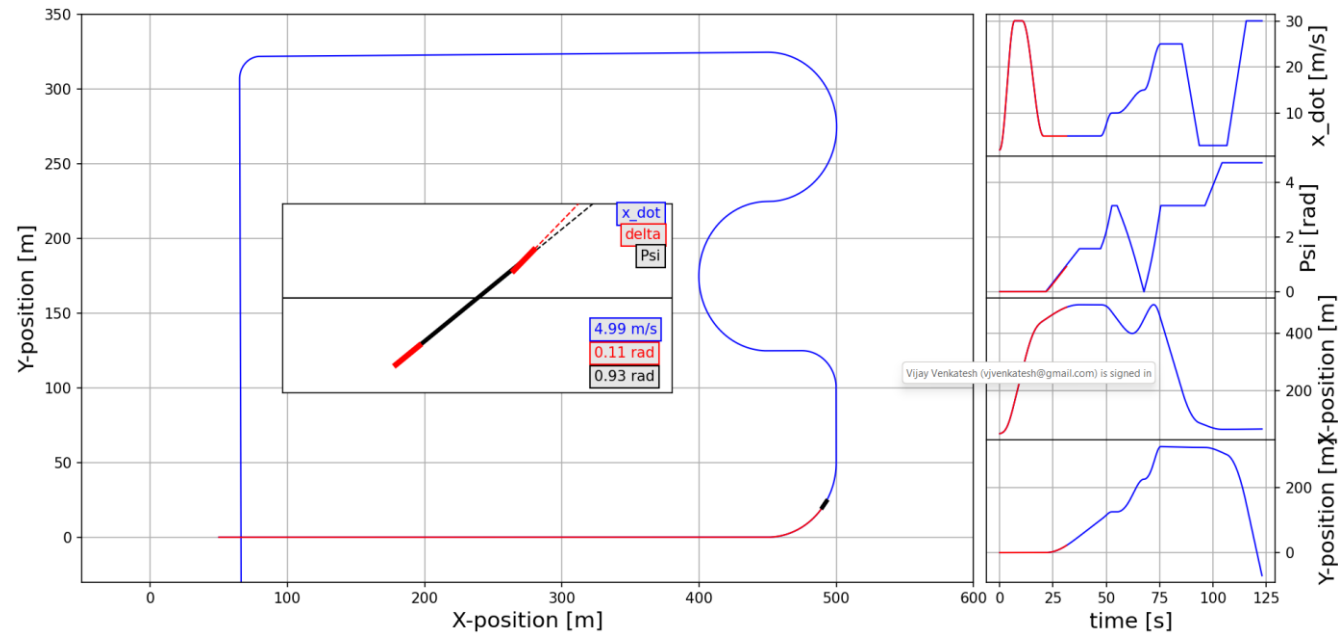
$$[Y, X, \Psi, \dot{\Psi}, \ddot{X}] = \ddot{\mathfrak{X}}$$

❖ Vehicle slows down during turn, but the look ahead by

N time-steps positions vehicle for reacceleration after turn.

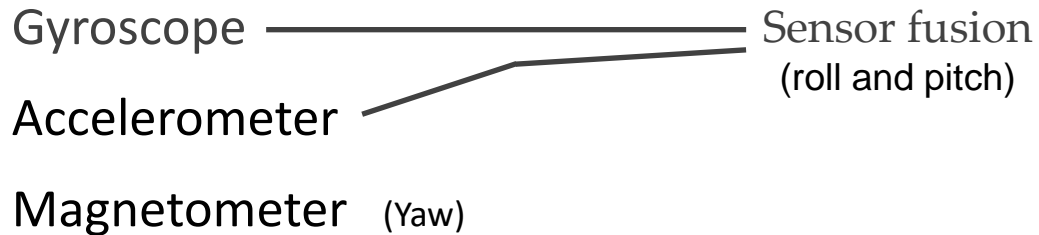
Pseudo-code

1. Import reference trajectory.
2. Initialize states.
3. Compute matrices A, B, C and D.
4. For t=0: 0.02: M*0.02
 - a. Compute augmented state vector
 - b. Compute error within horizon
 - c. Compute Hdb, Fdbt, Cdb, Adc
 - d. Compute
 - e. Compute
 - f. Limit steering angle based on friction ellipse
 - g. Compute new states
5. Visualize results



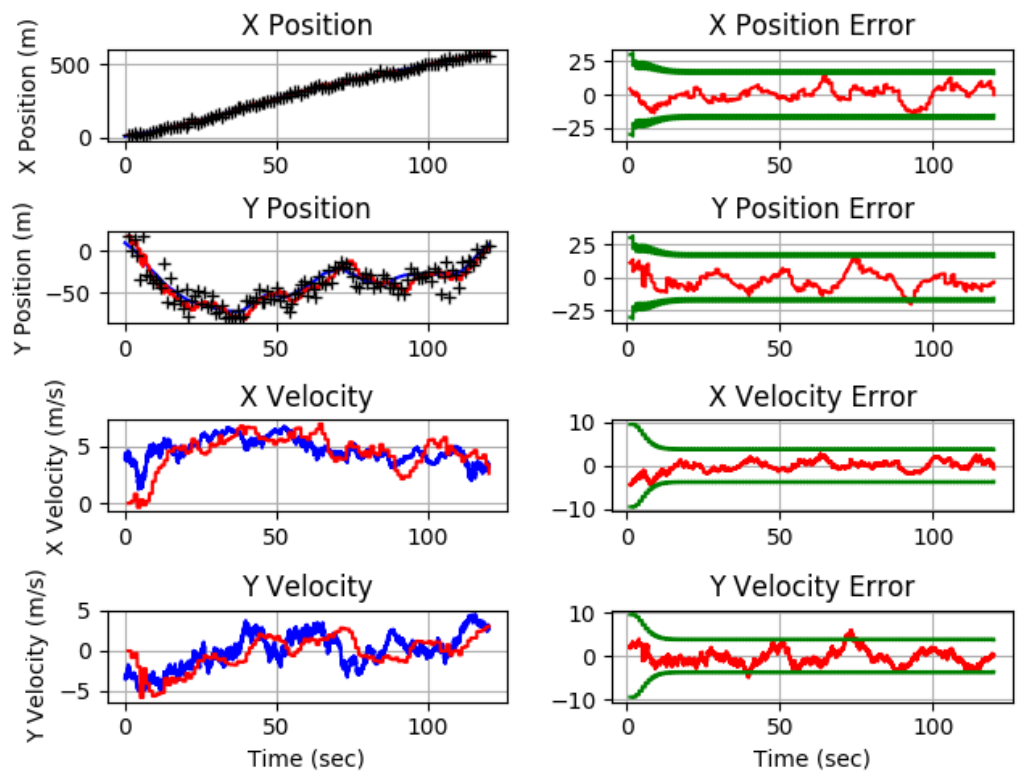
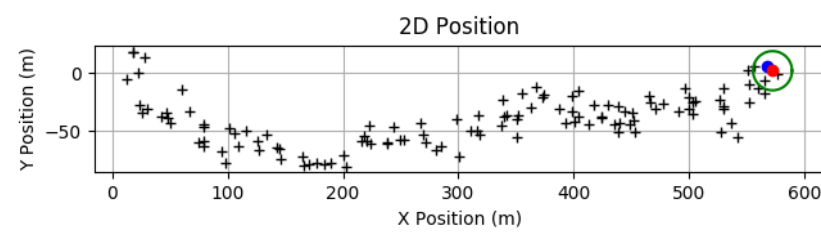
Sensors – Internal awareness

- ❖ Inertial motion unit for angular orientation sensing



- ❖ GPS for location sensing

Requires line of sight
communication with
at least 3 satellites



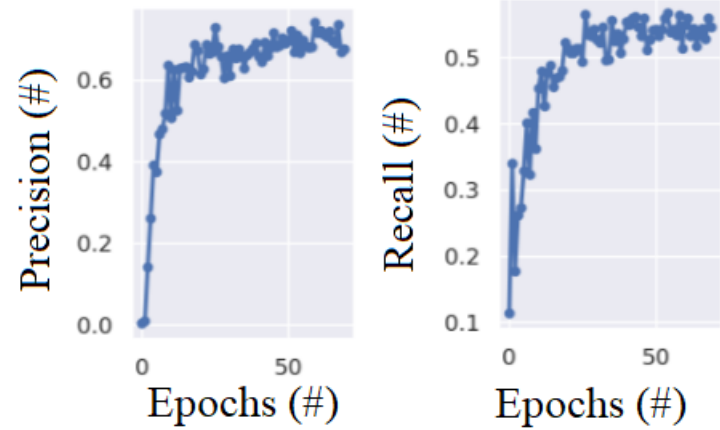
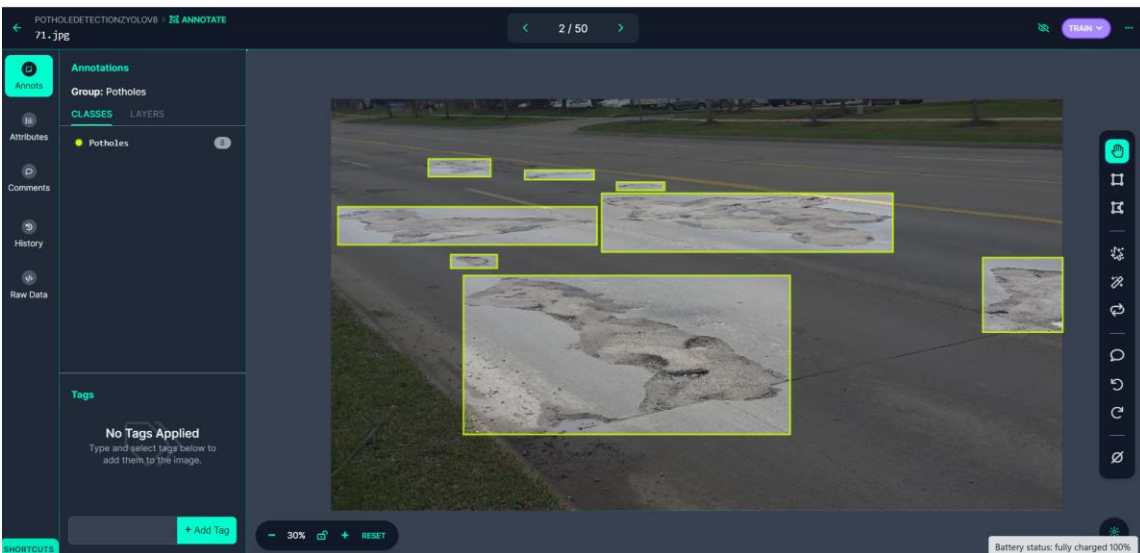
Sensors – Environmental awareness

- ❖ Camera
 - Dominant sensor as most information for driving is meant for visual cognition (e.g. lane markings, road signs, traffic lights)
- ❖ Radar
 - Critical for brake assistance at high speeds.
 - Blind spot monitoring.
 - Robust to all lighting conditions, rain and fog.
- ❖ Lidar
 - Localization with a 360 degree view



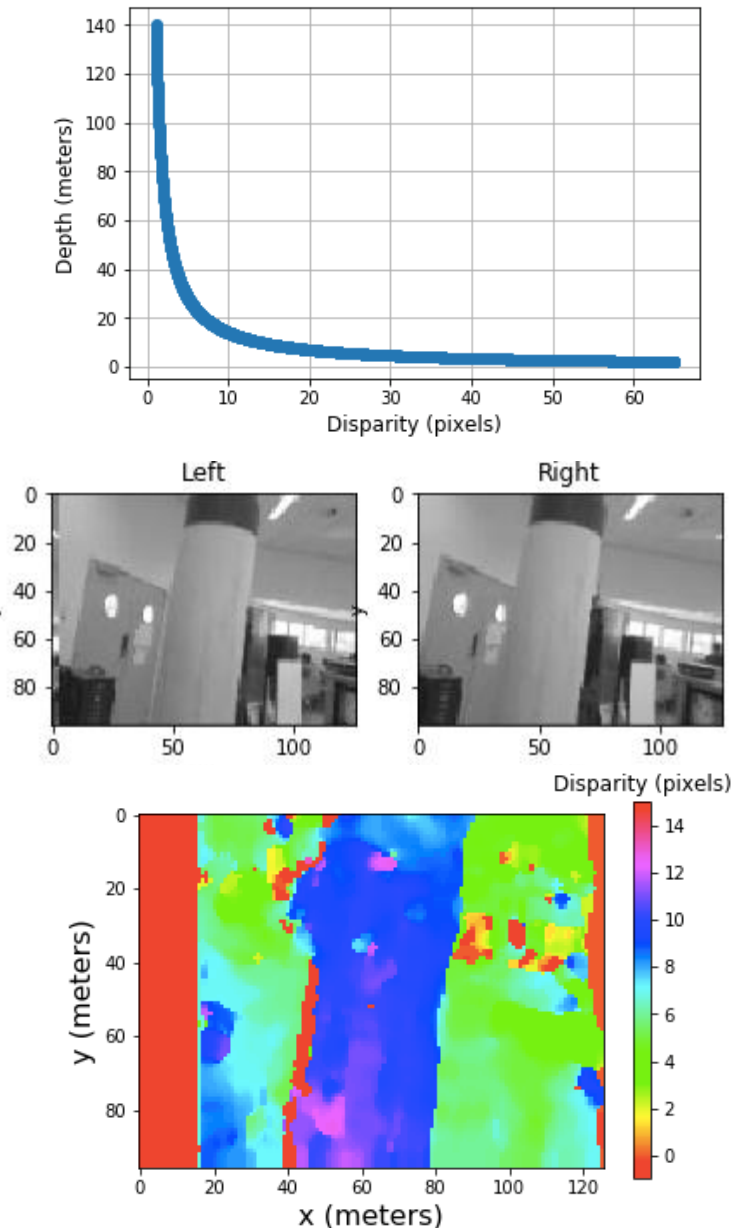
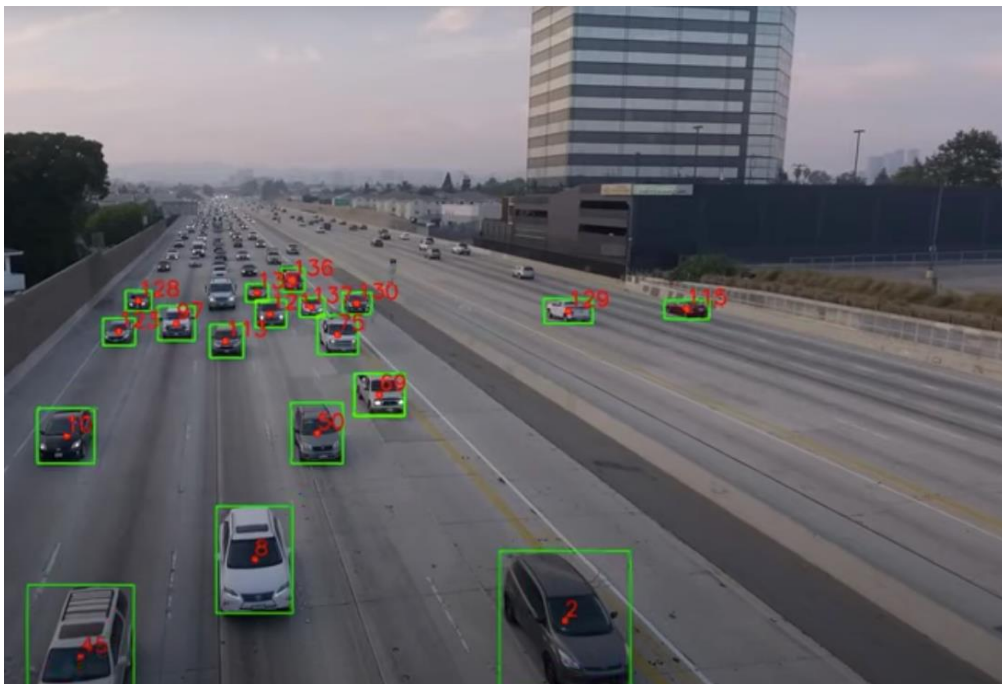
Sensors – Environmental awareness

- ❖ Pothole and traffic sign detection based on visual perception.
- ❖ Data annotation in example accomplished using Roboflow, and Google Colab was used for training.
- ❖ YOLO v8 used for object detection.



Stereo vision – limited to close range

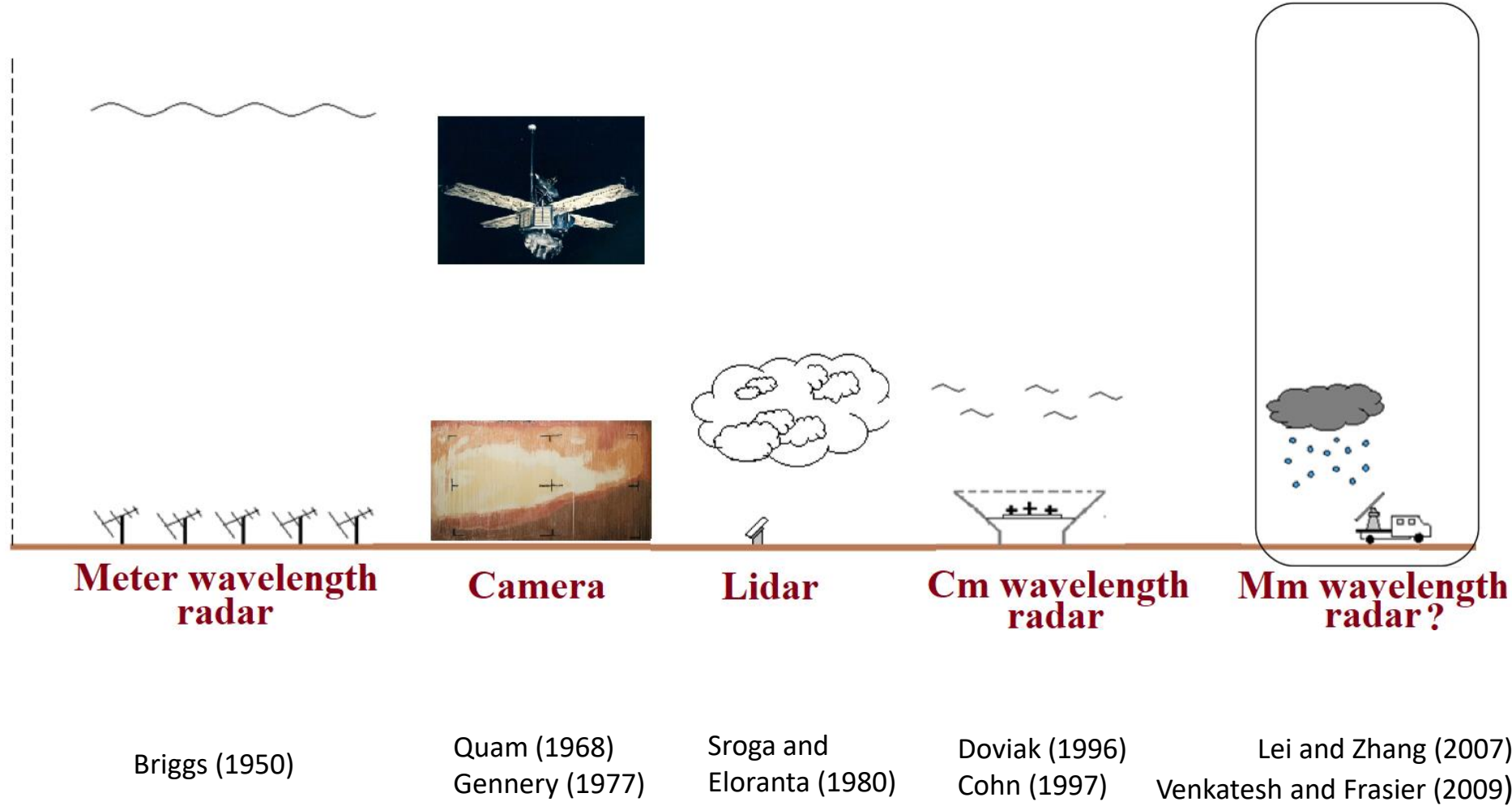
- ❖ Stereo vision limited to about 140 meters (right).
- ❖ YOLO object detectors also limited in range (below).
- ❖ Radars can provide long range tracking
necessary for braking decision at high speeds.



First compact stereo radar demonstration to sense 2-D velocity

- Motivation and problem description
- System implementation
- System performance
- Conclusions

Stereo sensors chronology



Radar sensor for 1-D velocity measurement



TRUCK MODIFICATIONS

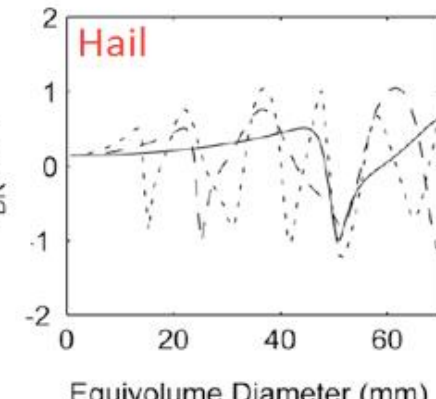
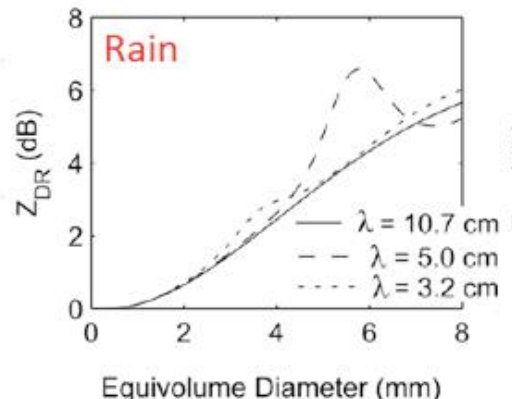
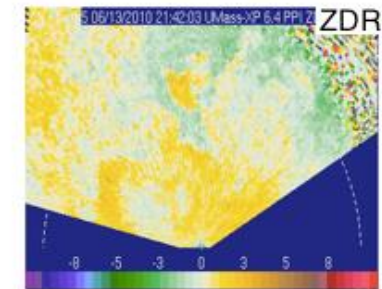
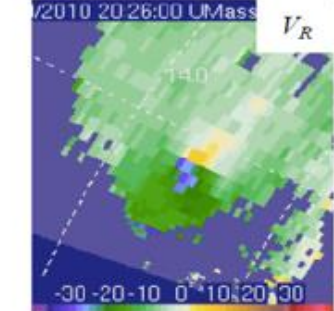
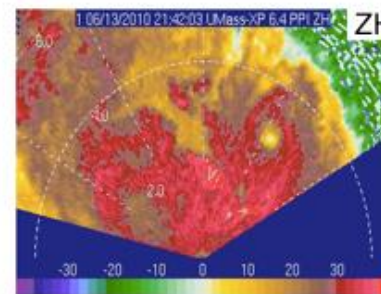
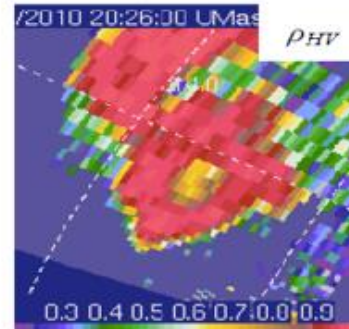
- Replaced alternator

TRUCK BED MODIFICATIONS

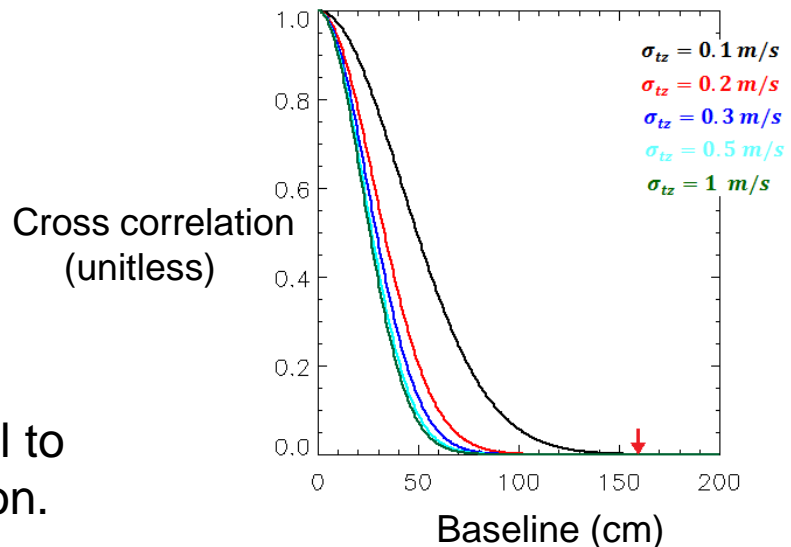
- Antenna
- Servo motor controller for mechanical scan
- Transmit and receive electronics
- Dedicated batteries and power management

LIMITATIONS

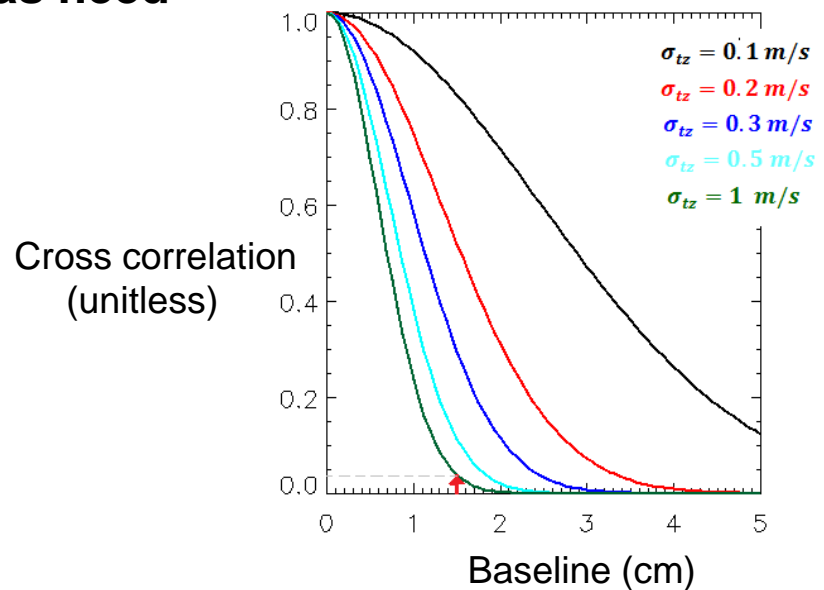
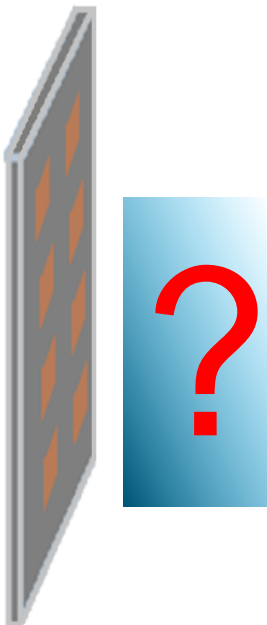
- Only measures radial component of velocity



Stereo radar for 2-D velocity estimation



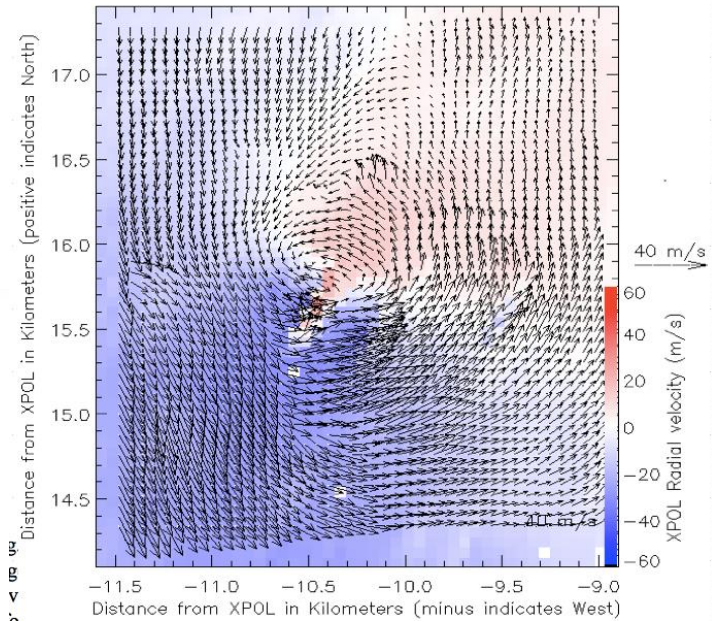
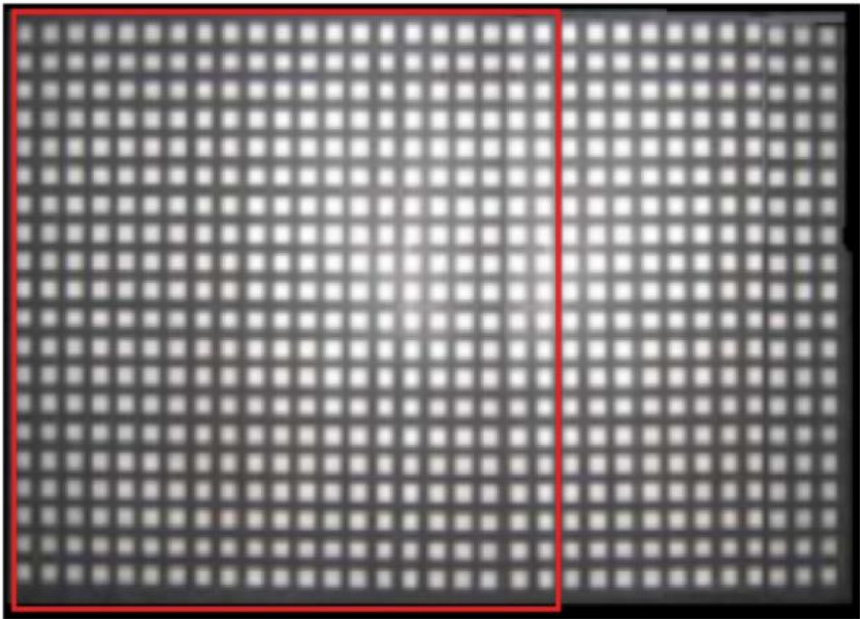
- Precision directly proportional to square of cross-correlation.
- At X- and W-band, antennas need to overlap.**



Stereo radar implementation

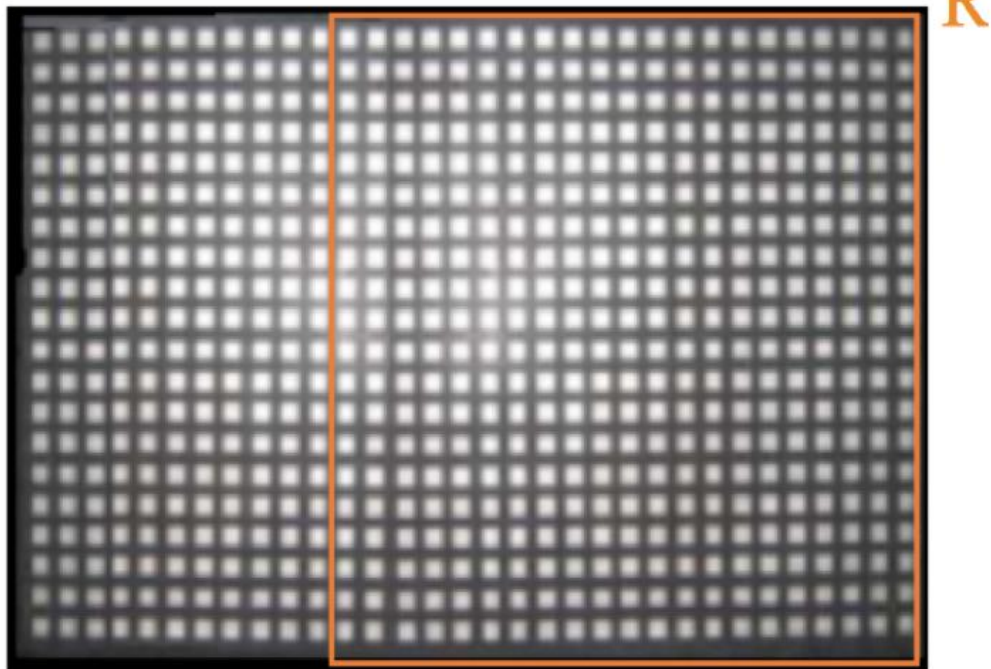
- Segment phased-array antenna face.
- Interleave sub-arrays on alternate pulses.

L



Stereo radar implementation

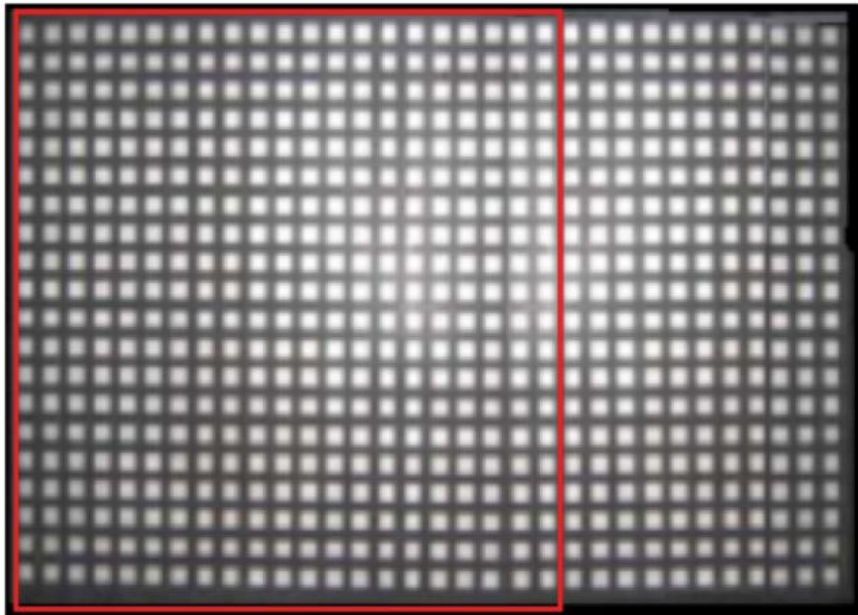
- Interleave sub-arrays on alternate pulses.



Stereo radar implementation

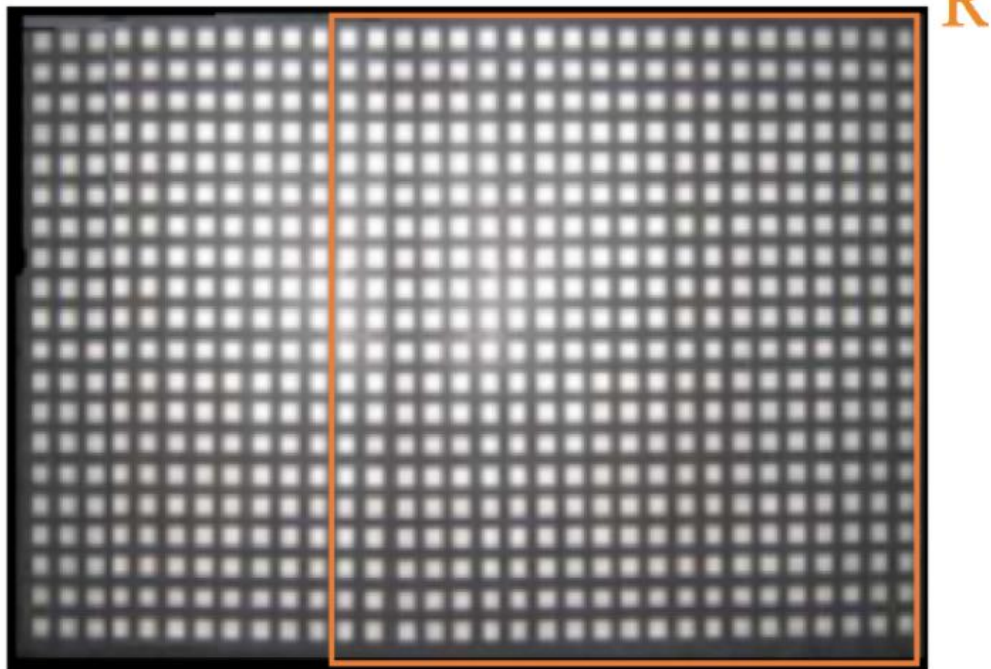
- Interleave sub-arrays on alternate pulses.

L

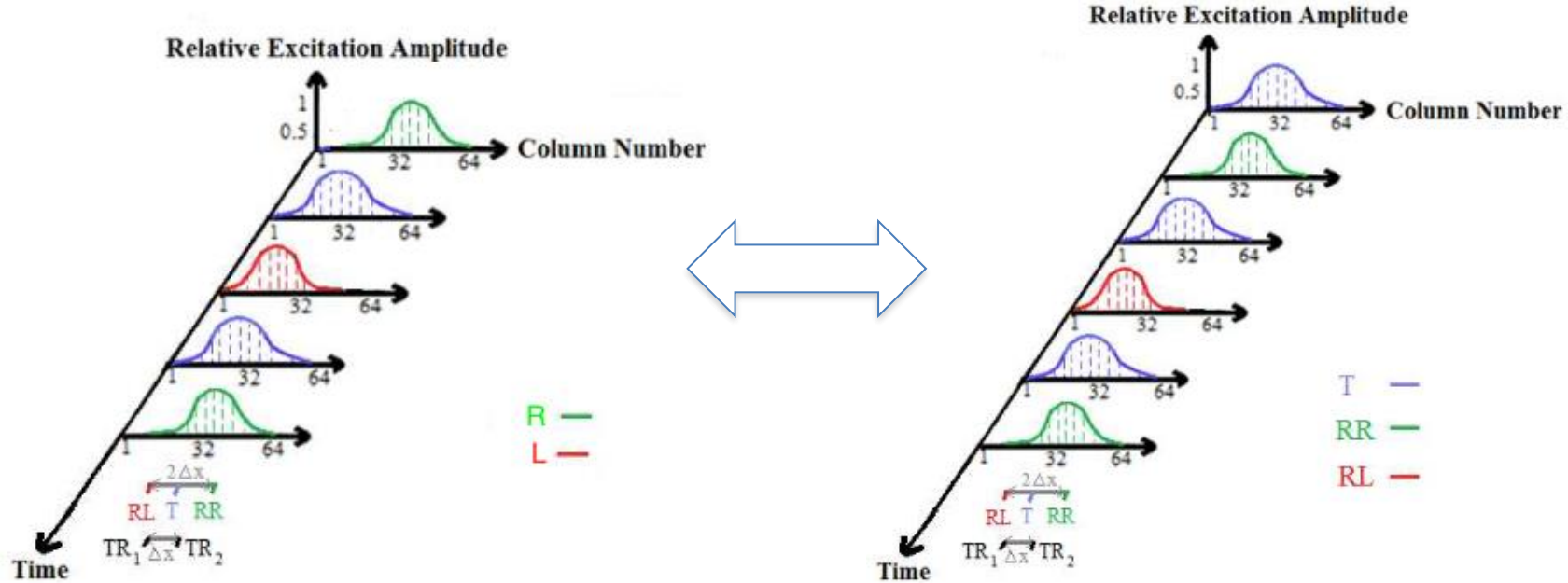


Stereo radar implementation

- Interleave sub-arrays on alternate pulses.

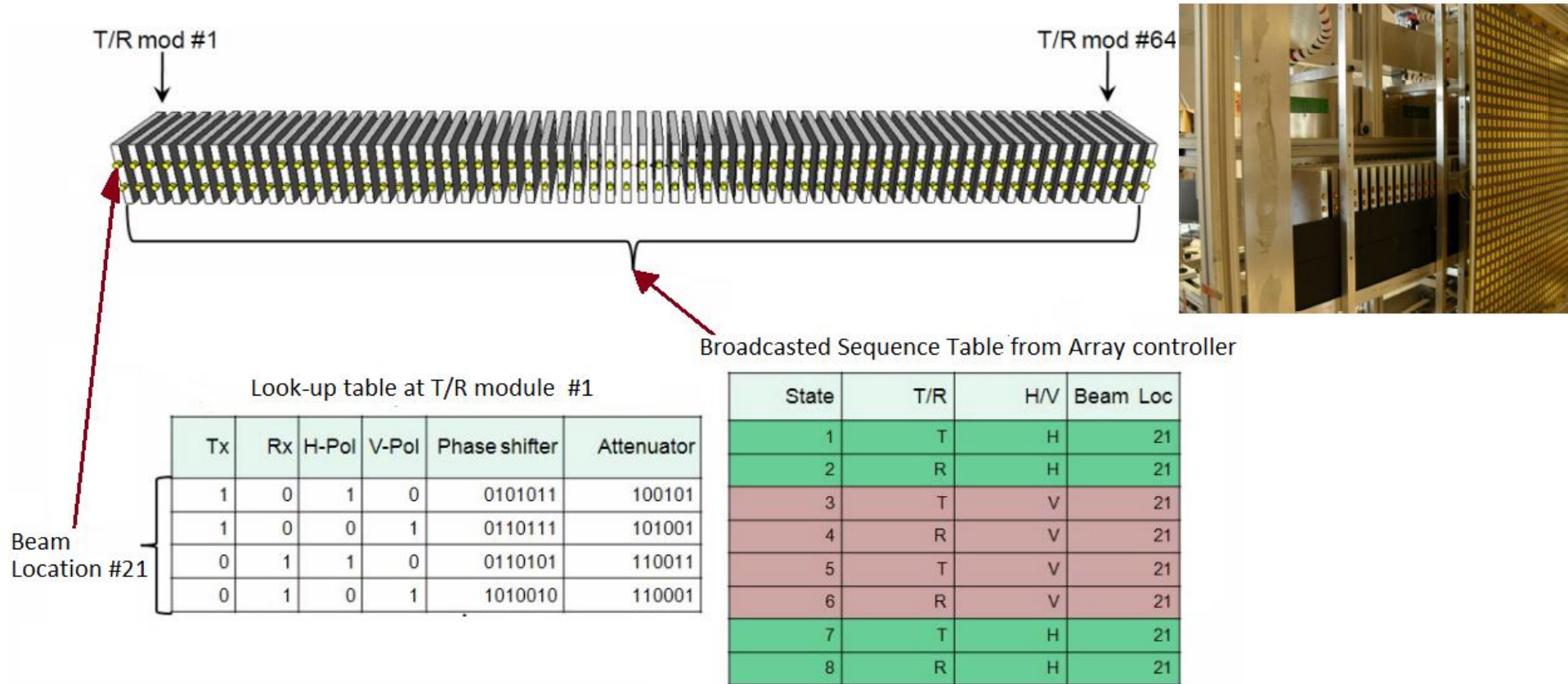


Stereo radar implementation

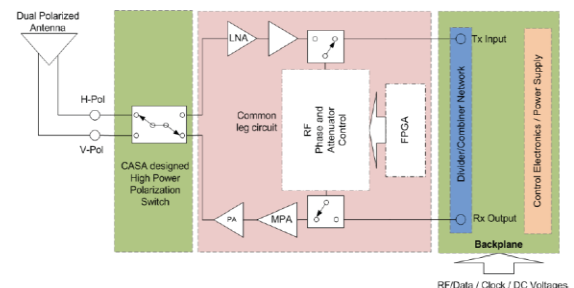


- Interleaved left and right antenna systems allow for spaced antenna implementation
- Monte-Carlo simulations employed to optimize array segmentation for spaced-antenna retrievals

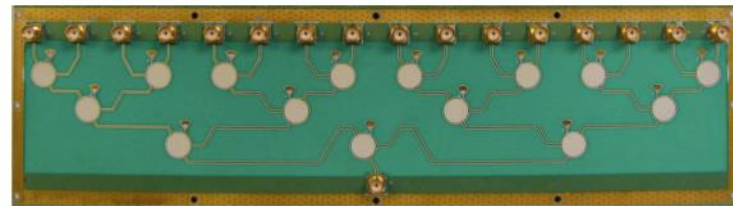
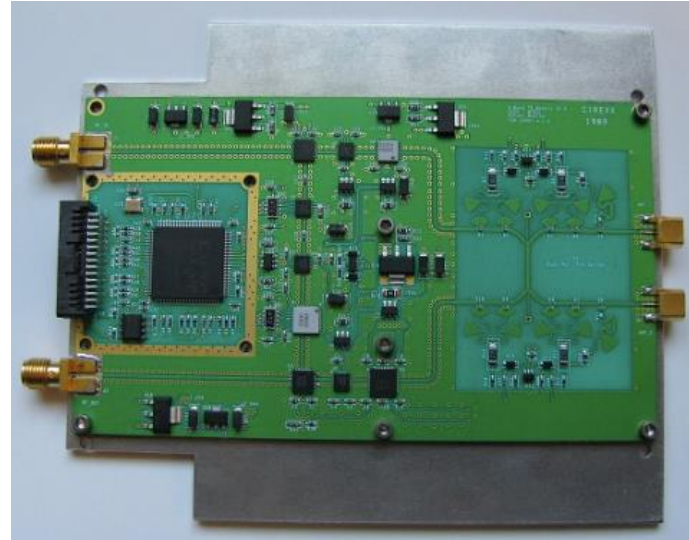
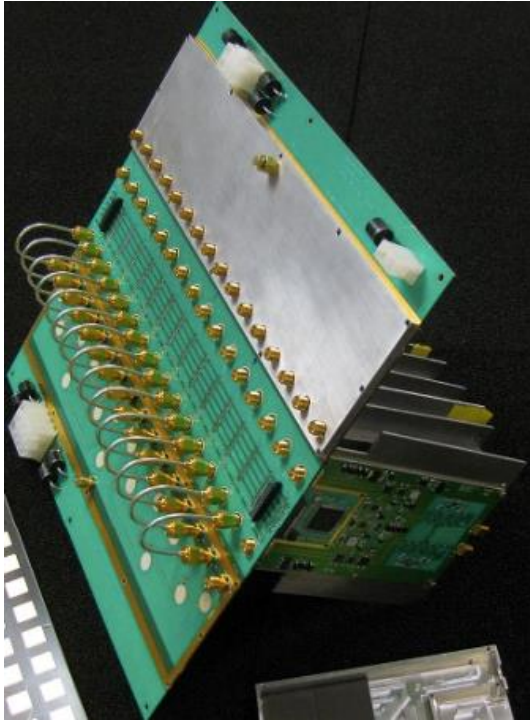
Stereo radar electronics



- Look-up tables stored in T/R module memory during calibration
- Spaced-antenna sub-arrays constitute additional beam “identities”

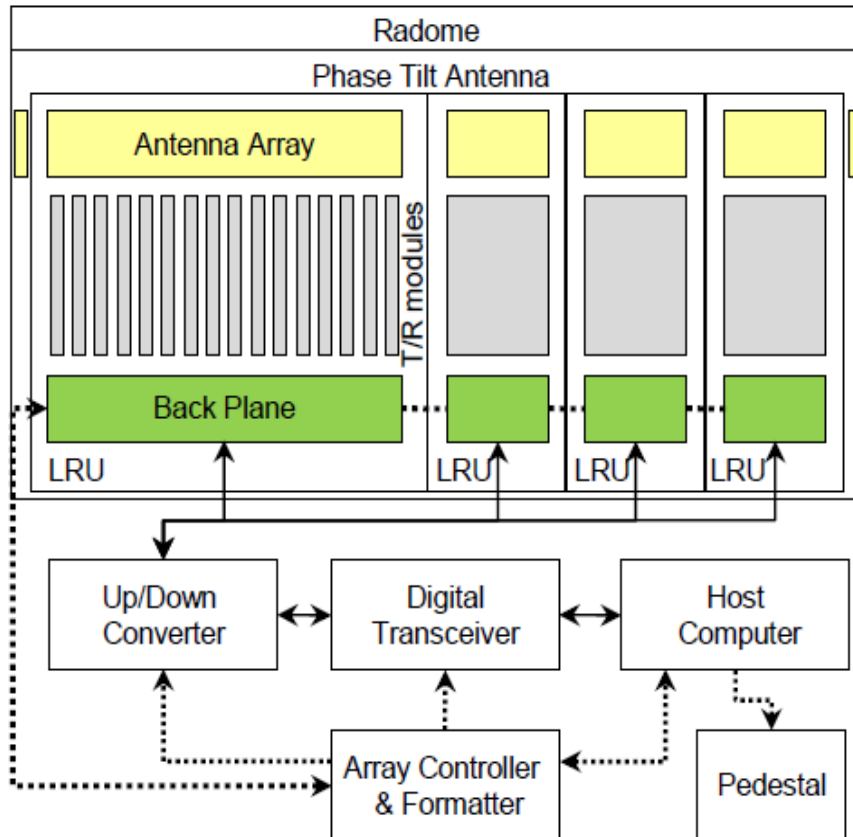


Stereo radar electronics



- About 70 Printed Circuit Boards designed, fabricated and tested.

Stereo radar electronics

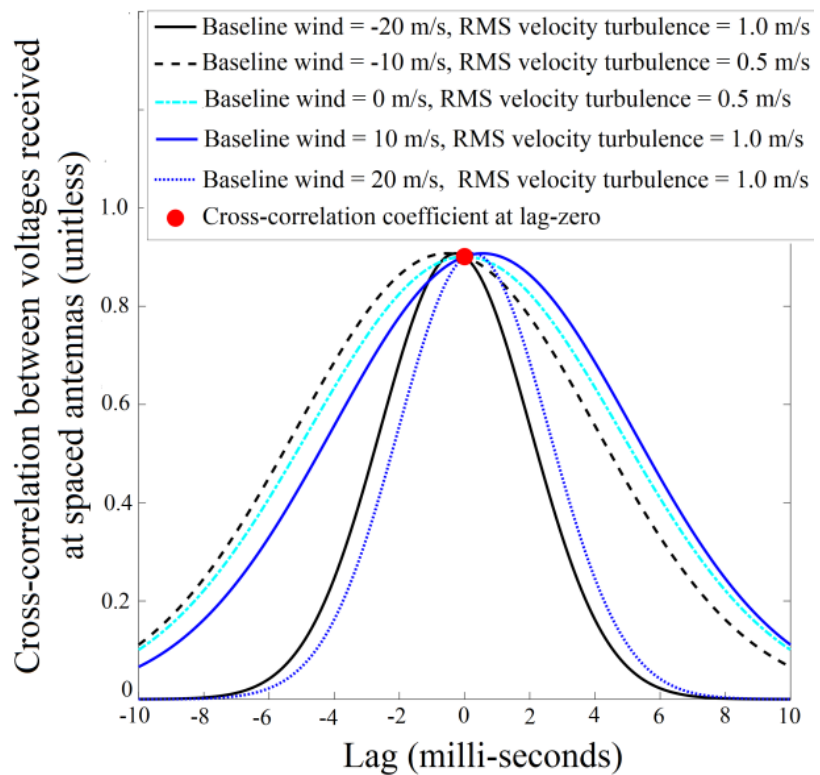


- Tx pulse generated on Host computer
- Up-converted copies fed to entire array
- “Controller” ensures synchronization
- Peak radiated power 64 Watts.

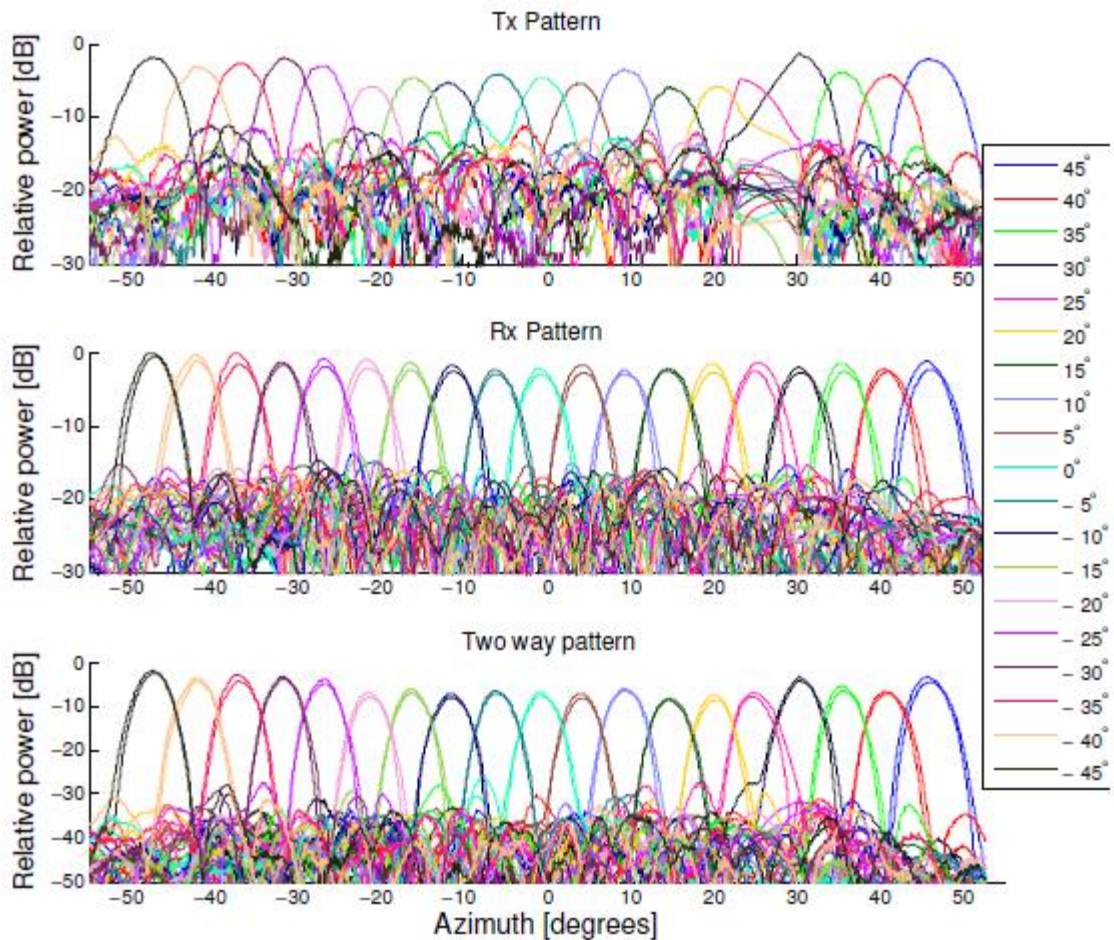


Stereo radar 2-D velocity measurement demonstration

- Motivation and problem description
- System implementation
- **System performance**
- Conclusions

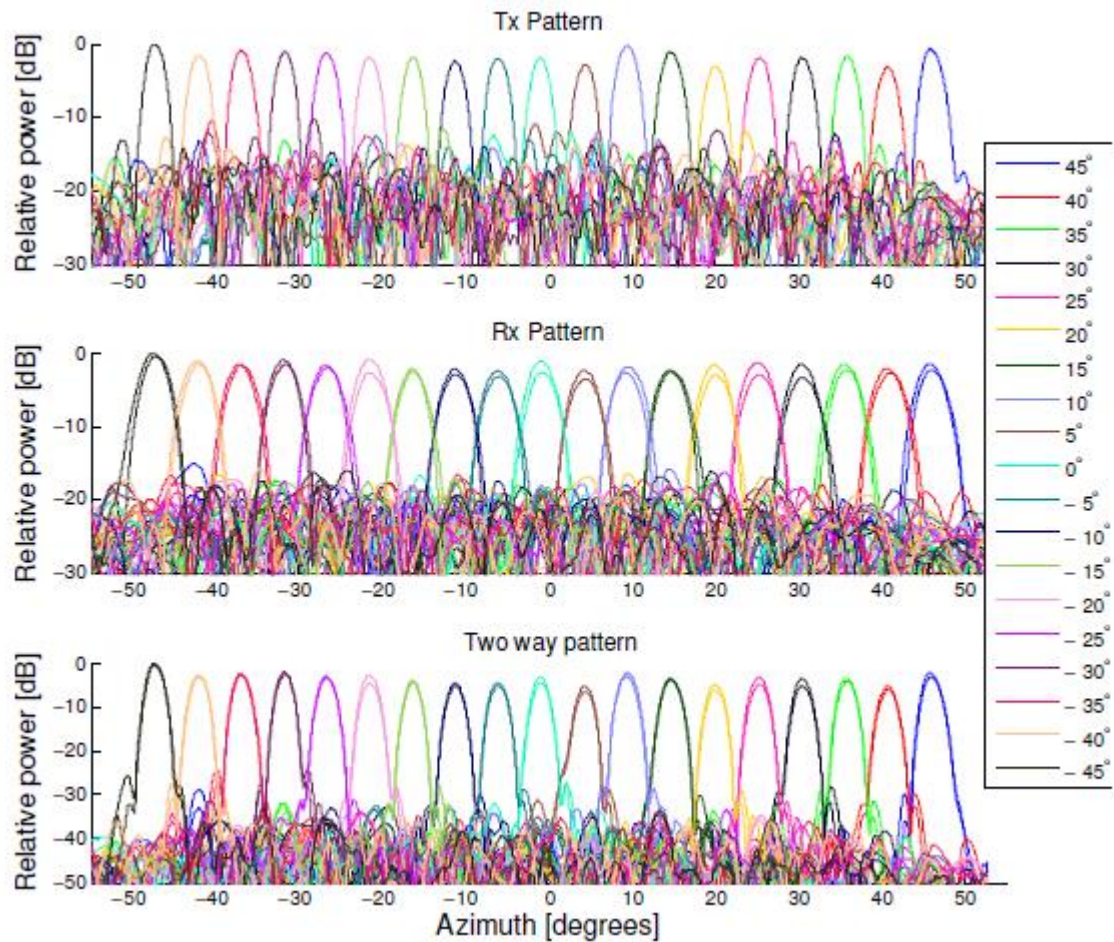


5 degree electronically scanned sub-arrays



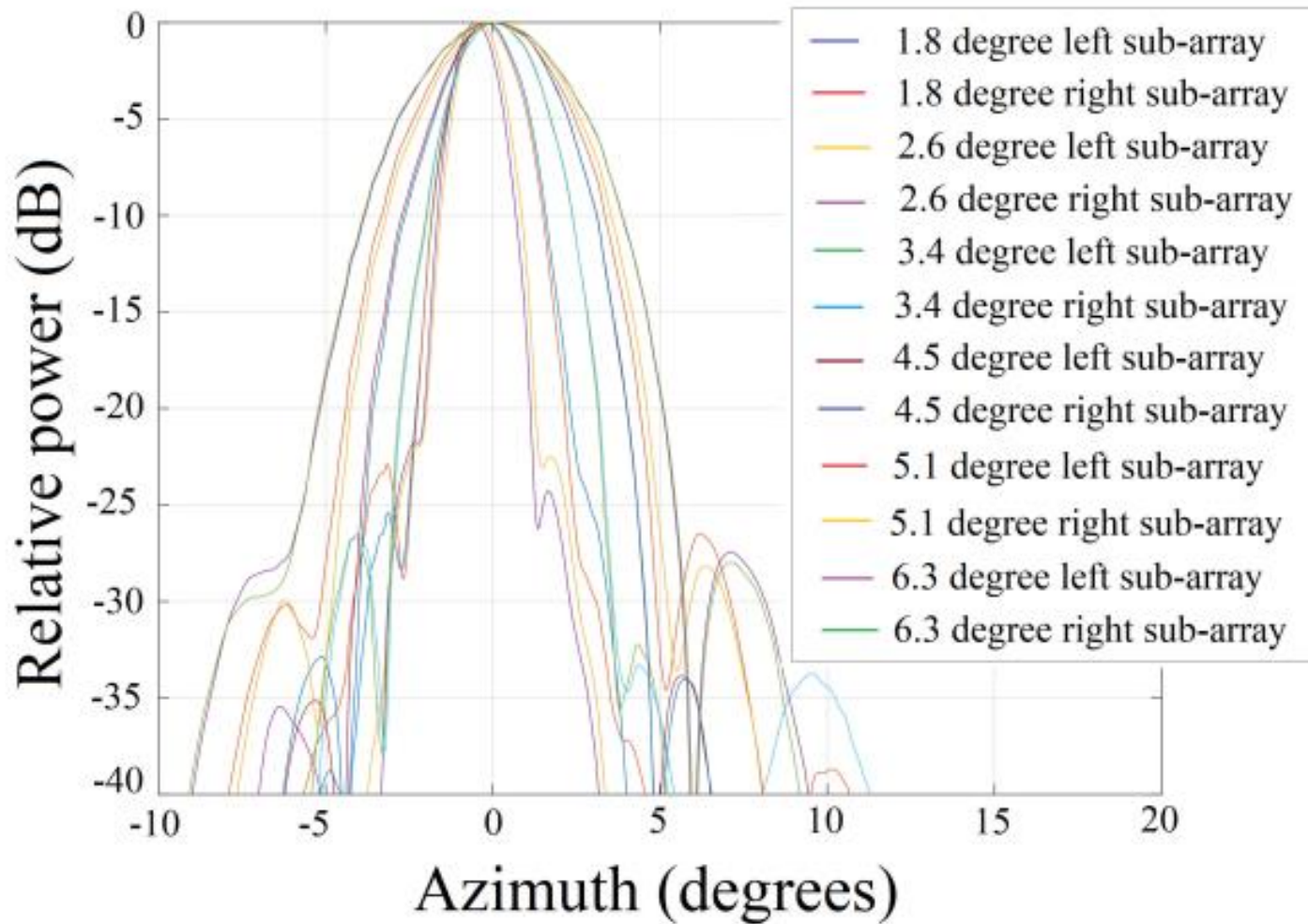
- “Tx” pattern affected by gap in data-collection
- Sidelobe levels appear worse than “desired”

2.7 degree electronically scanned sub-arrays



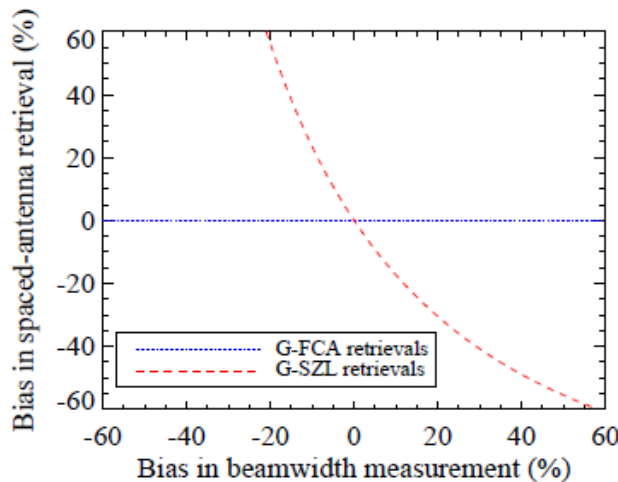
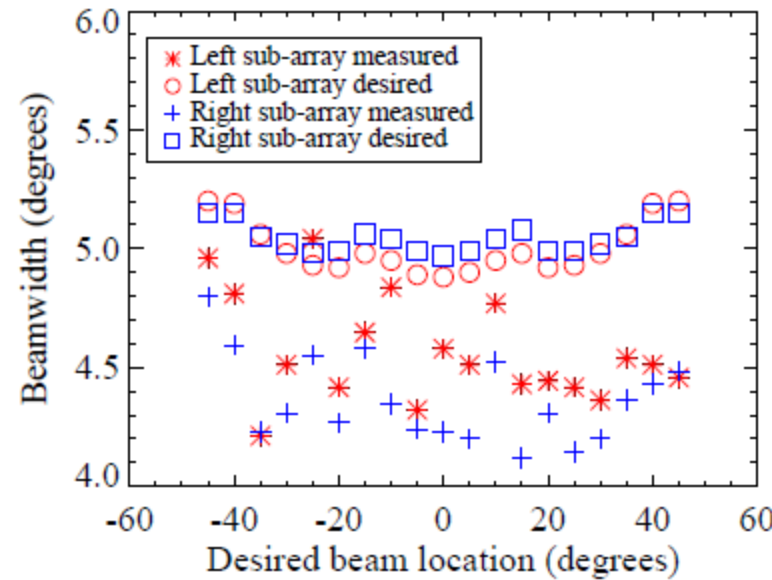
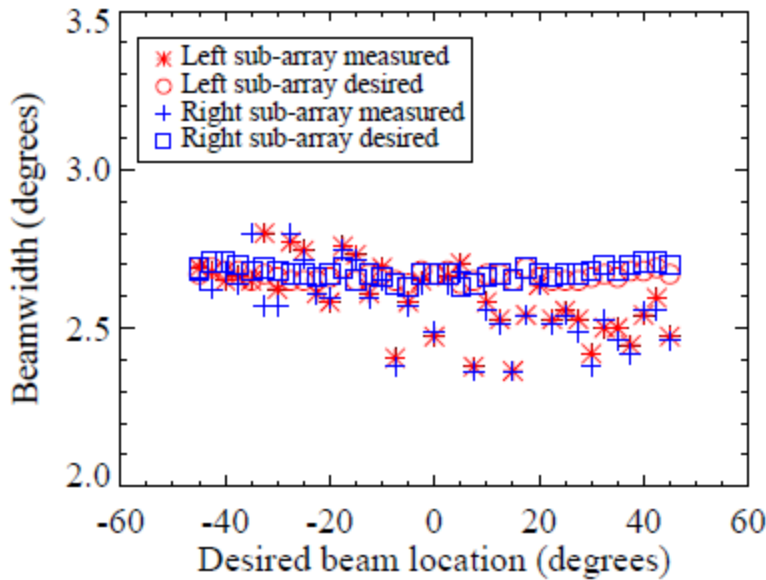
- Measured patterns only approximate “desired” patterns
- Equivalent left and right two-way patterns similar

Broadside sub-arrays



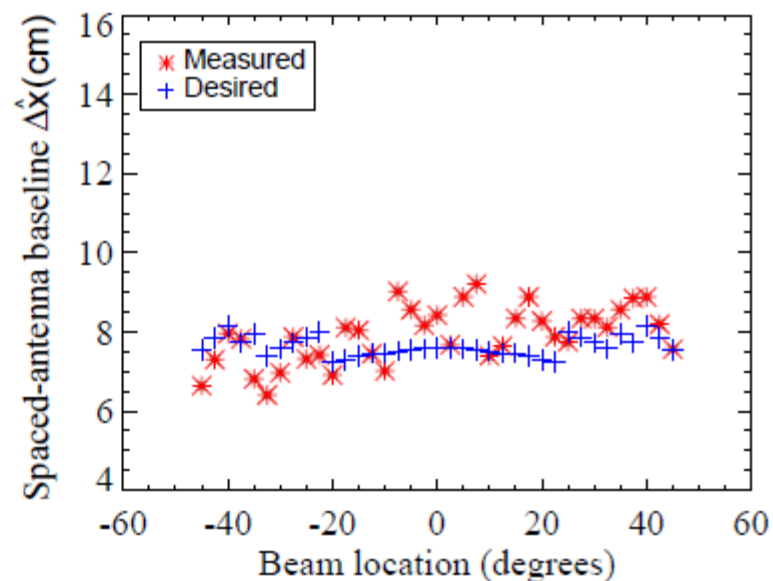
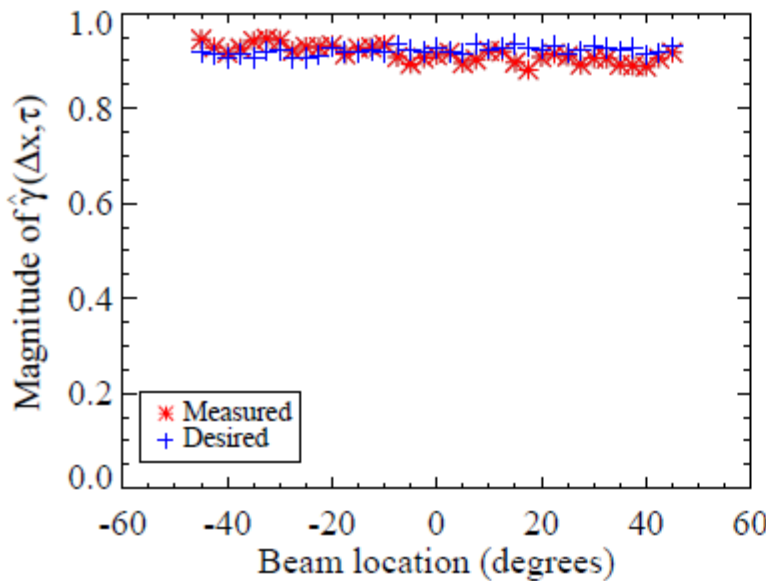
6 systems with beamwidths varying from 1.8 to 6 deg implemented

Beamwidth measurements for e-scan



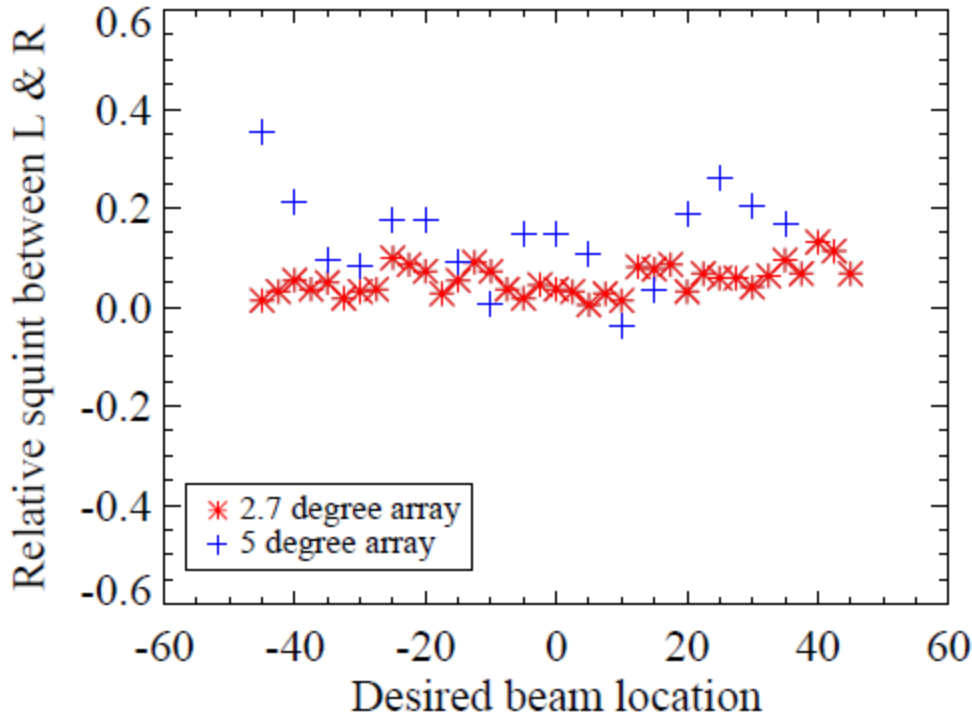
- 2.7 degree sub-array closer to “desired” patterns
- SZL algorithms sensitive to calibration errors

Baseline measurements for e-scan



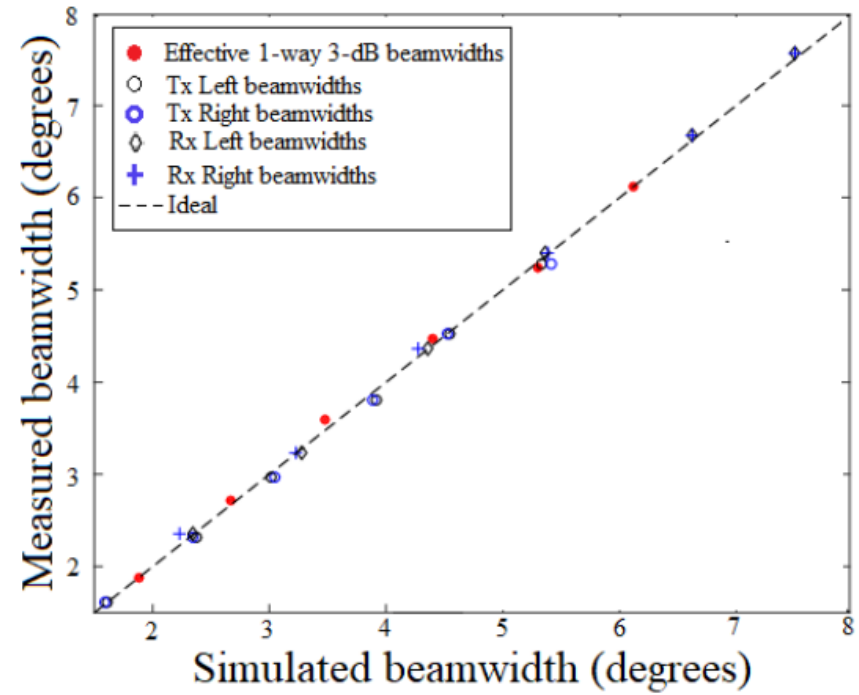
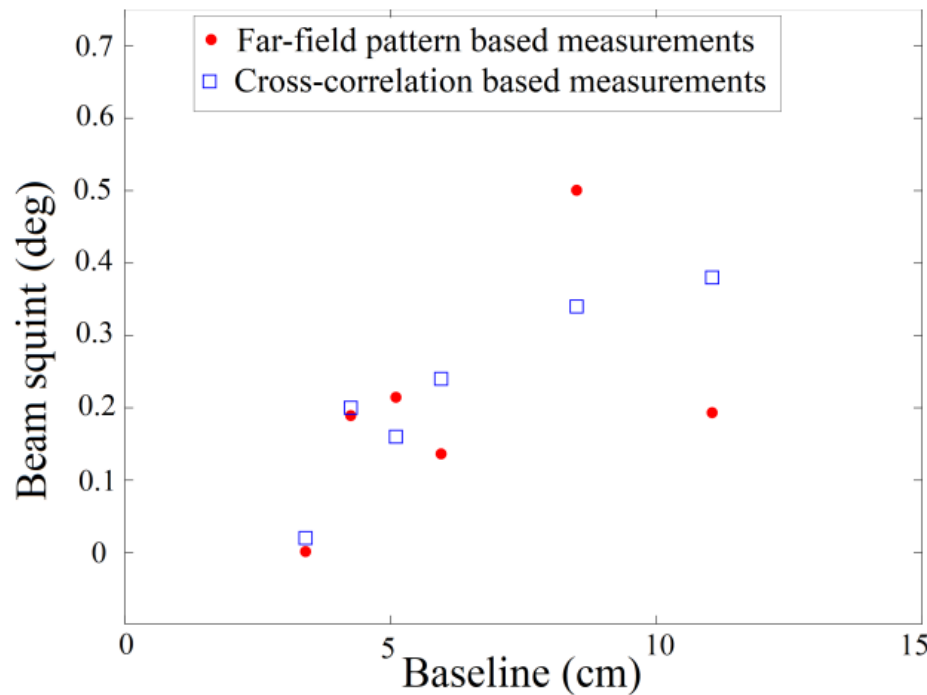
- Apriori knowledge of beamwidth
- Estimate $|\hat{\gamma}(\Delta x, 0)|$
- Retrieve baseline from $|\gamma(\Delta x, 0)| = \exp\{-2k^2\sigma_{e\phi}^2\Delta x^2\}$
- Provided baseline calibration for subsequent retrievals.

Beam squint measurements for e-scan



- Squint between left and right equivalent monostatic combinations measured.
- 2.7 degree array has less squint on average.

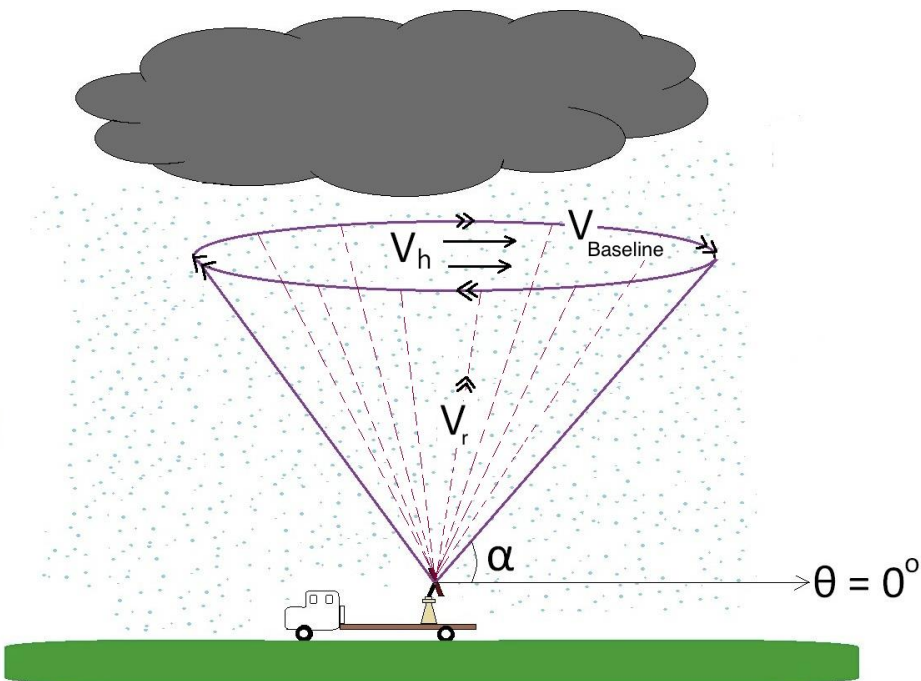
Beamwidth, baseline and beam squint measurements at broadside



- Aperture synthesis errors are lowest for low baseline and small beamwidth elements.
- This is because element level amplitude and phase errors are common to the left and right sub-arrays.

Experimental setup for stereo radar validation

- Compare stereo radar retrievals at broadside to DBS and VAD-like variational retrievals.



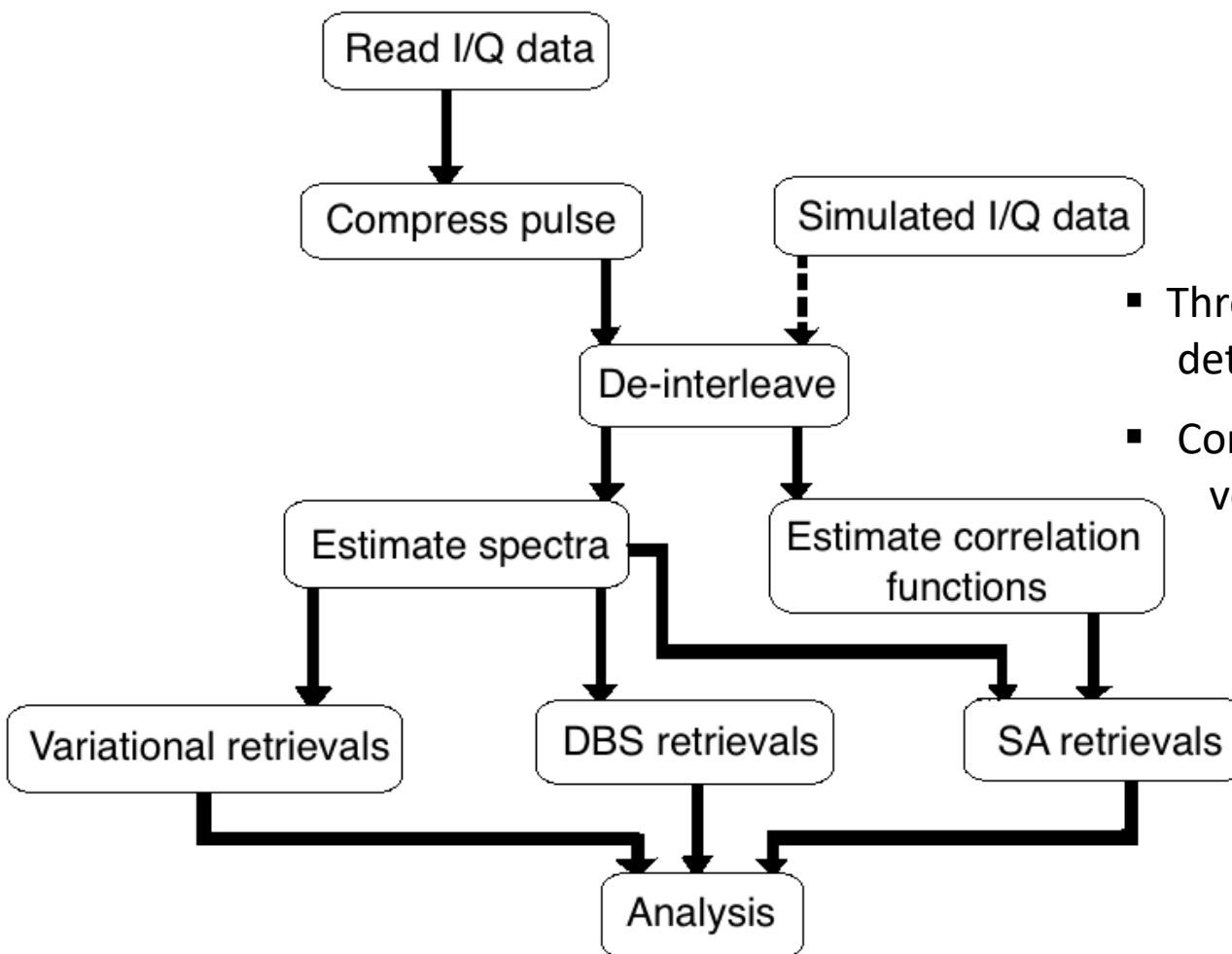
- “Stepped” mechanical scanning employed.
- No slewing during dwell.

Beamwidth = 2.7 degrees

Baseline = 8 cm

PRF = 5 kHz

Stereo radar performance analysis methodology

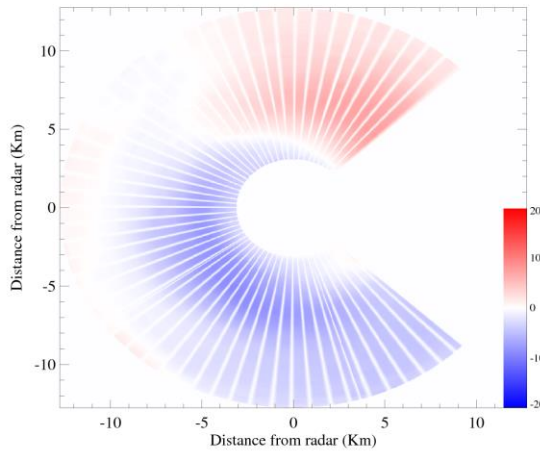


- Thresholds for quantitative analysis determined by simulations.
- Compare stereo radar cross-beam velocity with ground truth.

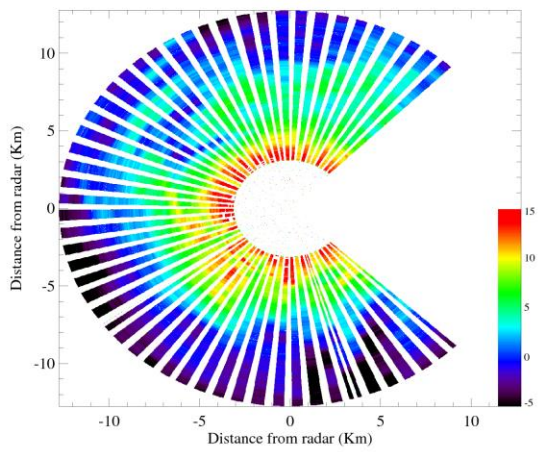
Data quality assessment

- Radial velocity signature similar to Wood and Brown (1986).

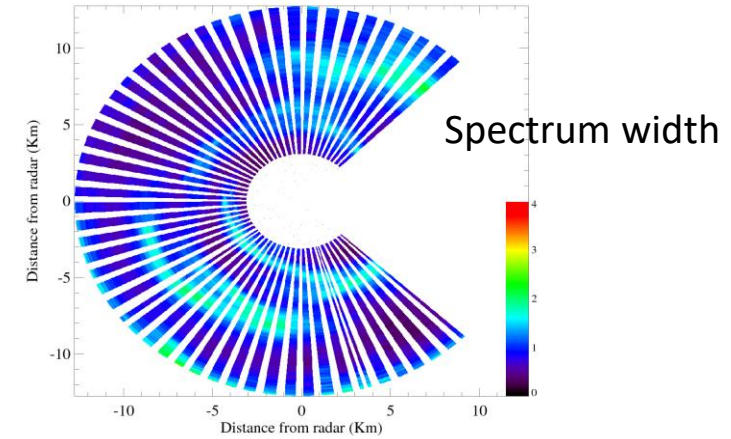
Radial velocity



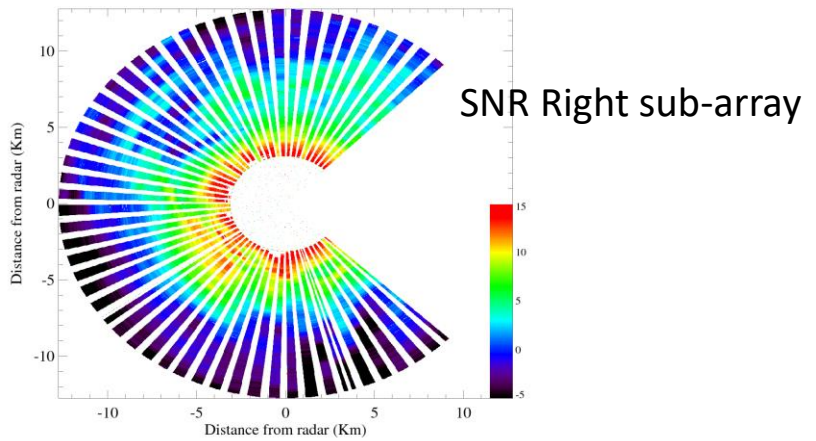
SNR Left sub-array



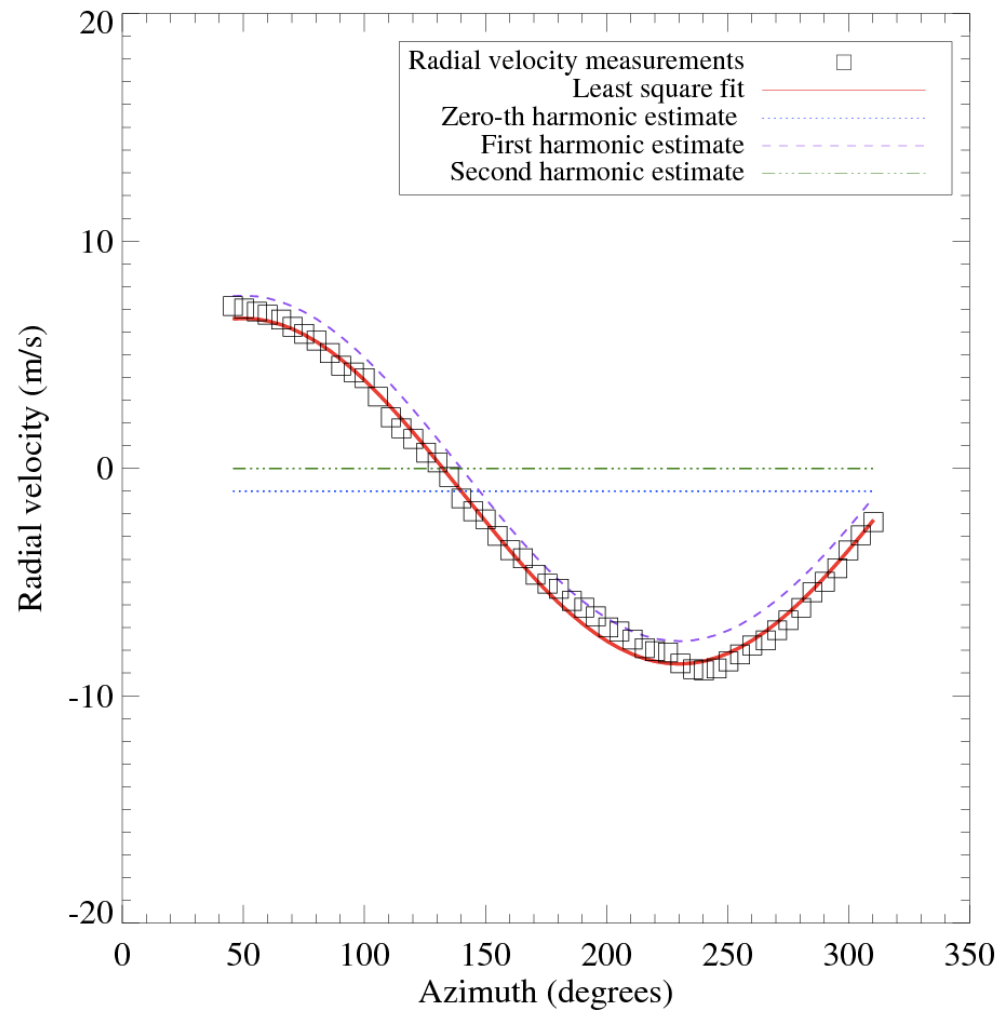
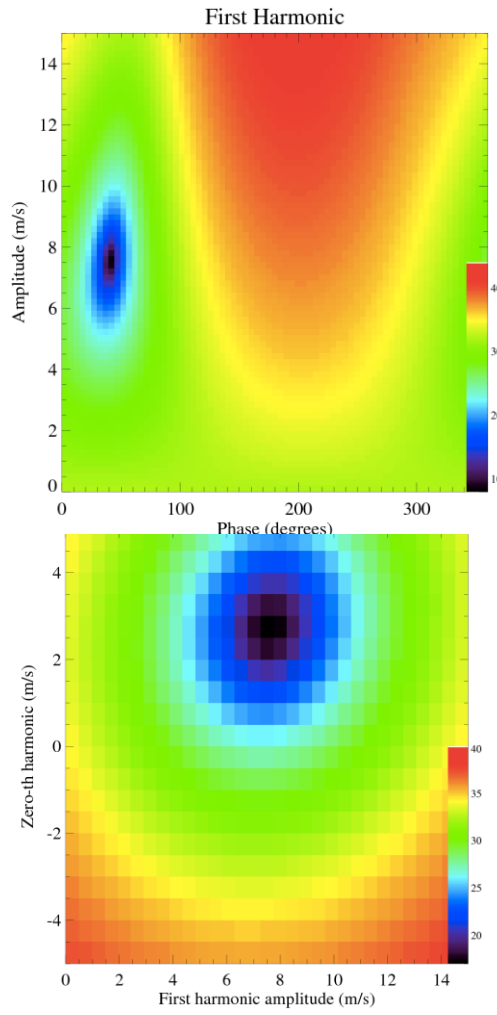
Spectrum width



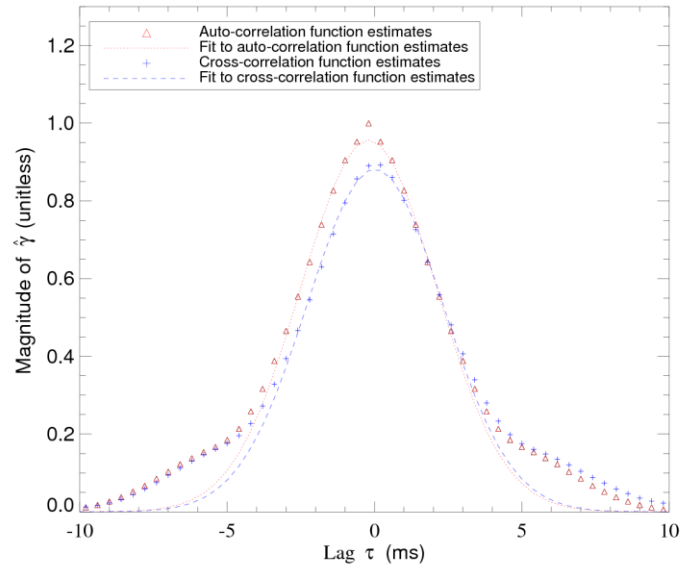
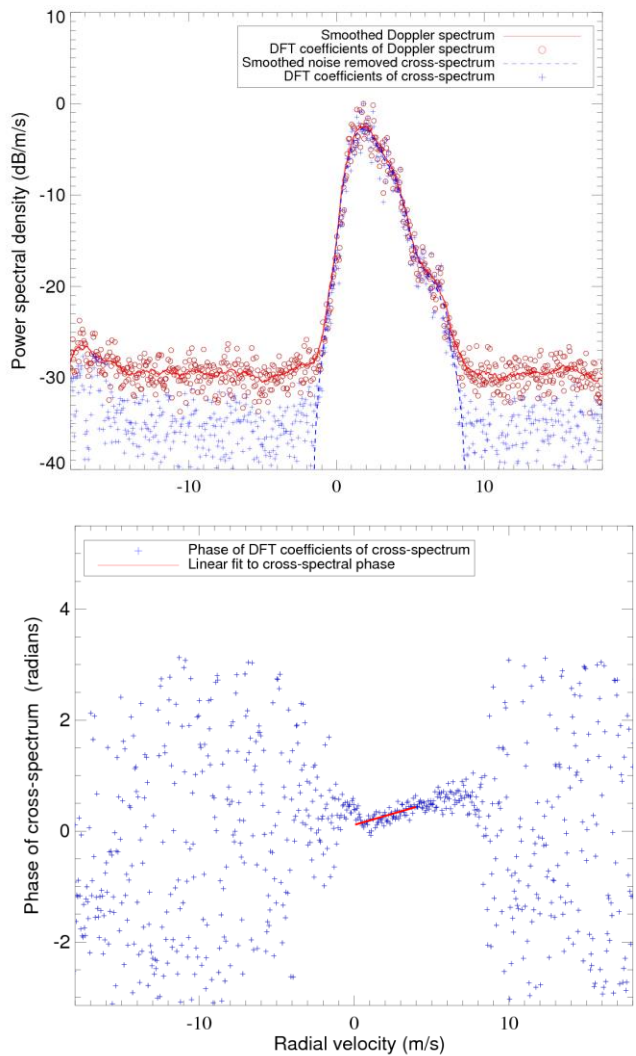
SNR Right sub-array



VAD-like variational retrievals



Spectra and correlation function estimation



$$v_{G-SZL} = 1.62 \text{ m/s}$$

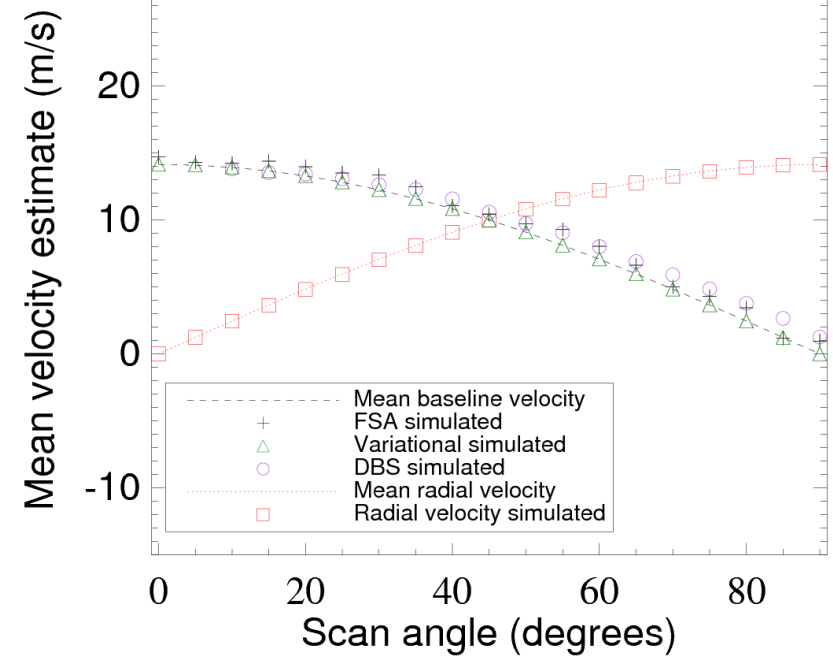
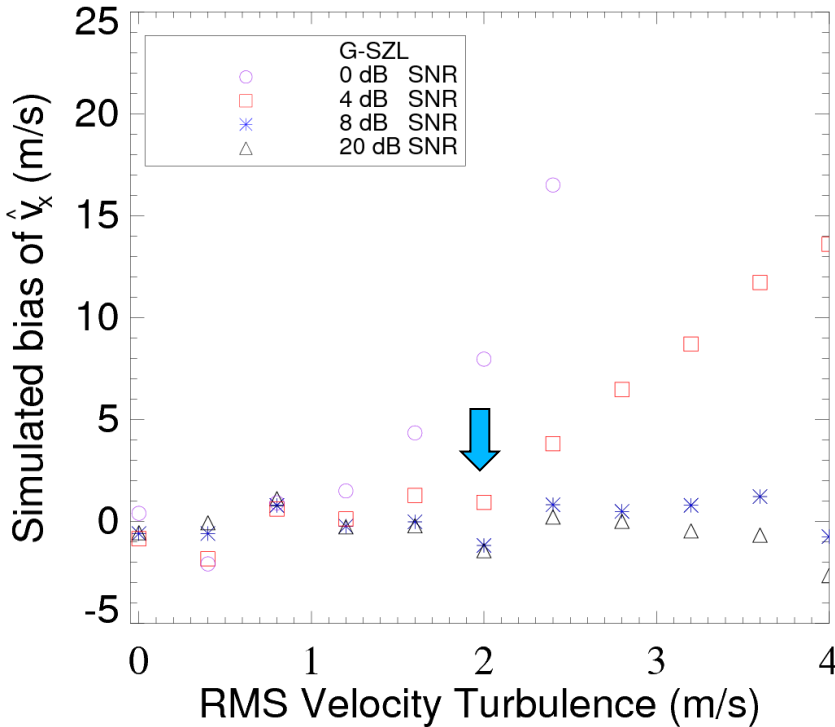
$$v_{FSA} = 7.9 \text{ m/s}$$

$$v_{DBS} = 10 . 35 \text{ m/s}$$

$$v_{VAD-Baseline} = 8.3 \text{ m/s}$$

Quality control based on simulations

- Threshold : Spectrum width ≤ 2 m/s, SNR ≥ 4 dB.
- At threshold point, baseline and radial velocities in quadrature.

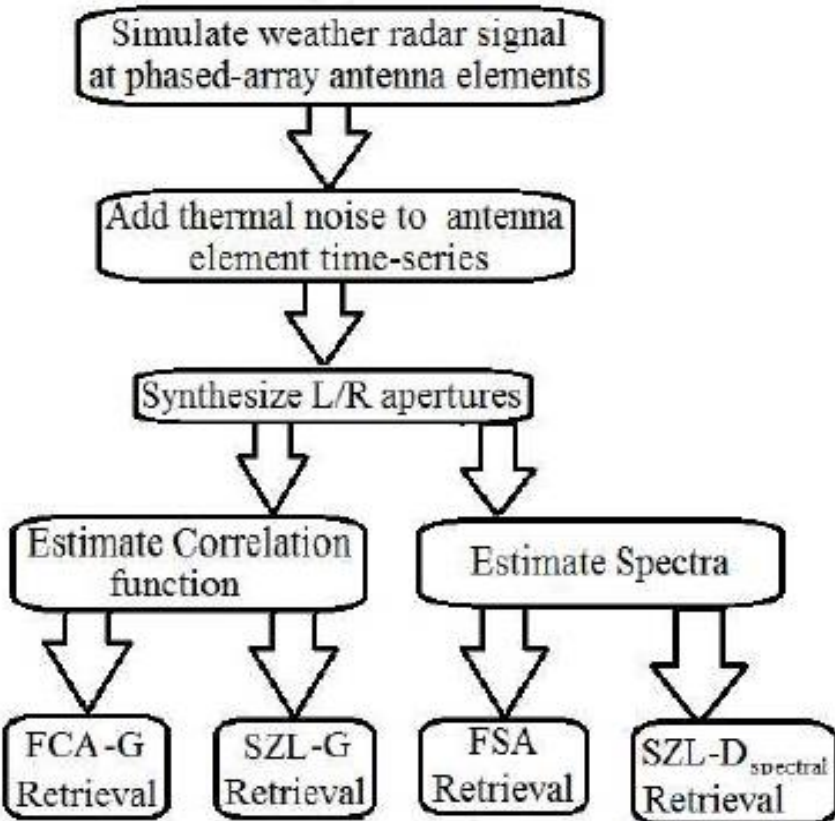


Simulation methodology

1. Generate voltage time-series at phased-array antenna elements.
2. Combine voltages to mimic left and right apertures.
3. Estimate spectra and apply phase compensation.

$$e_2(t + t_0) \iff e^{2\pi f t_0}$$

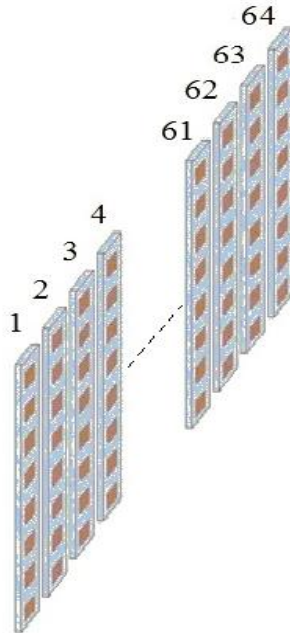
4. Spaced-antenna baseline wind retrieval.



- Goal - Minimize propagated error from thermal noise and velocity turbulence.

Monte-Carlo simulation methodology

$$V_J(t) = \sum_{n=1}^{n_s} A_{Jn} R_{Jn} \exp\{-jk[r + r_{nJ}]\}$$

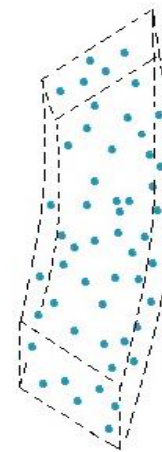


Phased array antenna elements

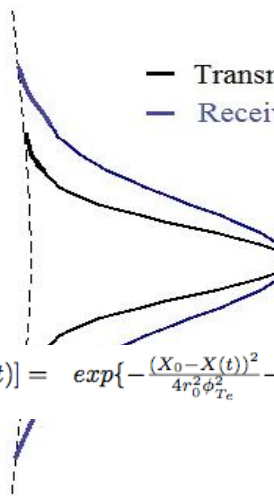


— Range Weighting function

$$R_n[r(t)] = \exp\left\{-\frac{(Z_0 - Z_n(t'))^2}{2\sigma_R^2}\right\}$$



Sampling volume at
chosen range bin



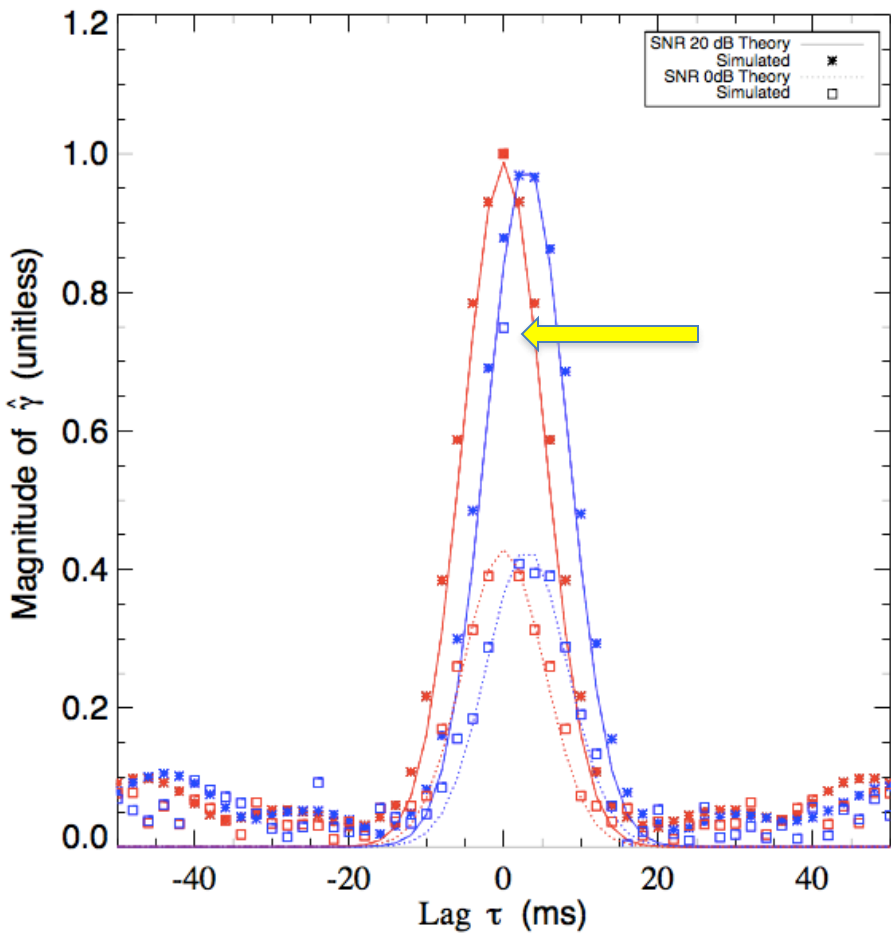
— Transmit antenna pattern
— Receive antenna pattern

$$A_{nJ}[r(t)] = \exp\left\{-\frac{(X_0 - X(t))^2}{4r_0^2 \phi_{Te}^2} - \frac{(X_J - X_n(t'))^2}{4r_0^2 \phi_{elem}^2}\right\} \exp\left\{-\frac{(Y_0 - Y_r^1(t))^2}{2r_0^2 \theta_e^2}\right\}$$

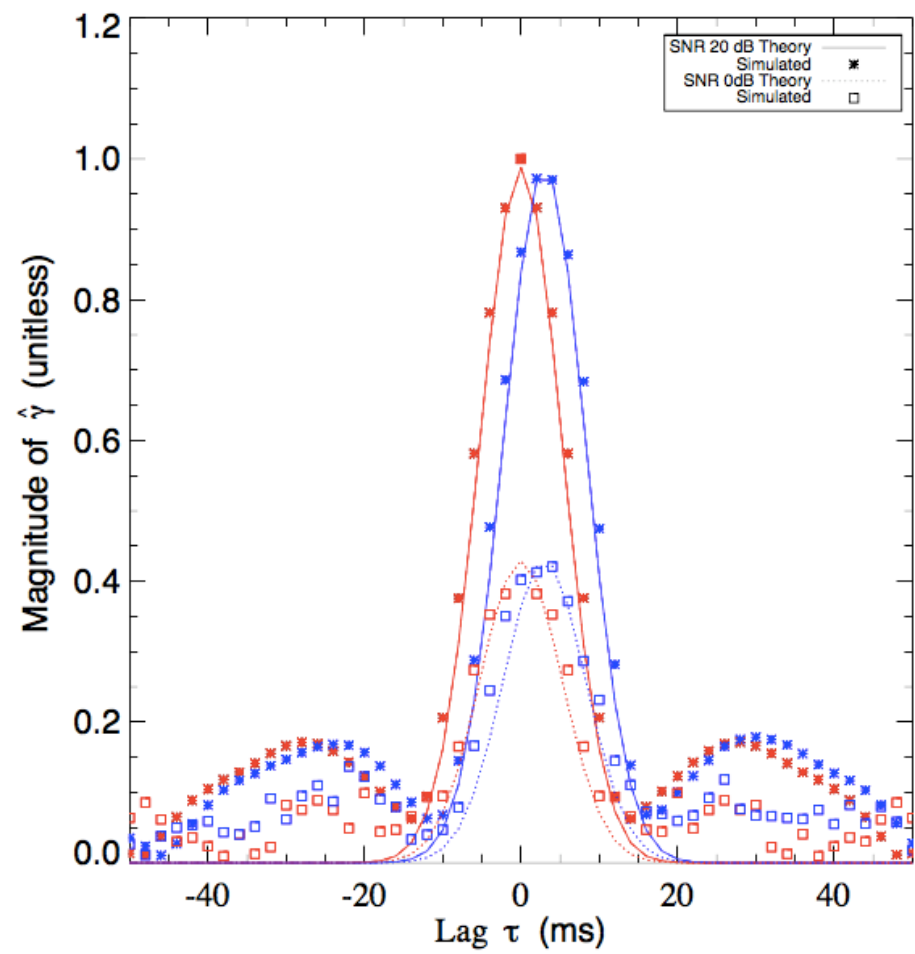
- Volume scattering evaluated by random sampling.
- Velocity to update scatterer position has mean and turbulent components.
- Turbulent components filtered to ensure temporal continuity.

Validation of correlation function estimates

Without interleaving processing



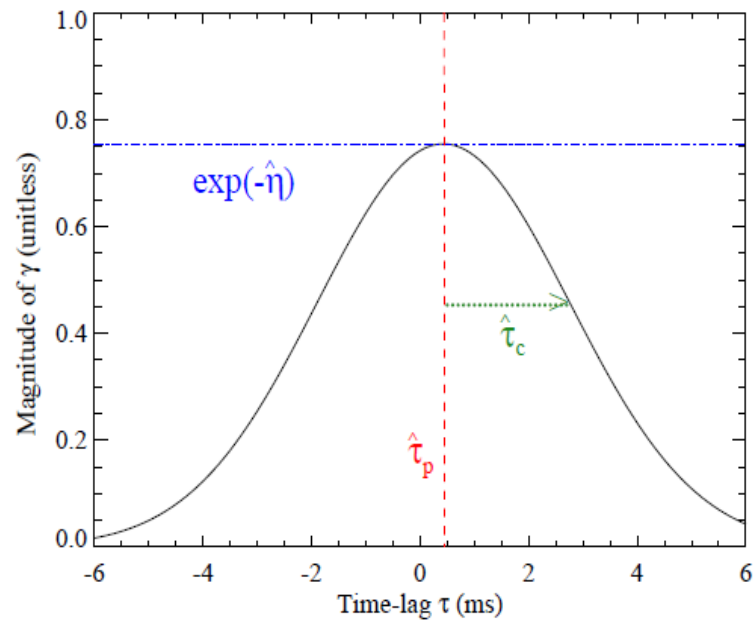
With interleaving processing



- Overlapping array elements in the left and right apertures, causes thermal noise in the left and right apertures to be partially correlated at zero-lag.

Algorithms for stereo radar cross-beam velocity retrieval

G-FCA algorithm



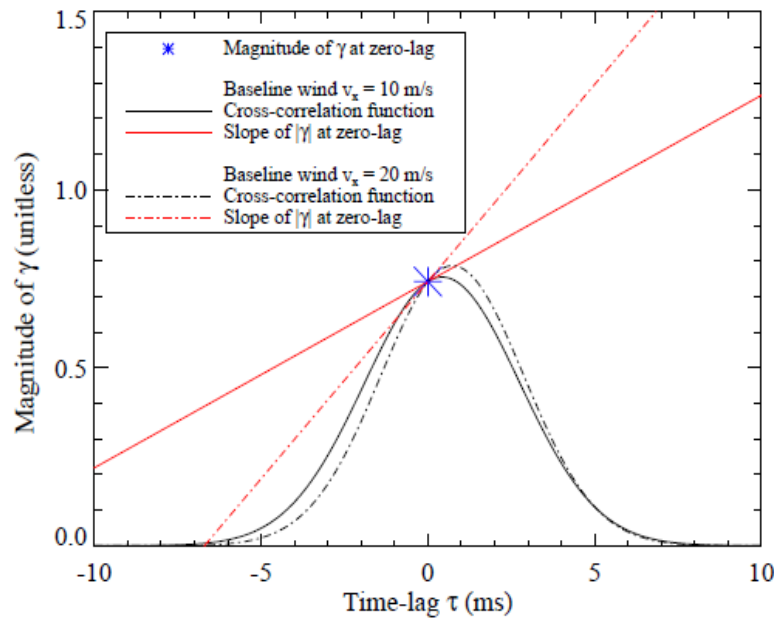
Full Correlation Analysis (G-FCA)

$$\hat{v}_x \text{ G-FCA} = \Delta x \frac{\hat{\tau}_p}{2\hat{\eta}\hat{\tau}_c^2 + \hat{\tau}_p^2}$$

Slope at zero-lag (G-SZL)

$$\hat{v}_{xG-SZL} = \frac{1}{2k^2\sigma_{e\phi}^2} \frac{\hat{\tau}_p}{\hat{\tau}_c^2}$$

Slope at zero-lag algorithms



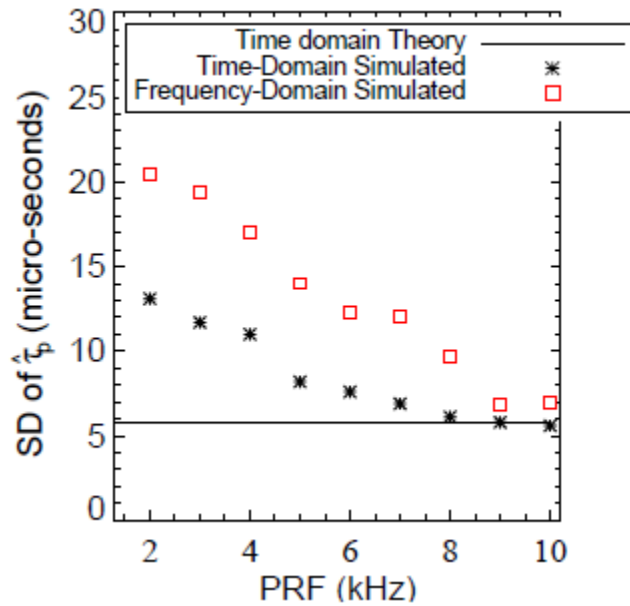
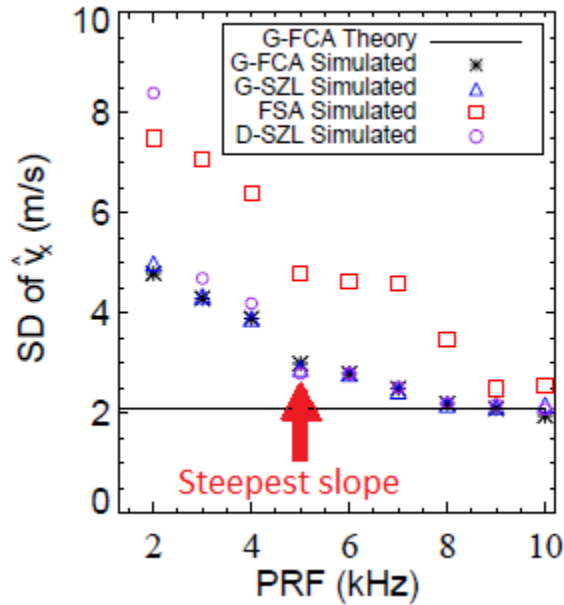
Full Spectral Analysis (G-FSA)

$$\hat{v}_{xG-FSA} = \frac{1}{2k^2\sigma_{e\phi}^2 \frac{\Delta x}{2k}} \widehat{m} \widehat{\sigma}_w^2$$

Slope at zero-lag (D-SZL)

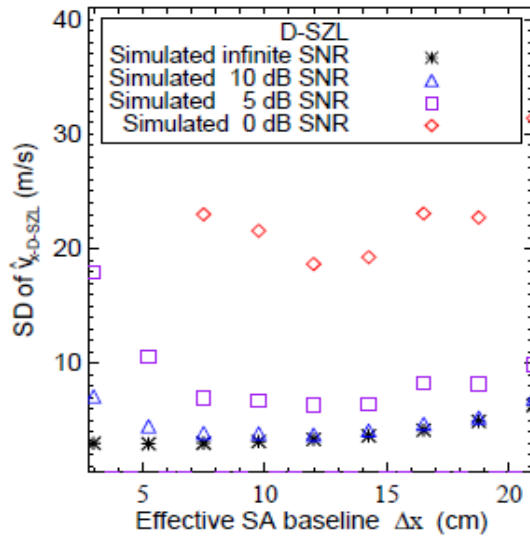
$$\hat{v}_{xD-SZL} = \frac{1}{2k^2\sigma_{e\phi}^2 \Delta x} \frac{d}{d\tau} \left[\frac{\widehat{\gamma}(\Delta x, \tau = 0)}{\widehat{\gamma}(\Delta x, 0)} \right]$$

Choice of Pulse Repetition Frequency

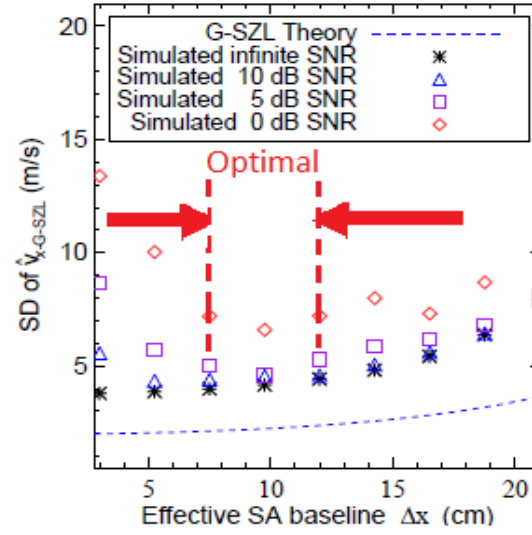
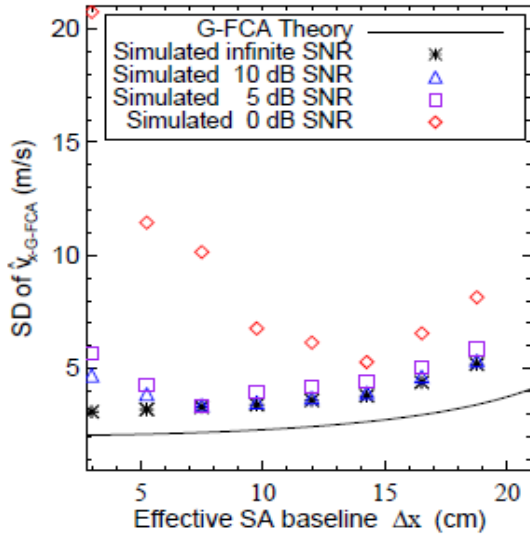


- PRF=5 kHz point of steepest retrieval uncertainty slope
- Higher PRFs require accepting larger range ambiguity

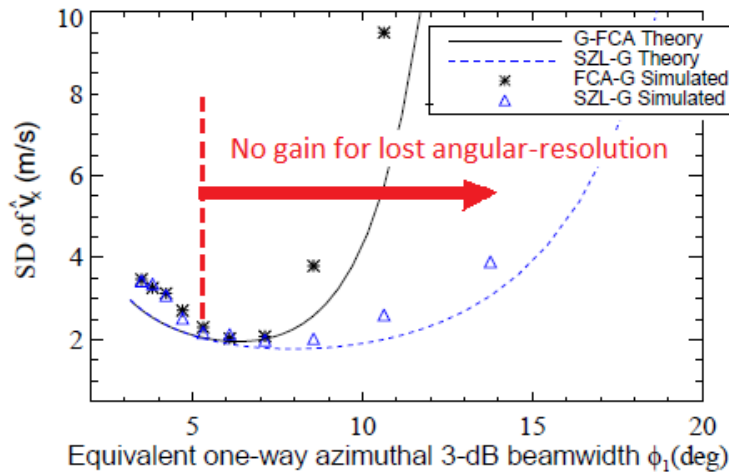
Choice of Baseline



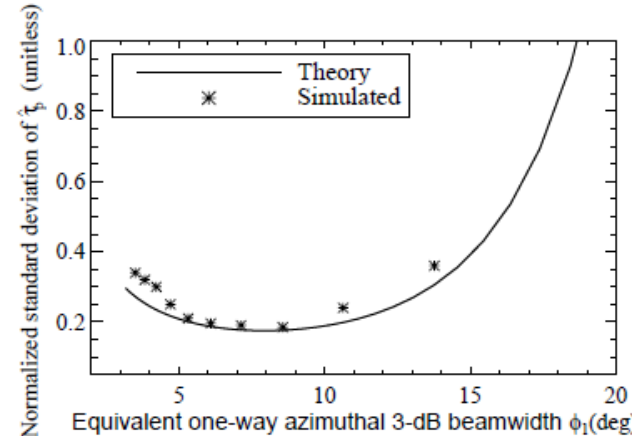
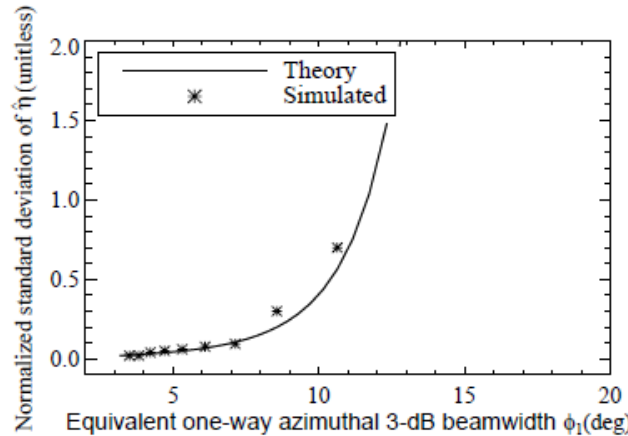
• $7.5 \text{ cm} \leq \Delta x \geq 12 \text{ cm}$



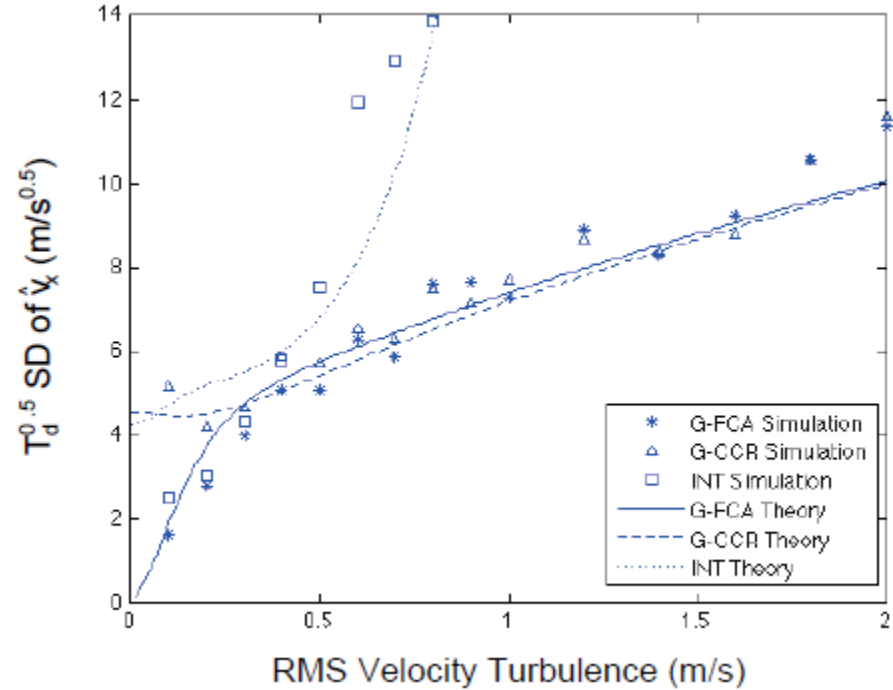
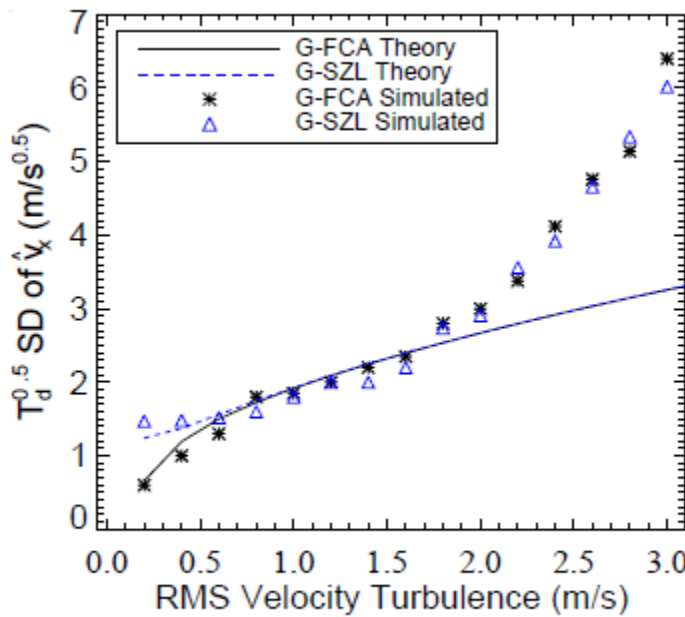
Choice of Beamwidth



- Beamwidth ≤ 5 degrees



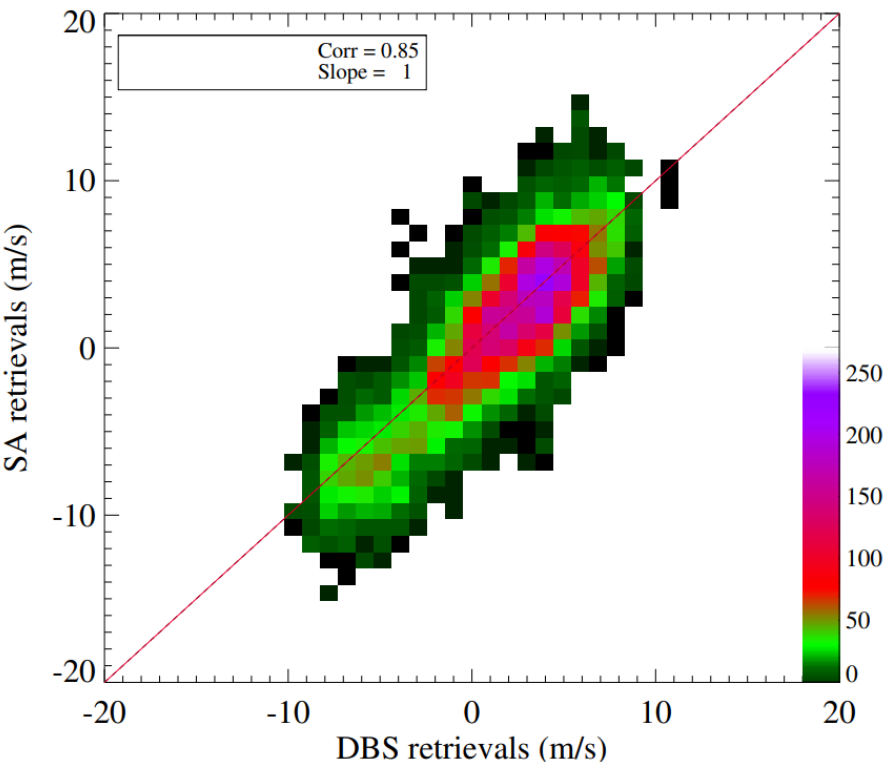
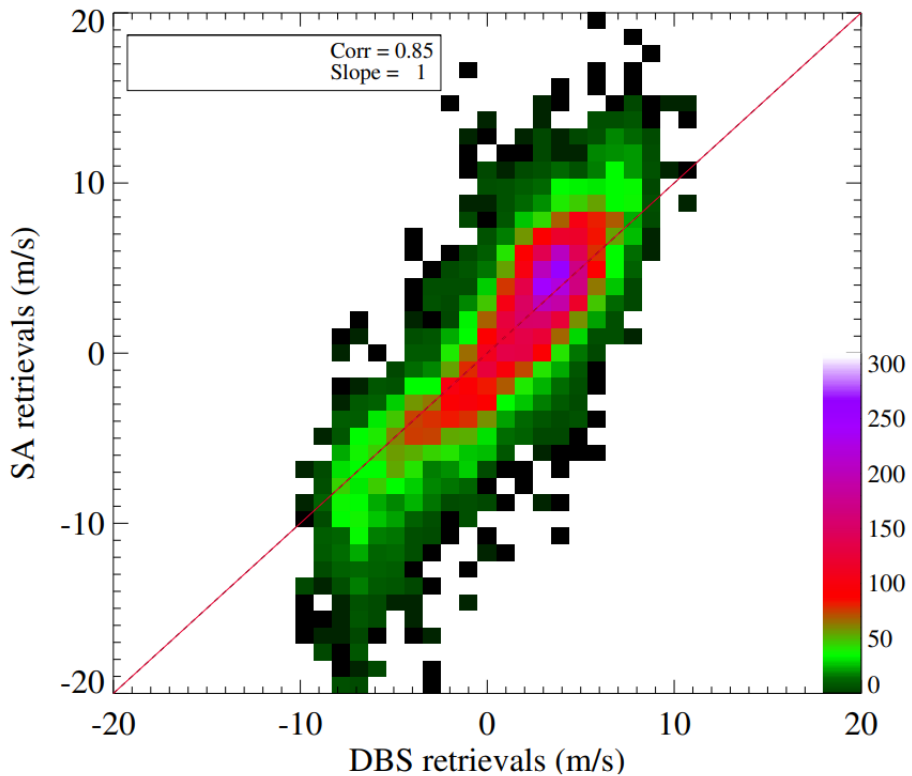
Relative performance evaluation



- 1. PRF = 5 kHz
- 2. $7.5 \text{ cm} \leq \Delta x \geq 12 \text{ cm}$
- 3. Beamwidth ≤ 5 degrees
- Designed X-band system has much less retrieval uncertainty than S-band “monopulse” NWRT spaced-antenna implementation.

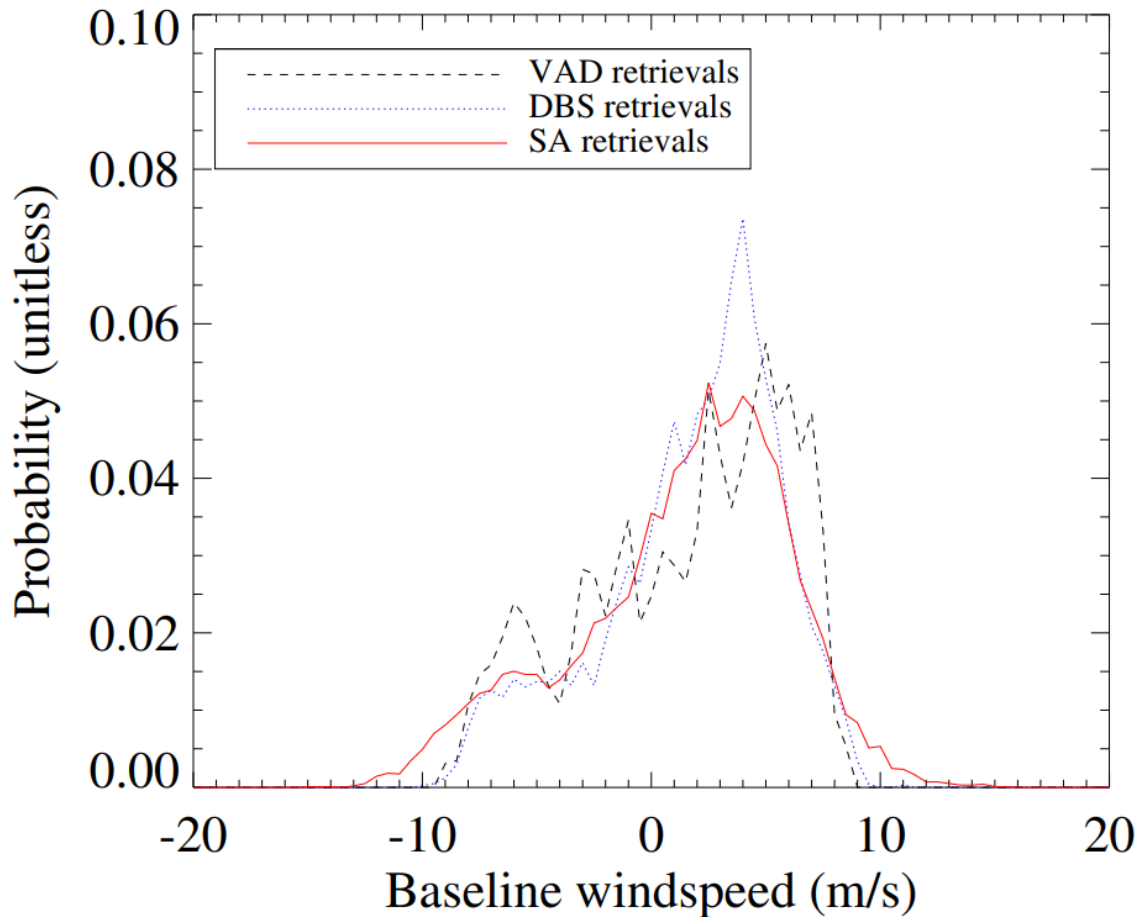
Quantitative comparisons with DBS

- Threshold based on simulations : Spectrum width $\leq 2 \text{ m/s}$, SNR $\geq 4 \text{ dB}$



Aggregated Quantitative comparisons

- Excellent agreement between stereo radar baseline velocity measurement and truth.
- First stereo radar concept validation at X-band.



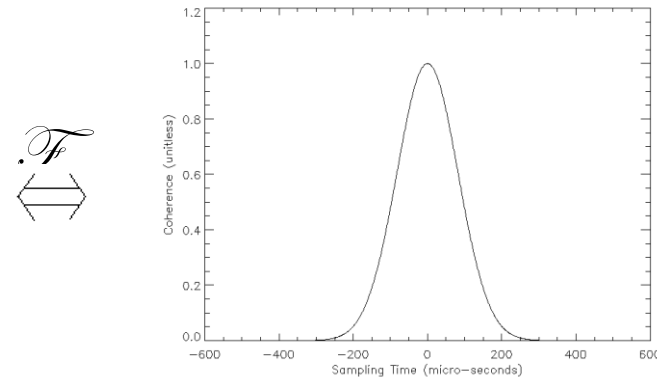
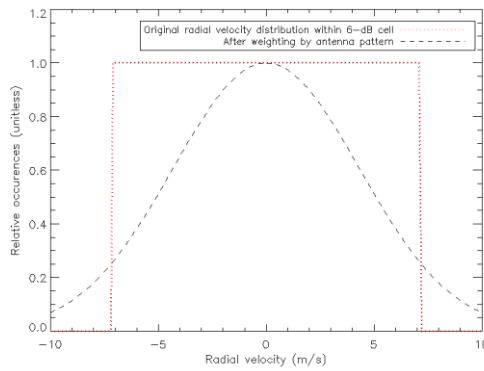
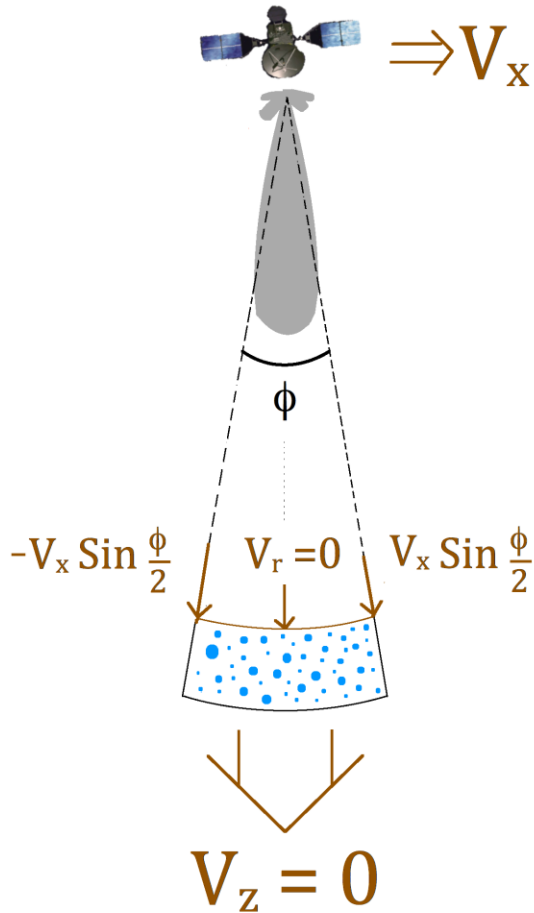
X-band Stereo radar 2D velocity retrieval conclusions

- High resolution stereo radar and Doppler beam swinging retrievals produced similar qualitative features.
- Local wind field features retrieved by stereo radar method modulated on large scale mean wind of VAD method.
- At a relatively high elevation of 10 degrees, G-SZL yielded slightly better results than FSA.
- Successful quantitative results limited to low-to-moderate wind-speeds (i.e. radial velocity < 10 m/s) and cases with smoothly varying wind-profiles.

Stereo radar demonstration at W-band

- Motivation and problem description for spaceborne Doppler cloud radars.
- High performance system formulation based on stereo radar concept.
- Low cost system formulation based on orthogonal waveform concept.
- Summary.

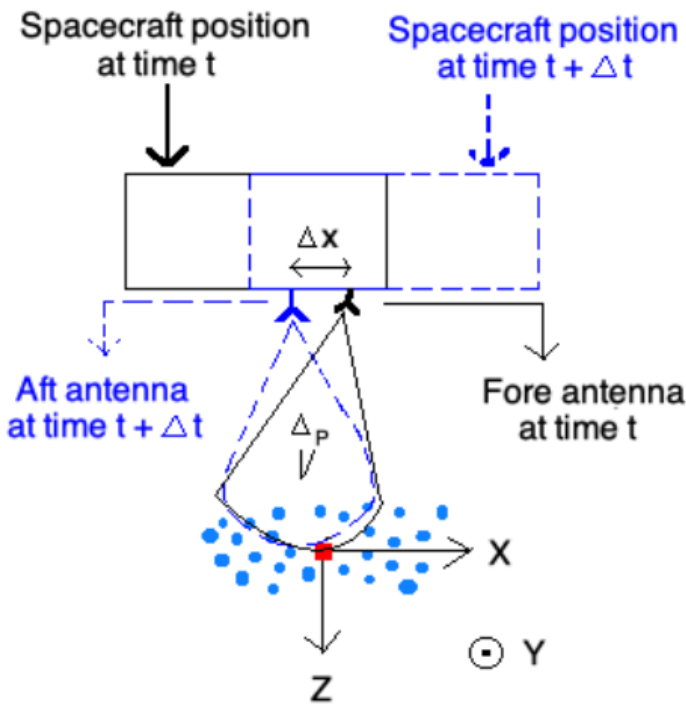
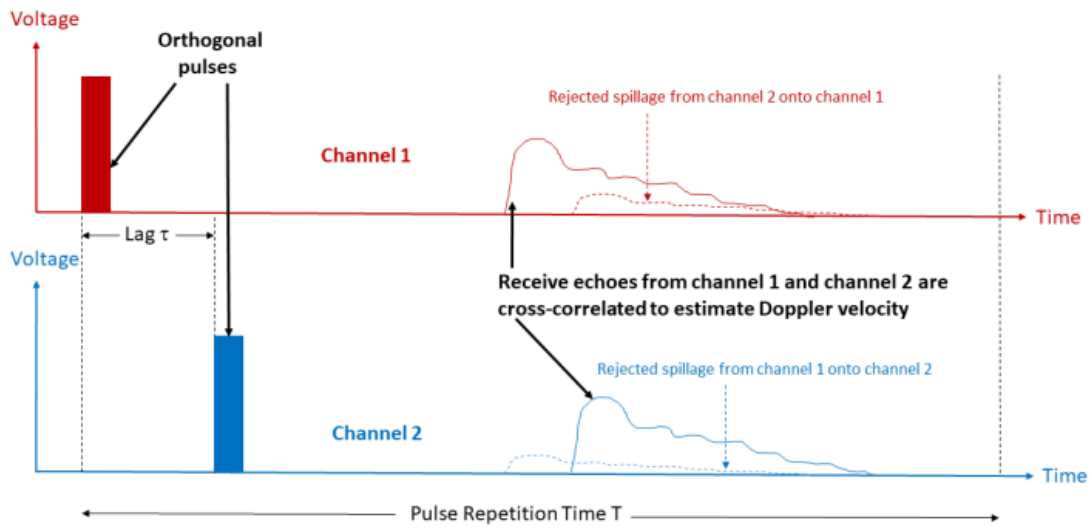
Challenges for space-borne Doppler measurement in clouds



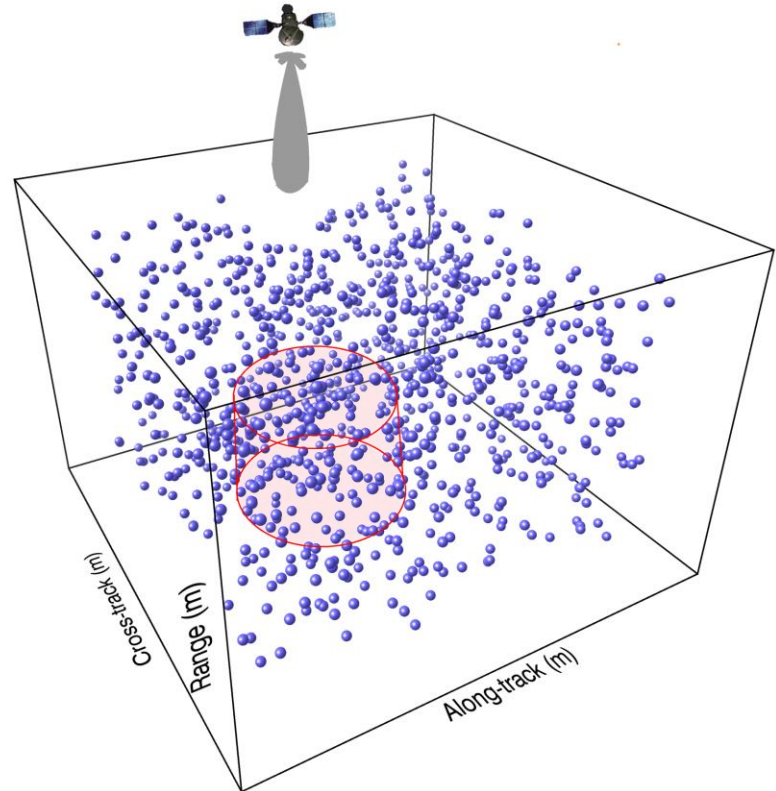
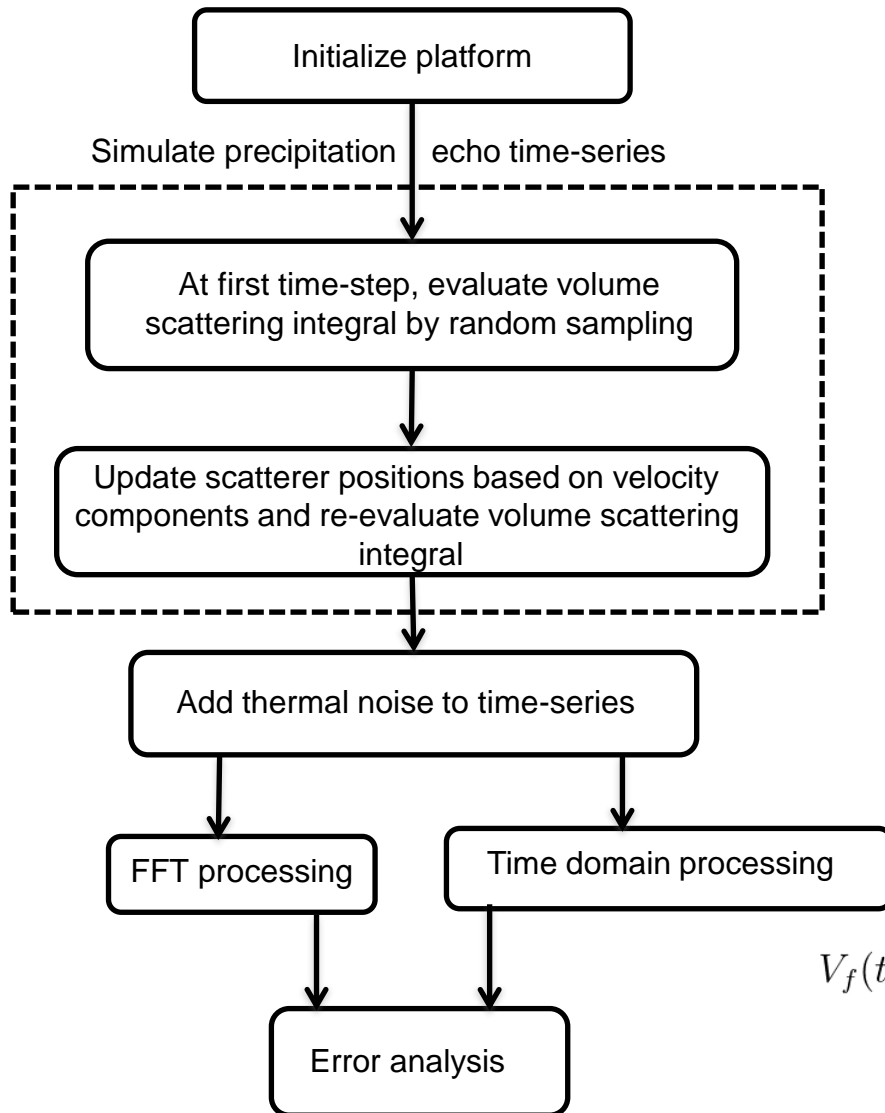
- Brief – Spacecraft velocity overwhelms cloud particle velocity.
- High speed platform motion limits signal coherence.
Doppler measurement error proportional to $\frac{1}{\text{Coherence}^2}$
- Prior attempts
 - Increasing antenna size so much that it was too large to be practical.
 - Averaging to a point where signal spatial non-stationarity contaminated measurements.

Stereo radar for first ever space-borne Doppler measurement at W-band

- Stereo system design that compensates for space-craft motion by steering beam backwards (Right)
- Orthogonal waveform design that allows Doppler measurement on short time-scales corresponding to low spacecraft displacement (Below).

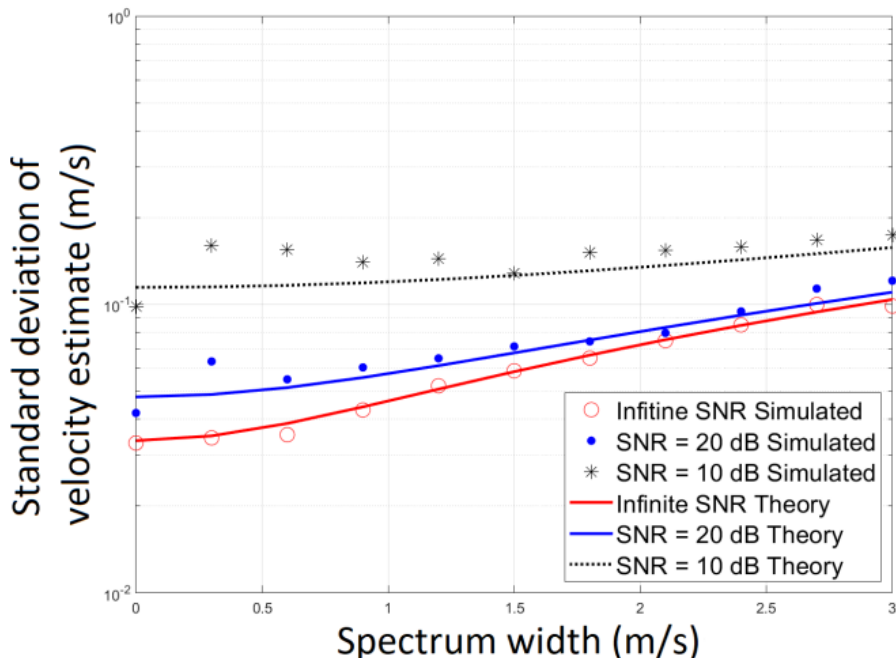
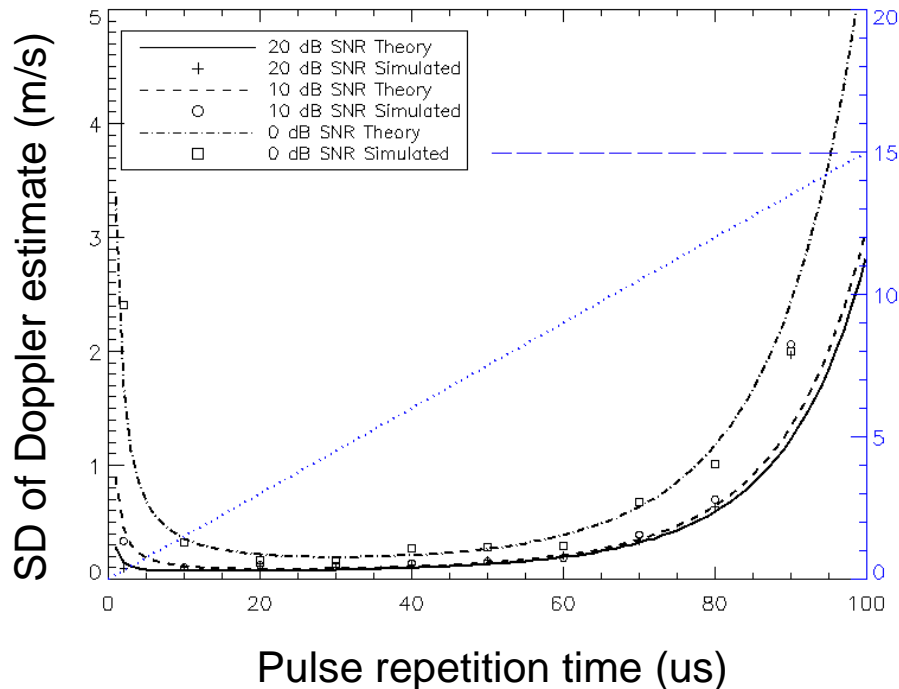


Monte-Carlo Simulation Methodology



$$V_f(t) = C \int_{V''} \sigma_{RCS}(r'') A(r'') W(r'') \exp\{-2j\vec{k}_f \cdot \vec{r''}(t)\} dV''$$

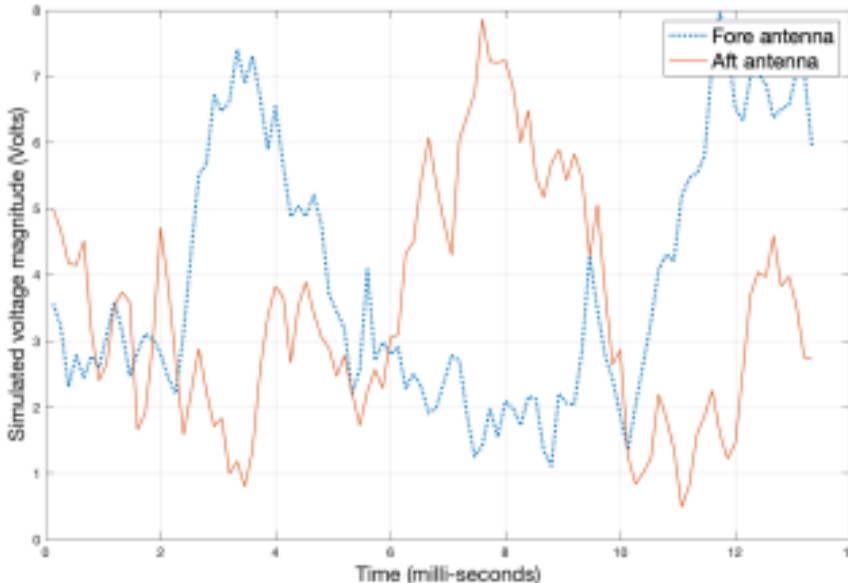
Simulation Validation



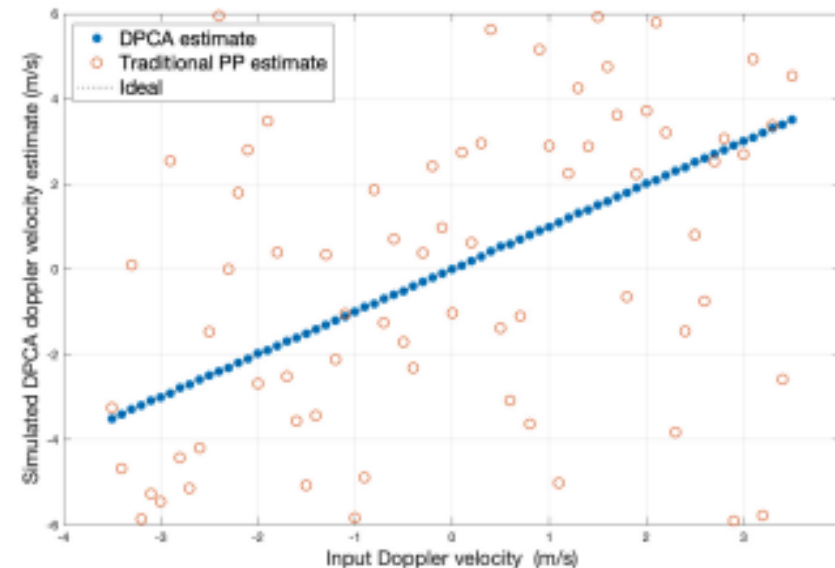
- Simulation code validated by virtue of agreeing with theoretical error statistics for traditional pulse-pair estimator.
- Increasing error on left side, due to thermal noise.
- Increasing error on right side due to loss of coherence.

- Simulations agree with theoretical prediction across the entire error space.

Stereo radar simulations at millimeter wavelength

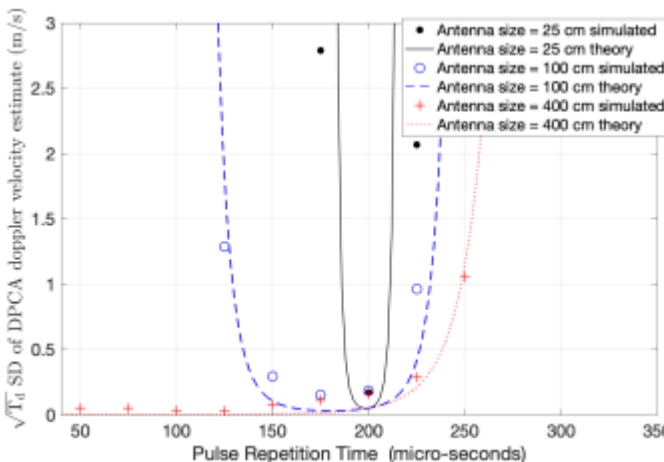
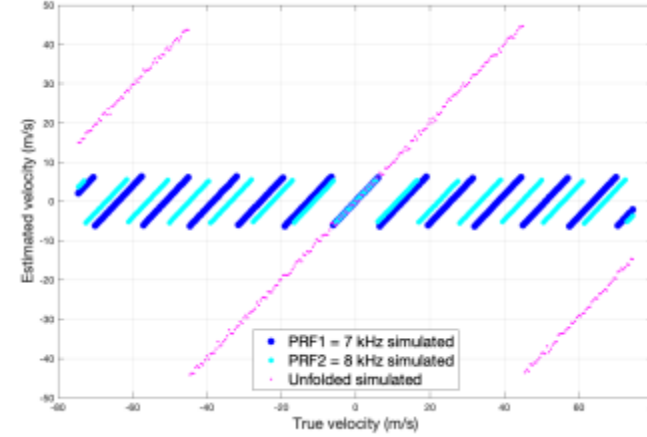
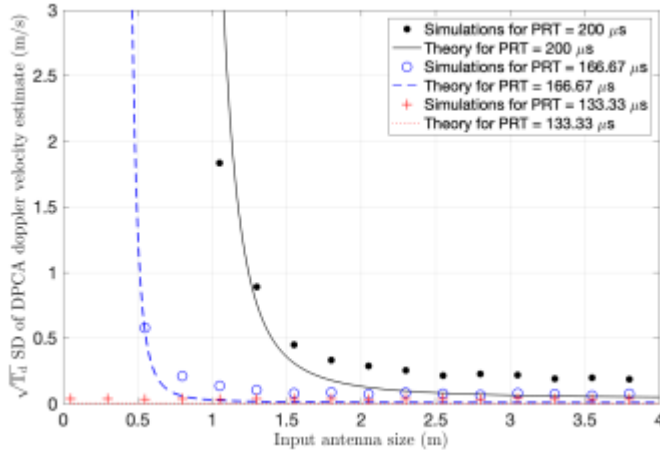


- The aft antenna received time-series is a delayed version of the fore antenna time series.
- Assumes relatively low RMS velocity turbulence.



- Doppler precision of stereo system is significantly better than earlier methods.
- On right, “DPCA” is the stereo concept. PP refers to traditional mono radar.

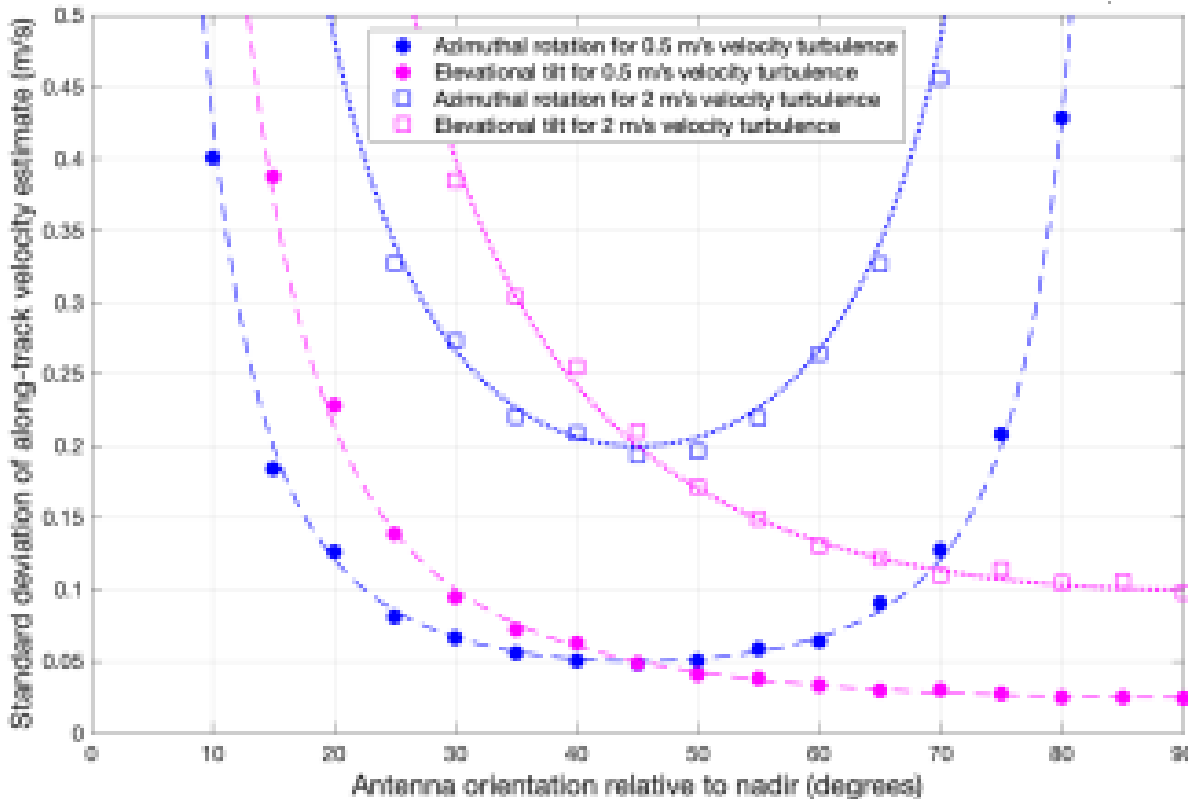
Stereo radar simulations at millimeter wavelength



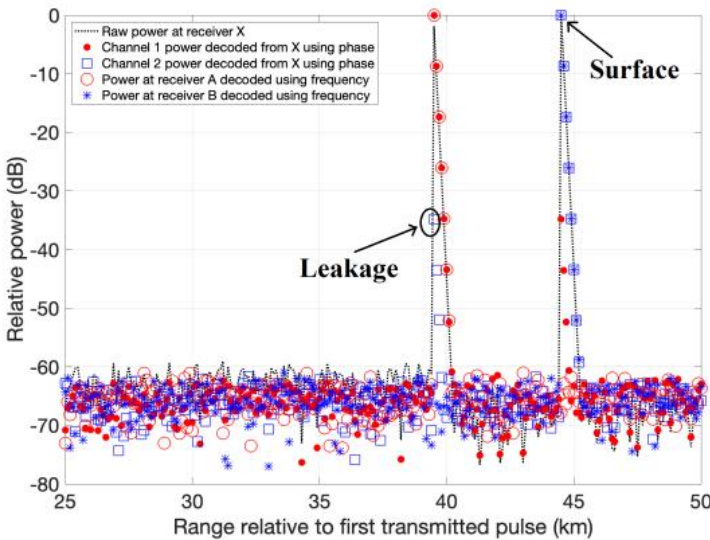
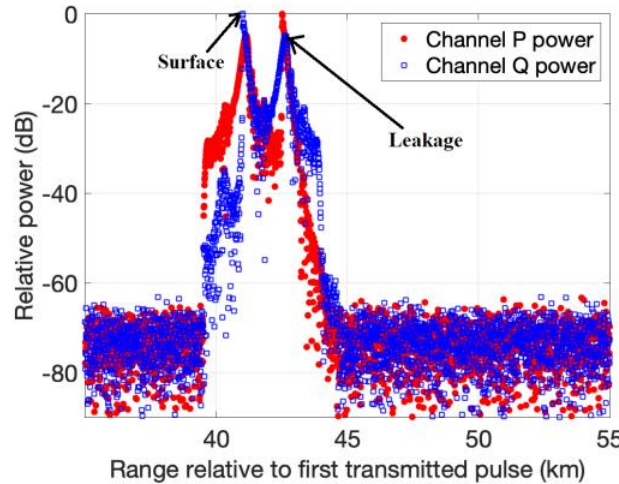
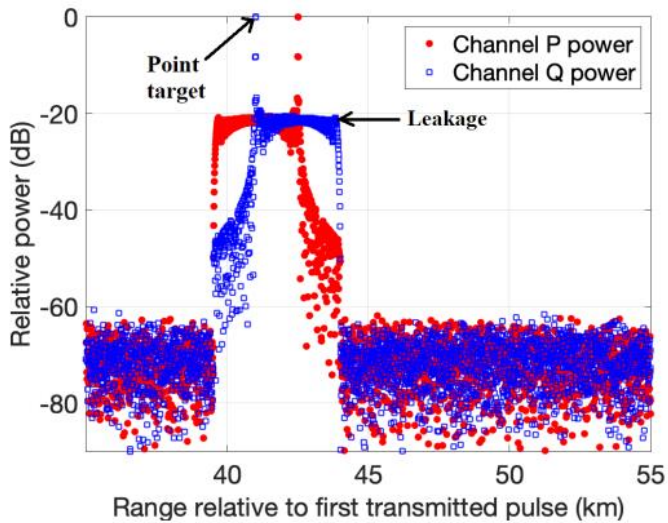
- Long pulse repetition times require relatively large antennas.
- Small antennas possible for rapid pulsing schemes.
- Doppler estimates across the entire Nyquist interval are robust.

Stereo radar simulations at millimeter wavelength

- Phased-array stereo radar allows for dual-Doppler retrieval of 2-D velocity.

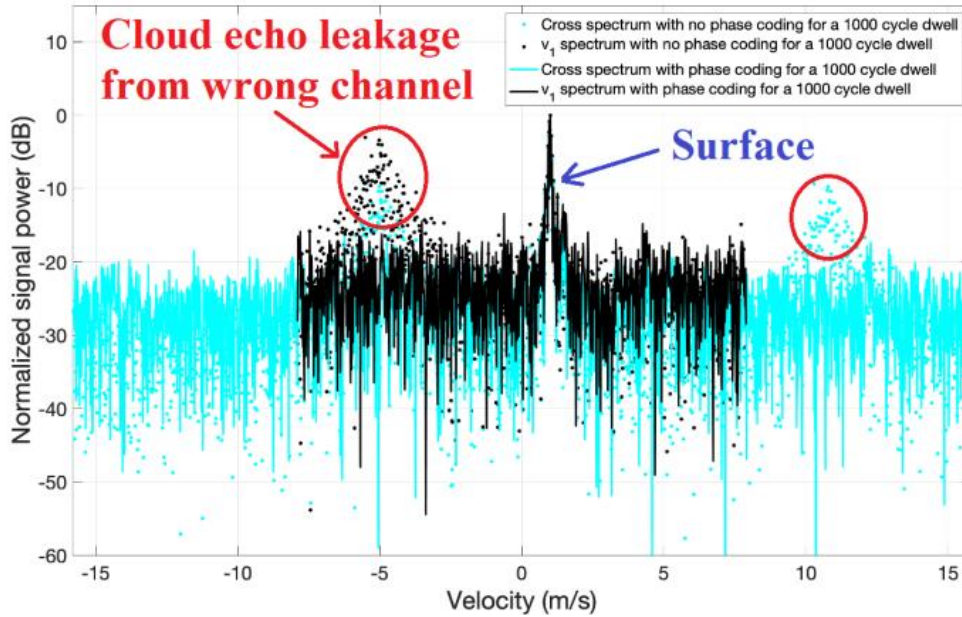


Orthogonal waveform concept simulations

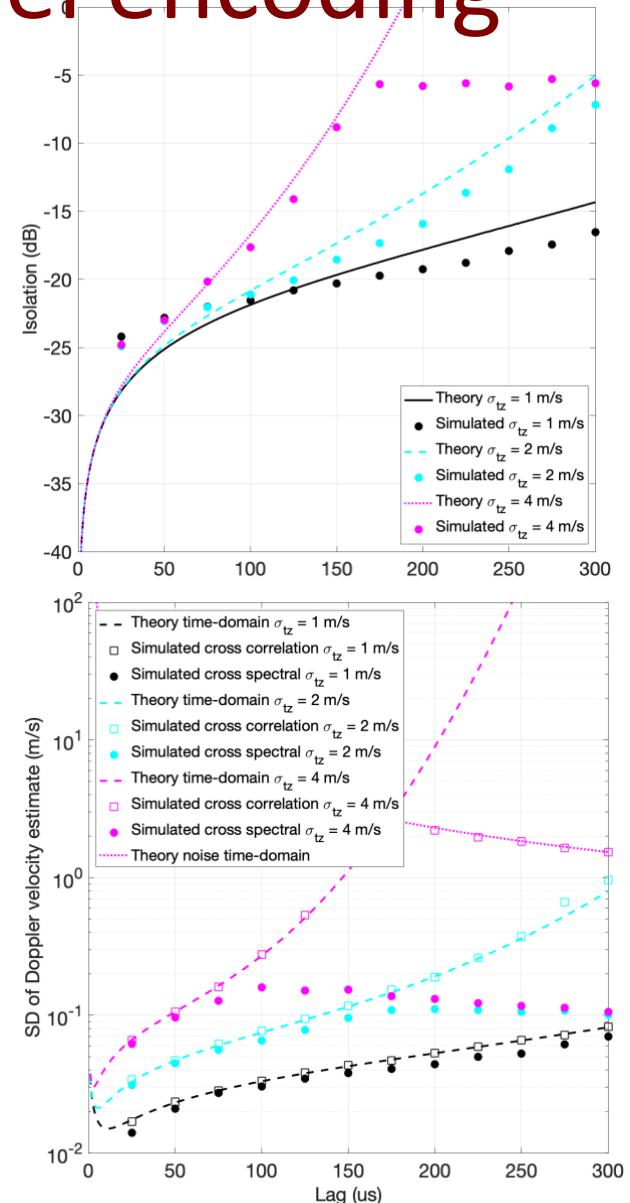


- Traditional orthogonal waveform designs such as up/down chirp pair work only for sparse targets (top left).
- Up/Down chirp pair fails for pulse limited surface echoes.
- OFDM and CDMA waveforms robust to all scenarios (bottom left).

Orthogonal waveform simulations – Channel encoding

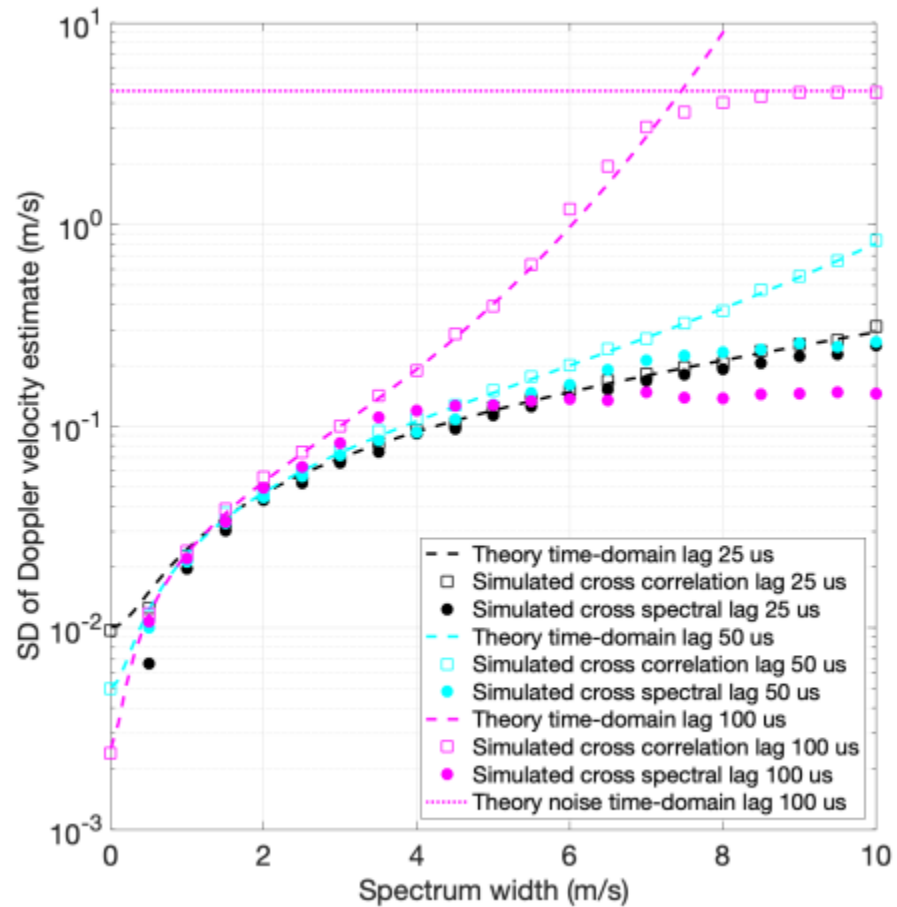
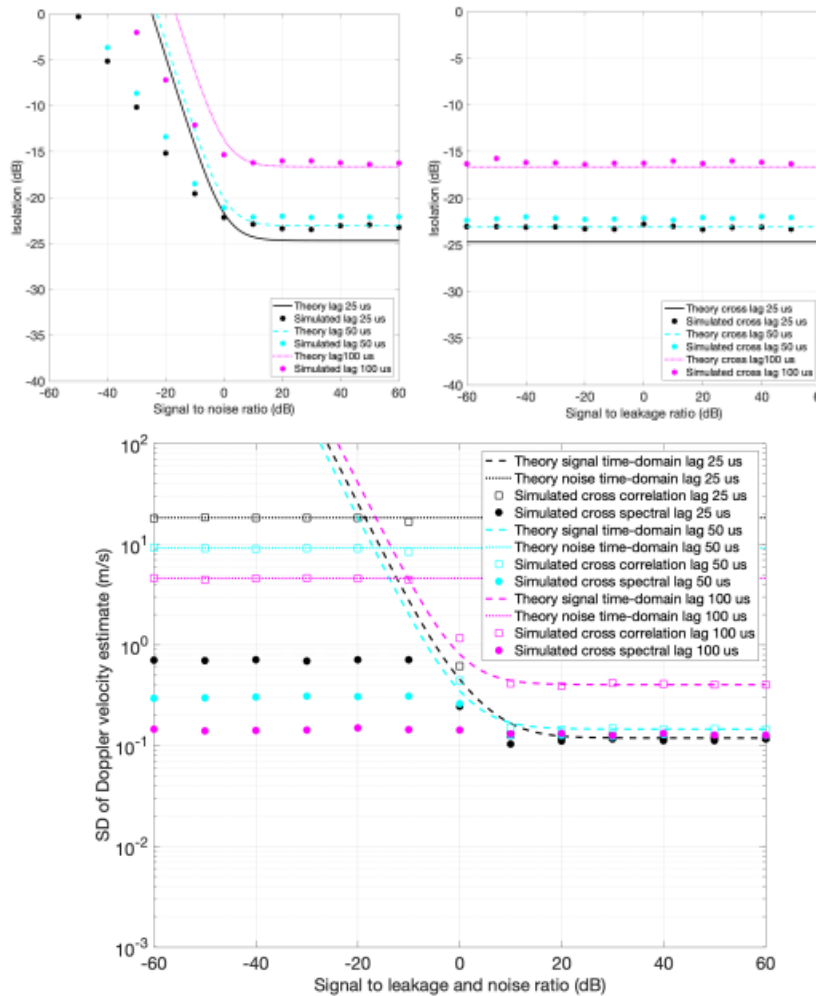


- Starting phase of waveform across N pulses of dwell can be used to smear leakage across power spectrum (top).
- Bound for inter-channel isolation approaches $1/N$.
- Many CDMA waveforms can be ported to radar applications
Performance is robust across design space
(top right and bottom right).



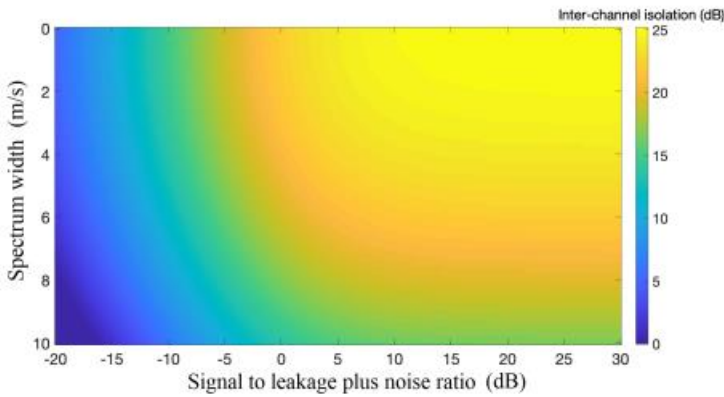
Orthogonal waveform simulations – Channel coding

- Theory and simulations agree when signal coherence is high.

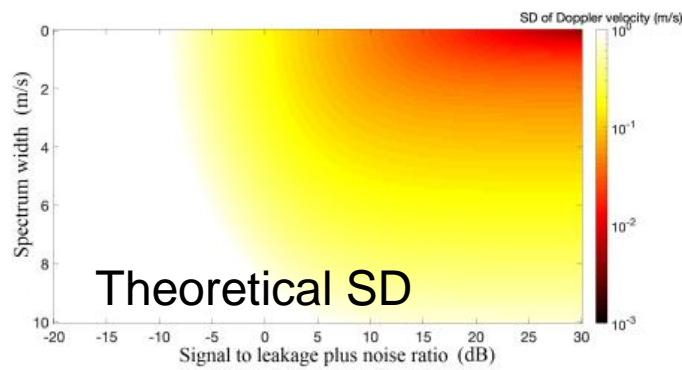
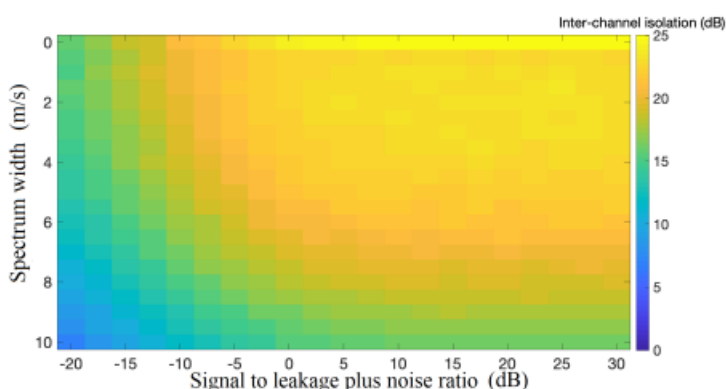


Orthogonal waveform simulations – Channel coding

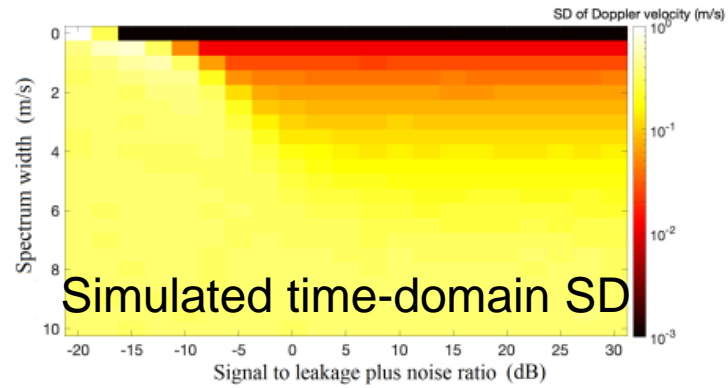
Theoretical Isolation



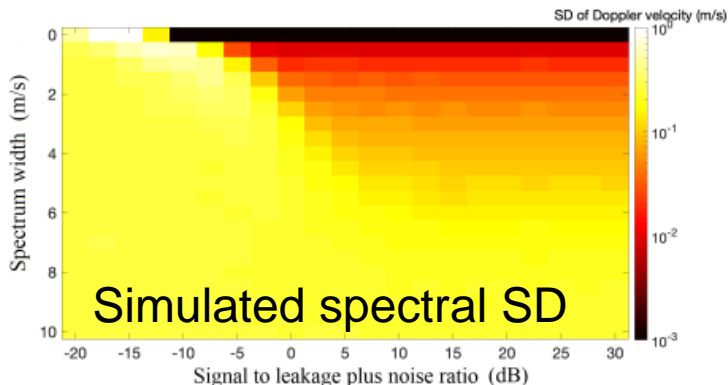
Simulated Isolation



Theoretical SD



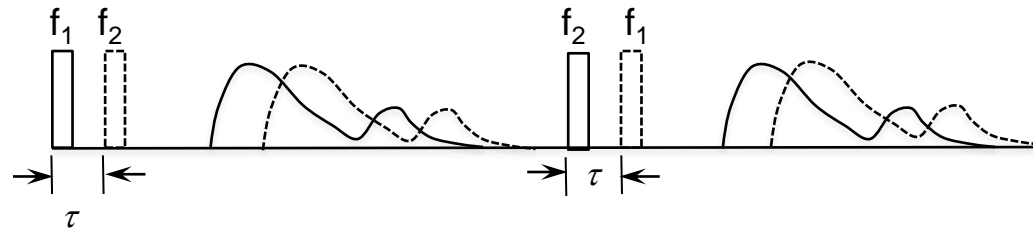
Simulated time-domain SD



Simulated spectral SD

- Theory and simulations both predict robustness across entire error space.

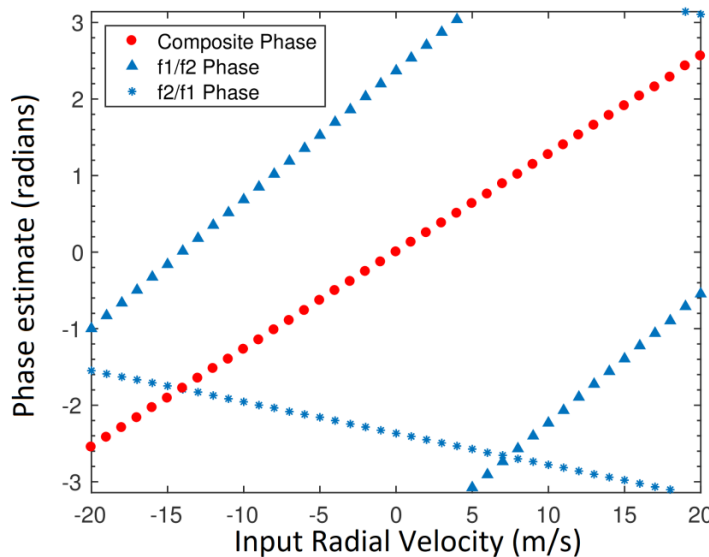
Orthogonal waveforms simulations - OFDM



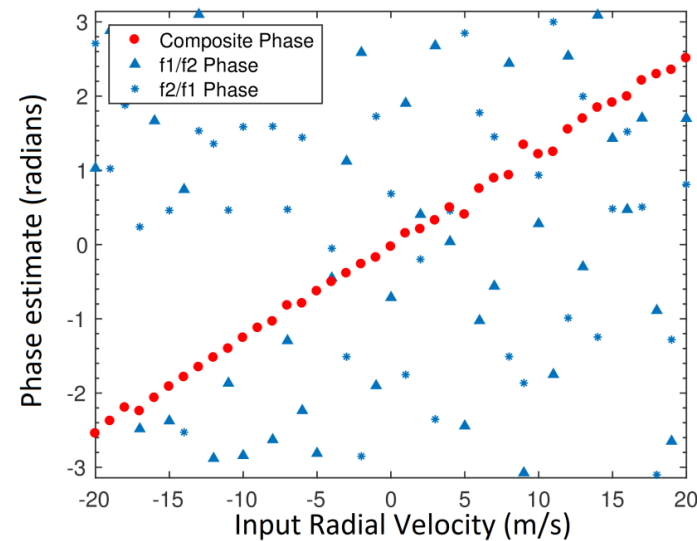
$$\Delta\Phi = 2[(k_2 - k_1)\tau + (k_1 + k_2)\Delta T]v_r$$

$$\rho(\Delta\Phi_{Order1}, \Delta\Phi_{Order2}) \rightarrow -1, \quad \sigma(\Delta\Phi) \rightarrow 0$$

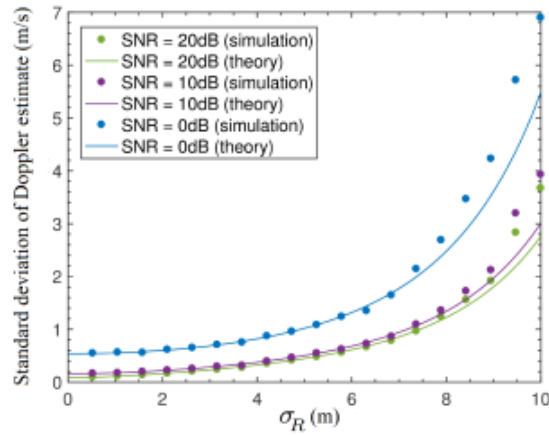
Alternating sequence cancels error due to “beat” phase.



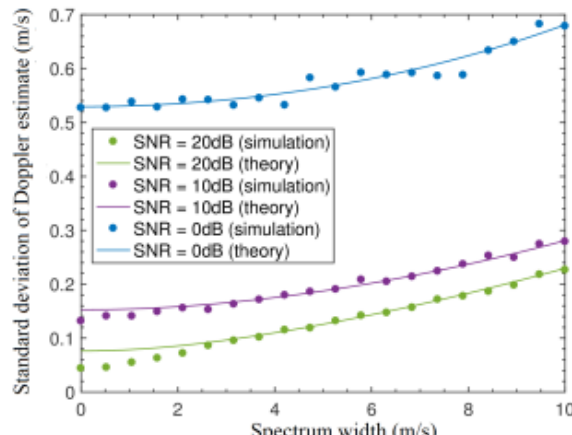
Loss of coherence compensated by high anti-correlation of phase between frequency reversed pairs



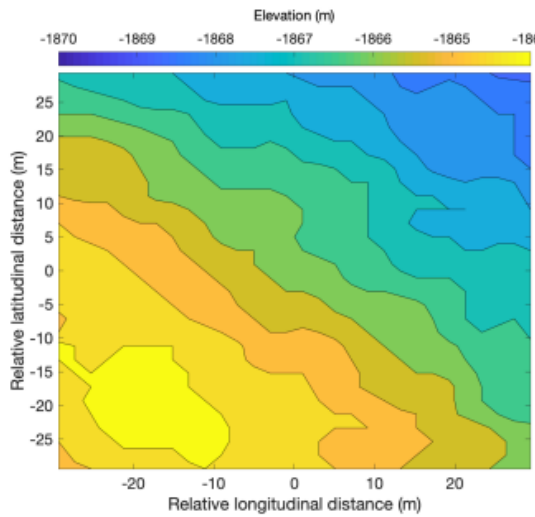
Orthogonal waveform simulations - OFDM



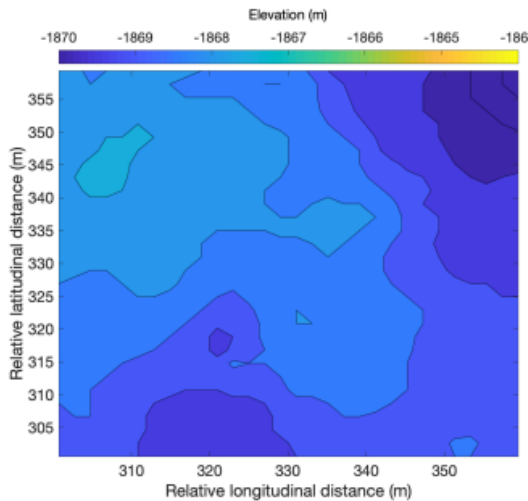
(a) Spectrum Width = 1 m/s



(b) $\sigma_R = 1$ m



Jezero crater
RMS surface roughness
 $\sigma_R = 1.22$ m

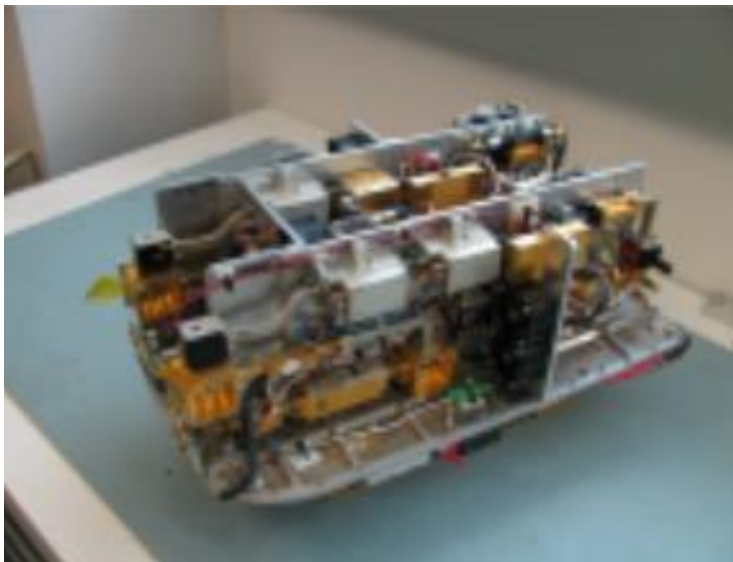
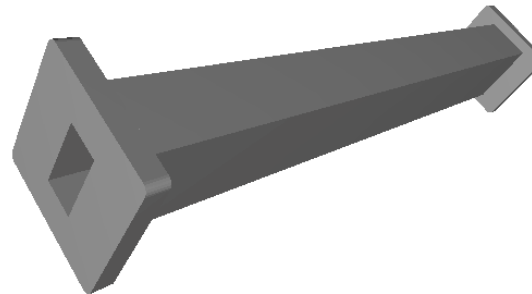


Mars DEM
RMS surface roughness
 $\sigma_R = 0.6$ m

- OFDM waveforms suitable for radar altimeters

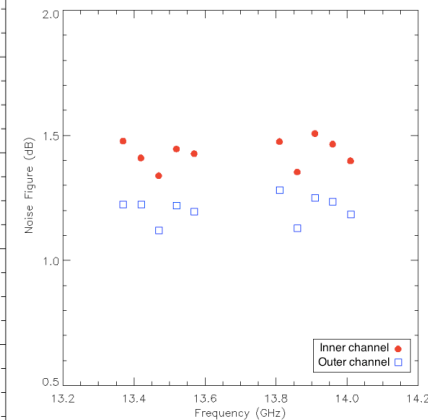
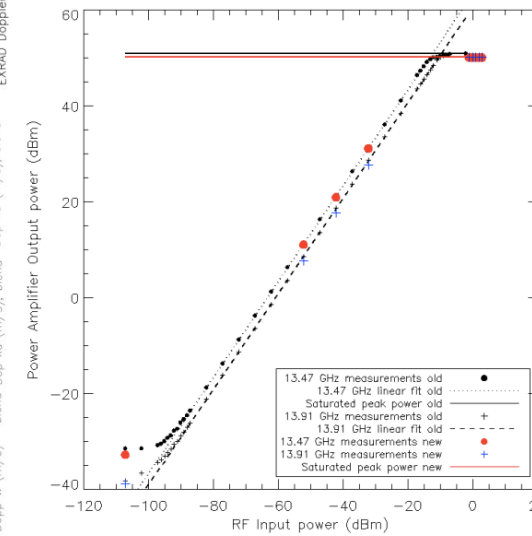
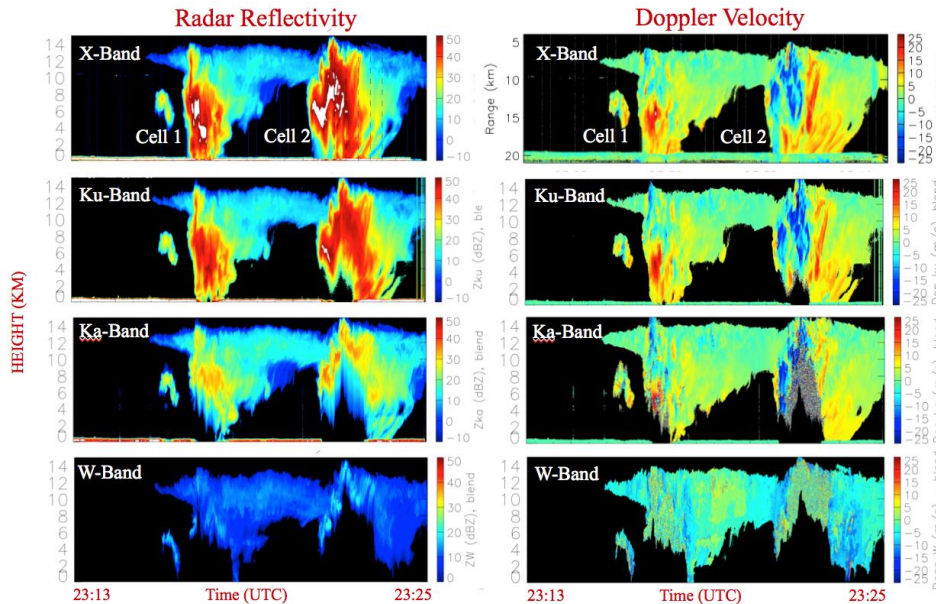
System implementation

- 95 GHz Cloud Radar System with digital receiver flew on ER-2.
- Engineered custom 3-D printed waveguides.

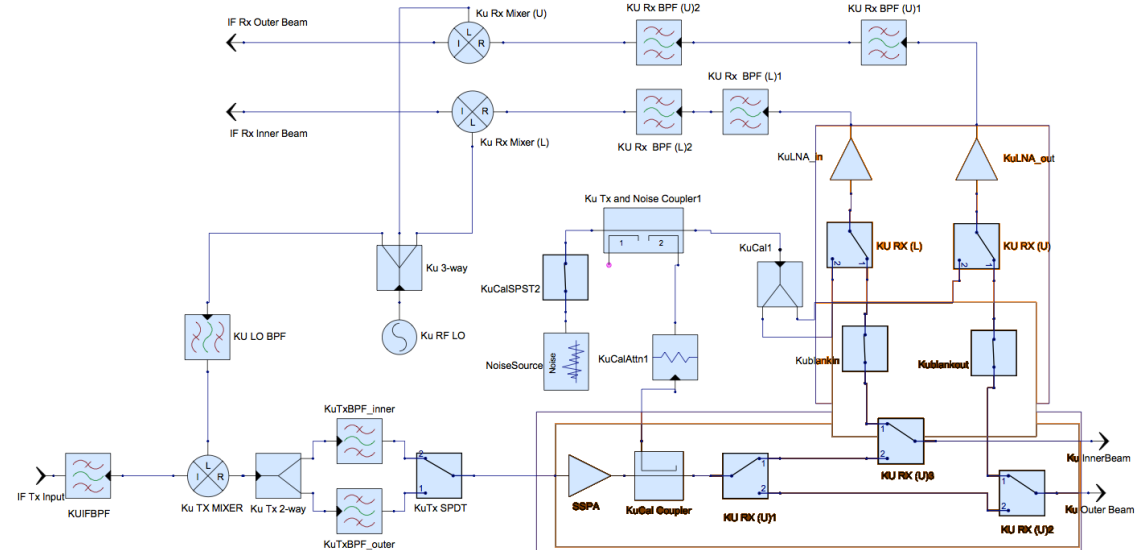


NASA ER-2

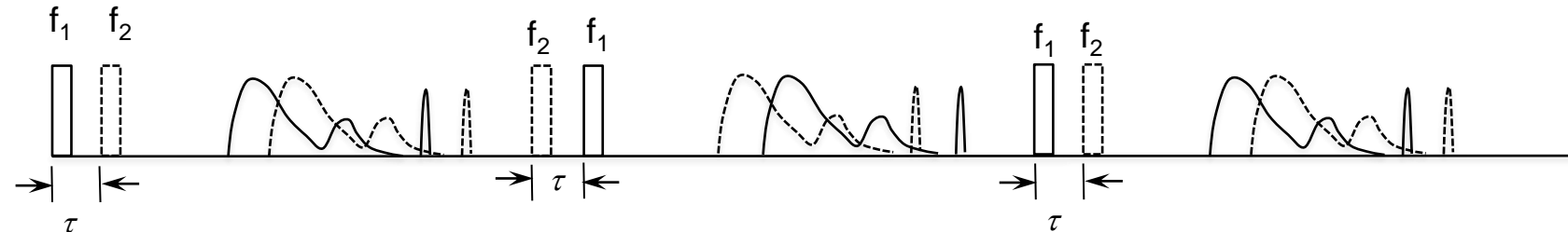
RF transceiver electronics



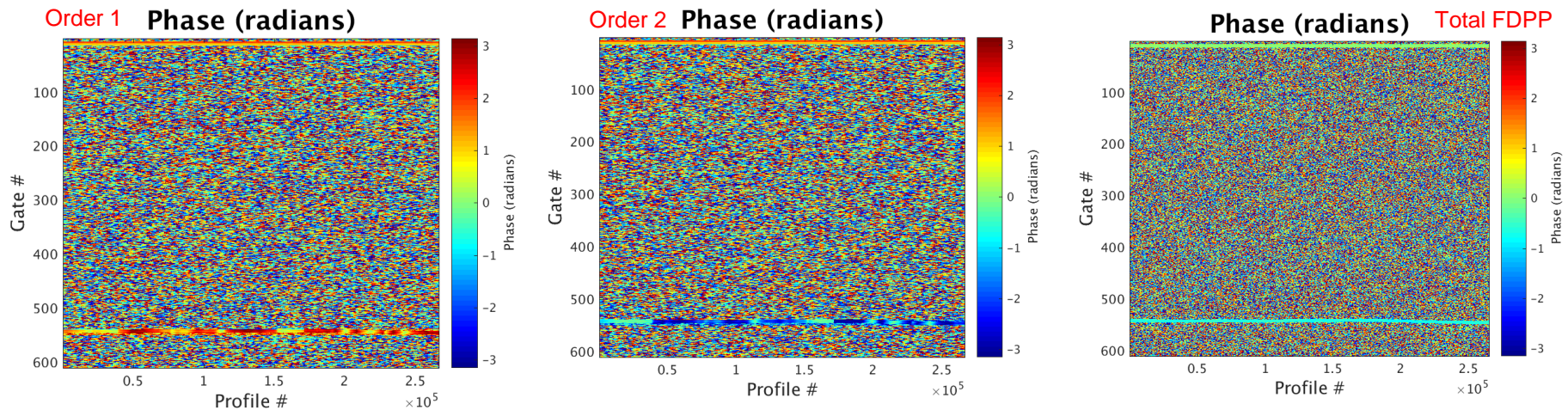
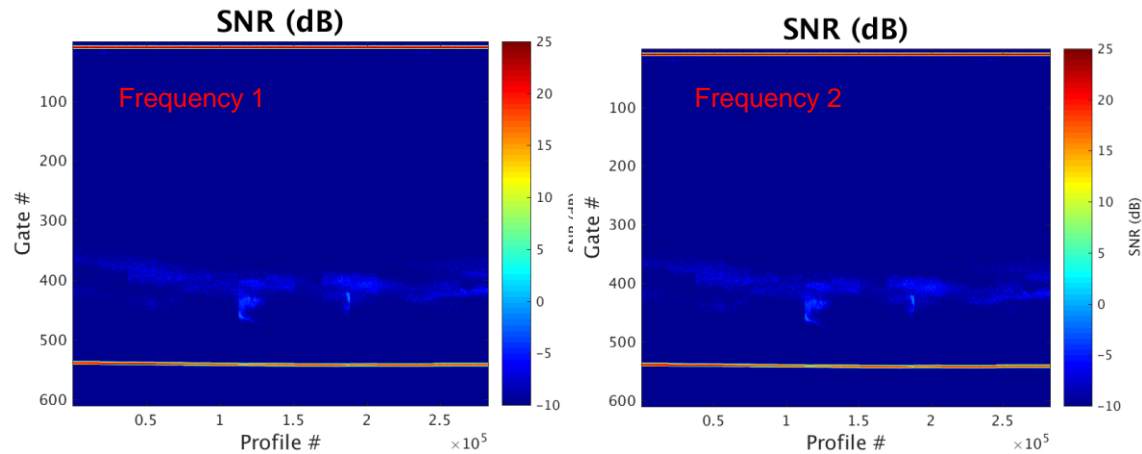
A multi-frequency view of precipitation from NASA's high-altitude radars



System implementation

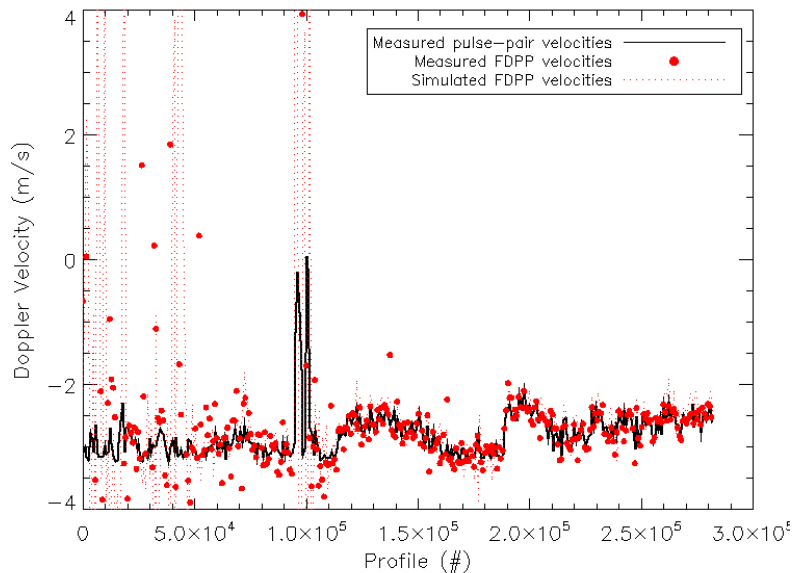
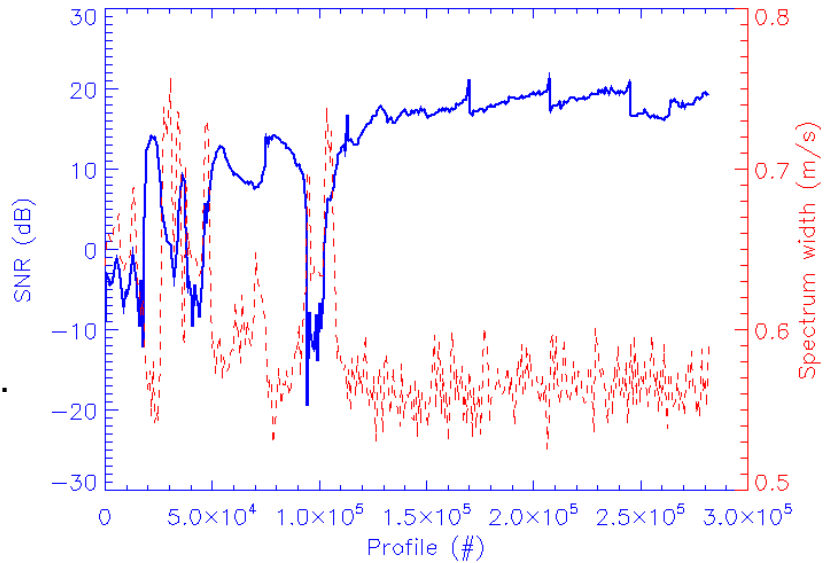


- Flight segment shows steps in retrieval process.
- Phase of f_1/f_2 and f_2/f_1 pairs both noisy, but sum is cleaner.
- High SNR surface echo alone used for subsequent analysis.

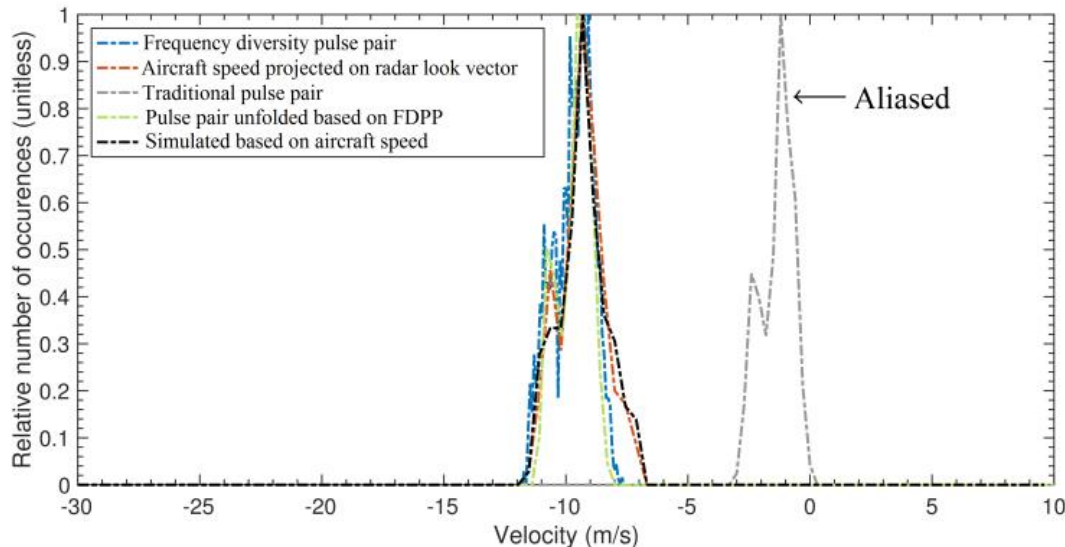
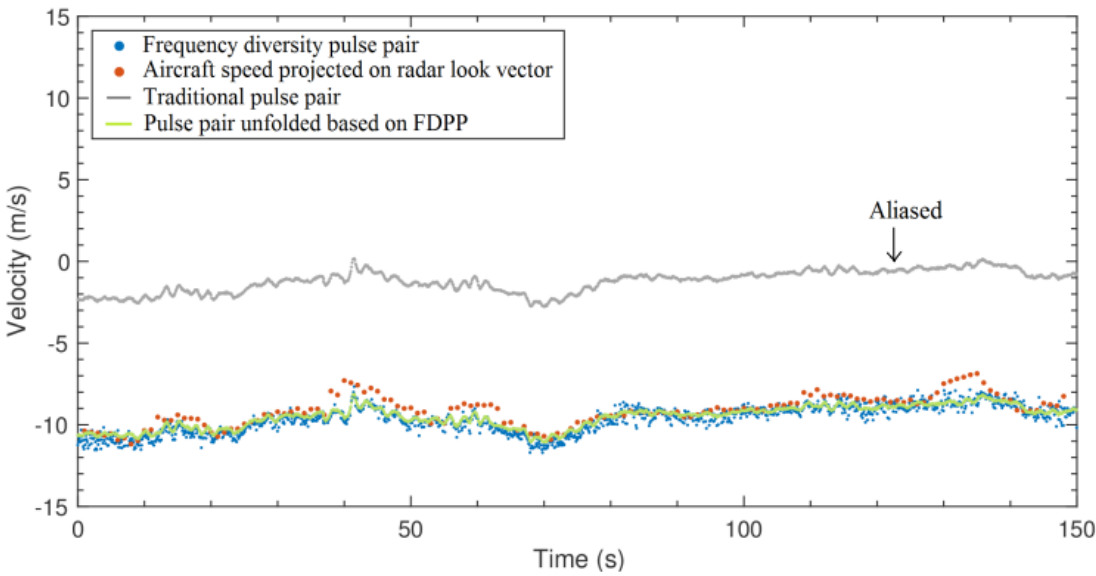


System implementation

- On an airborne data set using NASA's Cloud Radar System, FDPP Doppler estimates showed good agreement with traditional pulse-pair measurements.
- To first order, simulation predictions agree with measurements and theoretical expectations
- Simulations indicate potential for algorithm to be employed for hard-target tracking applications



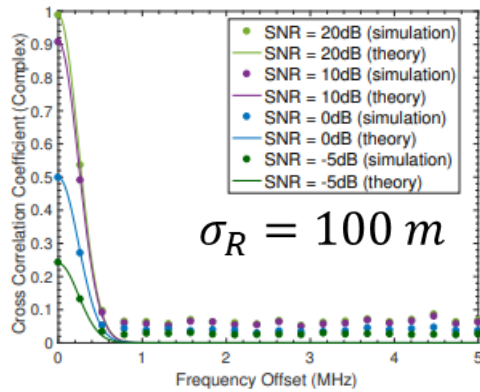
System implementation



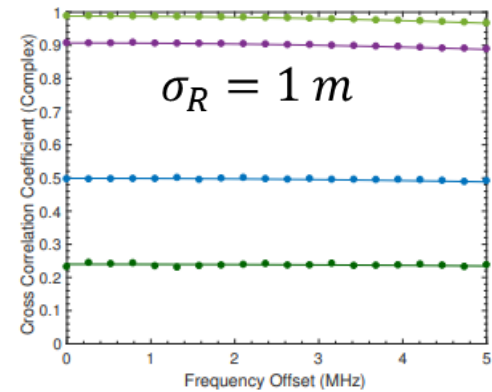
OFDM waveforms have much better immunity to aliasing.

System implementation

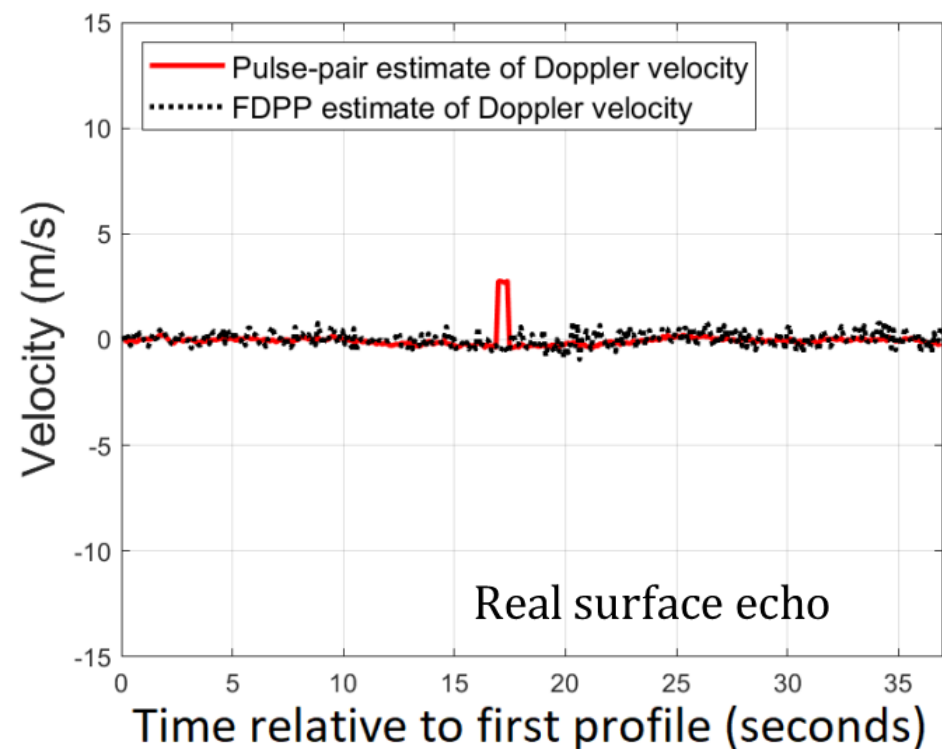
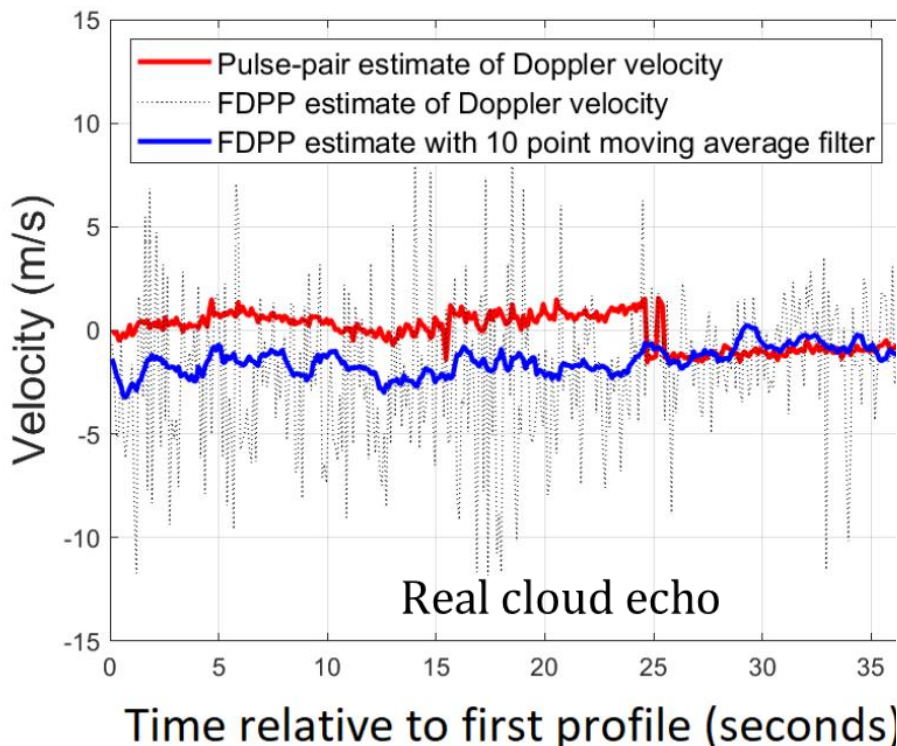
Simulated cloud echo



Simulated surface echo



Surface echo Doppler estimates perform better than cloud for OFDM waveforms.



Spaceborne stereo radar conclusions

- Spaceborne Doppler measurements in clouds are practical.
- Spaceborne stereo radars have performance that approaches a ground based Doppler measurements.
Drawback is high mass budget.
- CDMA technology enables single antenna solutions.
Performance worse than ground based systems but meets 0.5 m/s precision requirement.
- Stereo and CDMA solutions are superimposable, and constitute a new paradigm for spaceborne radars.